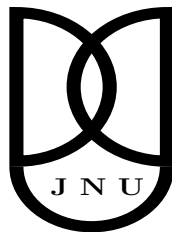# Inversion and Magnetic Quantum Oscillations in Kondo Insulators

A thesis submitted for the degree of
Doctor of Philosophy
by

PANCH RAM

School of Physical Sciences

Jawaharlal Nehru University
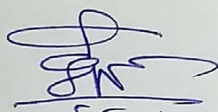
New Delhi - 110067 (INDIA)

July 2018

Dedicated to my loving parents
and respected teachers

Declaration

I hereby declare that the work reported in this thesis is entirely original, and has been carried out by me in the School of Physical Sciences, Jawaharlal Nehru University, New Delhi, under the supervision of Dr. Brijesh Kumar. I further declare that it has not formed the basis for the award of any degree, diploma, associateship or similar title of any university or institution.
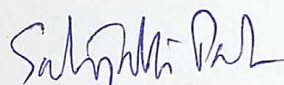
Date: July 2018

Panchram.
Panchram

Dr. Brijesh Kumar
(Thesis Supervisor)
School of Physical Sciences
Jawaharlal Nehru University
New Delhi - 110067

Prof. Satyabrata Patnaik
(Dean)
School of Physical Sciences
Jawaharlal Nehru University
New Delhi - 110067

Acknowledgements

At this moment, I feel the journey of my Ph.D., started about more than half a decade ago, is more like a mission of reaching the Everest step by step accompanying lots of encouragement, trust, hardship, and frustration, which took countless efforts, determination, and belief to successfully complete it. Even though eventually I find only my name printed on the thesis cover page, however, a great many people have supported me to complete this huge task.

In the very first place, I would like to express my sincere gratitude to my Ph.D. supervisor Prof. Brijesh Kumar for his continuous guidance, motivation and support throughout my Ph.D. research and thesis writing days. I am delighted to have a mentor like him who cared for my research work and responded so instantly to all kinds of doubts and queries. In my academic career, he is the one who majorly enlightens me through his constant hard work and honesty.

I would like to express my regard to Prof. Akhilesh Pandey and Dr. Nivedita Deo for being in my research advisory committee and also for their insightful comments, encouragements, and some hard questions which boosted me to comprehend my research in various ways.

I acknowledge the Council of Scientific and Industrial Research (CSIR), India and JNU for providing me financial support during my Ph.D. research days. I also acknowledge the HPC cluster at IUAC, and DST-FIST funded HPC cluster at SPS, JNU. I am also thankful to the SPS library staff and administrative staffs for their cooperation and consistent support in official work.

I thank Dr. Somenath Jalal, Dr. Bimla Danu, Dr. Ashwani Kumar Tripathy, Pratyay Ghosh, Meghadeepa Adhikary, and Deepti Sharma for being wonderful labmates, and I have been honoured by spending a quality time with you people. I thank Dr. Rakesh Kumar for his advice at the beginning of my PhD. I especially thank Dr. Somenath Jalal for collaborating with me on some problems, Pratyay Ghosh for helping me in learning parallel programming, and Meghadeepa Adhikary for the proof reading of this thesis.

List of Publications

1. **Theory of quantum oscillations of magnetization in Kondo insulators**
   <u>Panch Ram</u> and Brijesh Kumar
   Phys. Rev. B **96**, 075115 (2017)

2. **Phase diagram of the Hubbard-Kondo lattice model from variational cluster approximation**
   J. P. L. Faye, M. N. Kiselev, <u>Panch Ram</u>, B. Kumar and D. Sénéchal
   Phys. Rev. B **97**, 235151 (2018)

Contents

Chapter 1

Introduction

The work presented in this thesis is our contribution to the ongoing effort in understanding magnetic quantum oscillations, or the de Haas-van Alphen effect, in Kondo insulators. The Kondo insulators are a class of heavy-fermion systems that behave at lower temperatures as electrical insulators due to electron correlation and hybridization. The heavy-fermion systems make a vast area of research within the condensed matter physics. We begin this chapter with a basic introduction to the heavy-fermion systems, and to the Kondo insulators which are of primary interest to us here in this thesis. Then, we introduce the de Haas-van Alphen (dHvA) effect, which refers to the oscillations of magnetization as a function of

magnetic field. Historically, the dHvA effect has been considered to be a hallmark of metals. But recent findings of magnetic quantum oscillations in SmB_6, a Kondo insulator, poses a challenge to this conventional view. We briefly discuss the curious case of SmB_6, which motivated us to investigate the problem of dHvA oscillations in Kondo insulators. We conclude this chapter with an outline of the problems studied and the results obtained in this thesis.

1.1 Heavy Fermion Systems

The heavy-fermion (HF) systems are a family of rare-earth and actinide compounds with incompletely filled $4f$ or $5f$ shells [1, 2, 3]. The electronic properties of the HF materials are governed primarily by the strongly correlated and localized f electrons, and their hybridization with the conduction (say, d or s) electrons. The characteristic heavy fermion behaviour, which broadly defines this family, was first noted in 1975 by Andres, Graebner and Ott in $CeAl_3$ [4]. They observed that in the specific heat measurement, the coefficient, γ, of the term linear in temperature possesses an anomalously large value of 1620mJ/mole K^2 for $CeAl_3$, together with a T^2 behaviour of resistivity ($\rho \sim \rho_0 + AT^2$, $A = 35\mu\Omega cm/K^2$), at low temperatures. See Fig. 1.1(a)-(b) taken from this paper [4]. While the T^2 behaviour of low temperature resistivity implies that it is metallic, the hugeness of γ compared to its values in common metals suggests that the electrons in this material seem to be unusually 'heavy'. This opened up an exciting area of research that goes by the name of heavy-fermion systems.

To appreciate the largeness of γ in HF materials, let us recall the specific heat, C, of normal metals at low temperatures, given by the following simple formula that is standardly used to discuss the experimental data.

$$C = \gamma T + aT^3 \tag{1.1}$$

Here, the term linear in temperature, T, is the contribution of electrons to specific heat (derived by Sommerfeld for free Fermi gas), and the T^3 contribution comes from the acoustic modes of lattice vibrations (Debye's law). According to

(a) (b)
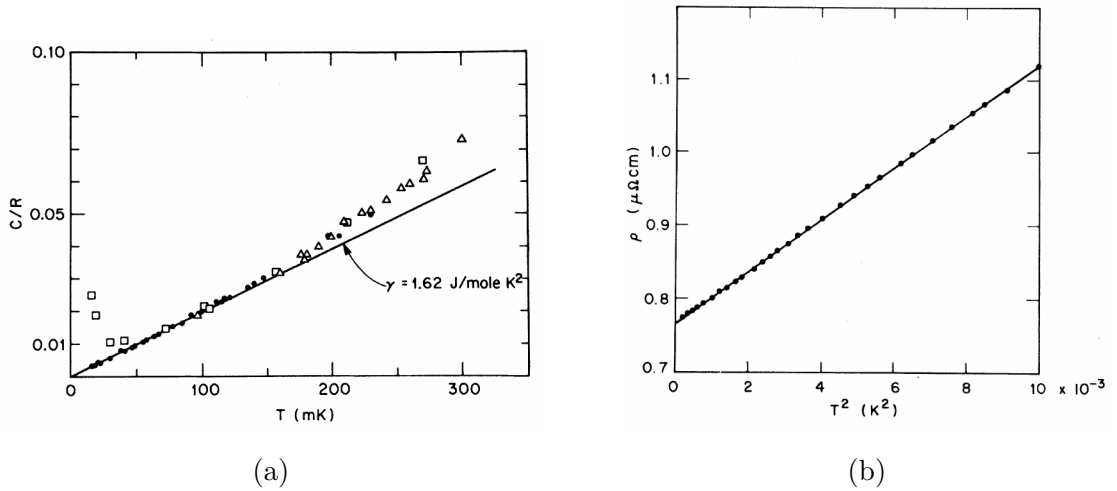
Figure 1.1: The heavy fermion nature of $CeAl_3$. (a) Specific heat vs. temperature (T), with huge γ at low temperatures. (b) Electrical resistivity (ρ) as a function of T^2 is very linear. Figures (a) and (b) are taken from Ref. [4].

Sommerfeld's theory of free electron gas [5, 6]

$$\gamma = \frac{2\pi^2}{3} k_B^2 \mathcal{D}(\epsilon_F) \tag{1.2}$$

where k_B is the Boltzmann constant and $\mathcal{D}(\epsilon_F)$ is the density of states at Fermi energy, ϵ_F. For free electrons, $\mathcal{D}(\epsilon_F) = \frac{3n}{4\epsilon_F}$, with number density, n, and $\epsilon_F = \hbar^2 k_F^2 / 2m$, where m is the free electron mass. In a real material, let the "effective" mass of electron be m^*, then using these, one arrives at the linear relation between γ and m^*.

$$\gamma = \frac{\pi^2}{2} \frac{n}{\epsilon_F} k_B^2 \propto m^* \tag{1.3}$$

Typical values of γ for metallic elements are: $\gamma_{Cu} = 0.695$ mJ/mole K^2, $\gamma_K = 2.08$ mJ/mole K^2 and $\gamma_{Ni} = 7.02$ mJ/mole K^2 [6, 1]. In comparison to these, the value of γ observed in $CeAl_3$, as mentioned above, is about 10^3 times larger [See Fig. 1.1(a)]. In view of the linear relation between γ and m^*, the most immediate implication of the the largeness of γ is that the effective mass of electrons in $CeAl_3$ and other such materials is very large (about 50 to 1000 times) compared to the free electron mass. This heavy fermionic behaviour consistently shows up not only as large γ of the specific heat, but also through enhancement of the Pauli susceptibility,

the coefficient of T^2 term of the low-T resistivity, highly temperature dependent amplitude of dHvA oscillations at low temperatures, etc.

The HF materials show a variety of interesting phenomena. For example, the discovery of superconductivity in $CeCu_2Si_2$ by Steglich et al. [7] intensified the interest in HF systems because of the coexistence of magnetism and superconductivity. Interestingly, in $CeCu_2Si_2$ the f-electrons are responsible both for local moments formation at high-T as well as superconductivity below critical temperature, T_c. Other HF systems like UBe_{13} shows superconductivity with non-Fermi liquid behaviour [8], and UPt_3 has antiferromagnetic (AFM) order below T_N [9]. The HF materials are too numerous to list here with all their properties. One can look up in the dedicated Handbooks for a detailed survey of this field [2]. We, instead, direct our attention towards a particular class of heavy-fermion systems called the Kondo insulators.

1.1.1 Kondo insulators: SmB_6, et cetera

The Kondo insulators (KI) are those HF materials which at sufficiently low temperatures behave as small-gap insulators exhibiting quantum paramagnetism. However, at higher temperatures, they behave as metals. In 1969, Menth et al. observed a change from metallic to insulating behaviour in samarium hexaboride, SmB_6, when temperature is lowered [10]. It is the earliest known case of a Kondo insulator. Many more Kondo insulating materials have been discovered over the years, for instance, YbB_{12}, $Ce_3Bi_4Pt_3$, CeNiSn, and so on [2]. Of these, SmB_6 has received much attention recently, and caused a stir in the condensed matter community by showing magnetic quantum oscillations at low temperatures, despite being an insulator [11, 12].

The SmB_6 forms the CsCl cubic structure, with lattice constant $a = 4.3$ Angstrom, in which Sm atoms sit at the corners and B_6 octahedra at the body centre, as shown in Fig. 1.2-(a). In this compound, samarium is in a mixed valence state of Sm^{2+} ($4f^6$) and Sm^{3+} ($4f^5$). For temperatures above 50 K, it is a Curie-Weiss metal. However, at lower temperatures, it opens up a gap and behaves like a paramagnetic insulator [2, 13, 14, 15]. The activated behaviour of electrical resistance with temperature, as shown in Fig. 1.2(b), gives an activation gap of

about 40 K for SmB_6 [12].

<div align="center">(a)   (b)</div>
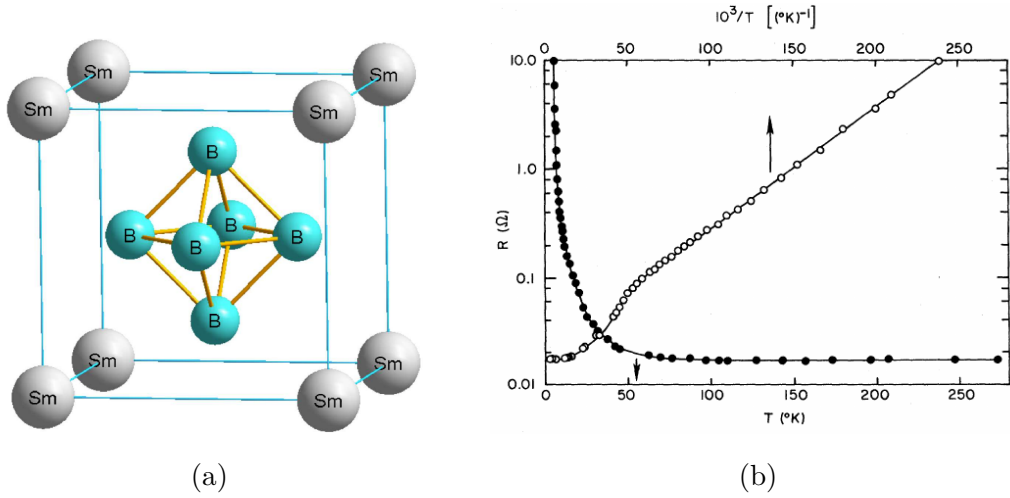
Figure 1.2: (a) Crystal structure of SmB_6, where the samarium ions are sitting at the corners. This figure is taken from Ref. [16]. (b) Resistivity vs. temperature of SmB_6 shows exponential rise in resistivity at low temperatures. This figure is taken from Ref. [10].

The Kondo insulating behaviour in these materials is caused by a combination of hybridization (between the conduction and f electrons) and strong correlation (of the f electrons), for suitably commensurate electron fillings. In case of SmB_6, for instance, the relevant hybridization process is: $4f^6 \rightleftharpoons 4f^5 5d$. The effective Kondo exchange, that results from hybridization and strong correlation, causes the formation of singlet between the conduction and localized electron spins, and opens a charge gap leading to insulating behaviour, at low temperatures. Recall that the metals (such as Au, Ag or Cu) with a dilute concentration of magnetic impurities (say, Fe or Mn) show an increase in the resistivity at low temperatures [17, 18, 19]. Jun Kondo famously solved this resistivity minimum problem by invoking 'Kondo' exchange as a scattering channel for the conduction electrons that gives a $\log T$ correction to the resistivity [20]. In contrast, the Kondo insulators are highly 'concentrated' or 'dense' Kondo impurity systems, where the metallic state completely gives way to an insulating state at low enough temperatures.

1.1.2 Models of Kondo insulators

The microscopic setting of a Kondo insulator can be described as having a band of conduction electrons, the localized and correlated f-electrons (or impurity spins), and their mutual coupling. Like in the Mott-Hubbard insulators, the electron filling is also an important parameter in the realization of a KI. For the basic case of a single conduction band filled with one electron per site (of some lattice), it would need exactly one localized f-electron (or spin-1/2 impurity) on every site, for this system to behave as Kondo insulator. This is commonly known as the "half-filled" case[1]. The microscopic physical models that are used to discuss Kondo insulators are the Kondo lattice model [21] and the periodic Anderson model, both at half-filling.

1.1.2.1 Kondo lattice model at half-filling

When the conduction and f electrons are weakly hybridized, the f electrons essentially behave as localized spin-1/2's interacting locally with the conduction electron spins via Kondo exchange. The minimal model that describes this physical setting is the Kondo lattice model (KLM). The Hamiltonian of the KLM can be written as follows:

$$\hat{H}_{\mathrm{KLM}} = \sum_{\mathbf{k}} \sum_{s=\uparrow,\downarrow} \epsilon(\mathbf{k}) \; \hat{c}^{\dagger}_{\mathbf{k},s} \hat{c}_{\mathbf{k},s} + \frac{J}{2} \sum_{\mathbf{r}} \mathbf{S_r} \cdot \boldsymbol{\tau_r} \tag{1.4}$$

Here, the first term is the kinetic energy of conduction electrons, with $\epsilon(\mathbf{k})$ as the dispersion of the conduction band. For instance, on square lattice, $\epsilon(\mathbf{k}) = -2t(\cos k_x a + \cos k_y a)$ with nearest-neighbour hopping, t. The $\hat{c}_{\mathbf{k},s}$ ($\hat{c}^{\dagger}_{\mathbf{k},s}$) are the annihilation (creation) operators of the conduction electrons. The second term, with $J > 0$, is the Kondo exchange interaction between the localized spin-1/2 moment described by the Pauli operators, $\boldsymbol{\tau_r}$, and the conduction electron spin, $\mathbf{S_r}$, on every lattice site $\mathbf{r}$. In more general cases, $\boldsymbol{\tau_r}$'s could be taken as larger than 1/2, or even classical moments. But we in this thesis will always consider $\boldsymbol{\tau_r}$ as quantum spin-1/2.

---

[1]To completely fill a single conduction band, we need two electrons per site. Hence, a filling of one conduction electron per site is called the half-filled case.
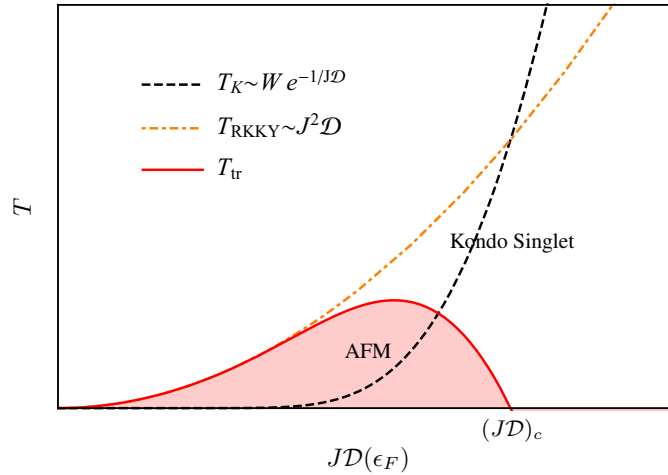
Figure 1.3: Doniach's phase diagram of the Kondo lattice model. For $T_K > T_{RKKY}$, i.e. for stronger Kondo couplings, the Kondo singlet phase is realized. When $T_K < T_{RKKY}$, a magnetic order is expected to appear. Here, T_{tr} denotes the line of phase transition.

As we will see in the following chapter, it is the Kondo coupling, J, that drives the formation of charge gap and Kondo singlet phase, when sufficiently strong. However, for weaker J's, the KLM realizes an indirect exchange interaction between the magnetic moments, which is mediated by the conduction electrons. It is known as Ruderman-Kittel-Kasuya-Yosida or RKKY interaction [22, 23].

$$\hat{H}_{\text{RKKY}} = \frac{1}{4} \sum_{\mathbf{r},\mathbf{r}'} J_{\text{RKKY}}(|\mathbf{r} - \mathbf{r}'|)\boldsymbol{\tau}_{\mathbf{r}} \cdot \boldsymbol{\tau}_{\mathbf{r}'} \tag{1.5}$$

The competition between Kondo and RKKY interactions can be illustrated using Doniach's well-known phase diagram, shown in Fig. 1.3. It is obtained by comparing the two energy scales present in the system: the Kondo temperature, $T_K \sim We^{-1/J\mathcal{D}}$, and the magnetic ordering temperature, $T_{\text{RKKY}} \sim J^2\mathcal{D}$, where W is the bandwidth and $\mathcal{D}$ is the density of states at Fermi surface. For strong Kondo couplings, we get Kondo singlet phase, but for weak Kondo couplings, we expect to get a magnetically ordered phase.

1.1.2.2 Symmetric periodic Anderson model

The periodic Anderson model (PAM) is the lattice version of the celebrated single impurity Anderson model [24]. It is more microscopic than KLM, because it treats the localized f electrons not merely as spin-1/2's, but as full dynamic electrons

which hybridize with the conduction electrons. The Hamiltonian of PAM can be written as:

$$\hat{H}_{\text{PAM}} = \sum_{\mathbf{k},s} \epsilon(\mathbf{k})\hat{c}^\dagger_{\mathbf{k},s}\hat{c}_{\mathbf{k},s} + \epsilon_f \sum_{\mathbf{r},s} \hat{n}^f_{\mathbf{r},s} + U_f \sum_{\mathbf{r}} \hat{n}^f_{\mathbf{r},\uparrow}\hat{n}^f_{\mathbf{r},\downarrow} - V \sum_{\mathbf{r},s} \left[\hat{c}^\dagger_{\mathbf{r},s}\hat{f}_{\mathbf{r},s} + \text{h.c.} \right]$$
(1.6)

where $\hat{c}^\dagger_{\mathbf{k},s}(\hat{c}_{\mathbf{k},s})$ are the creation (annihilation) operators of the conduction electrons with momentum $\mathbf{k}$ and spin $s = \uparrow, \downarrow$, and likewise, $\hat{f}^\dagger_{\mathbf{r},s}(\hat{f}_{\mathbf{r},s})$ are operators for the f electrons at site $\mathbf{r}$. Moreover, $\hat{n}^f_{\mathbf{r},s} = \hat{f}^\dagger_{\mathbf{r},s}\hat{f}_{\mathbf{r},s}$ is the number operator of an f electron. The $\epsilon(\mathbf{k})$ is the dispersion of the conduction band, ϵ_f and U_f are respectively the local energy and Coulomb repulsion of the f electrons, and V is the hybridization between the conduction and f electrons. The PAM, with all these key ingredients necessary to discuss heavy fermion physics, is indeed the basic model of the HF systems.

To see its utility for Kondo insulators, consider the PAM without U_f, which can be diagonalized by Fourier transforming $\hat{f}_{\mathbf{r},s}$ to $\hat{f}_{\mathbf{k},s}$ and then mixing $\hat{f}_{\mathbf{k},s}$ with $\hat{c}_{\mathbf{k},s}$. The resulting band dispersions of this non-interacting PAM are given as follows:

$$\lambda_\pm(\mathbf{k}) = \frac{1}{2}\left[\epsilon(\mathbf{k}) + \epsilon_f \pm \sqrt{[\epsilon(\mathbf{k}) - \epsilon_f]^2 + 4V^2} \right]$$
(1.7)

They are shown in Fig. 1.4. In order for the non-interacting PAM to describe an insulator, it is clear that the band with lower energy, $\lambda_-(\mathbf{k})$, must be fully occupied, while the higher energy band should be empty. It implies that the number of electrons per site should be $n_e = 2$, which is the half-filled case[2]. Thus, the non-interacting PAM has an insulating ground state at half-filling. But this is just a band insulator, without Kondo singlet formation. For the Kondo singlet, we need to turn on U_f, which makes the PAM a difficult many-body problem. But U_f does not alter the electron filling. Thus, the half-filled PAM with $U_f > 0$ describes a Kondo insulator.

Now the question is how to realize and maintain half-filling, while doing the calculations. It so happens that a neat and simple way of exactly guaranteeing half-filling is to consider the PAM on a bipartite lattice with $\epsilon_f = -U_f/2$. One can

---

[2]On every site there are two orbitals, c (conduction) and f (localized). Therefore, the maximum number of electrons per site could be 4. Hence, $n_e = 2$ is the case of half-filling.
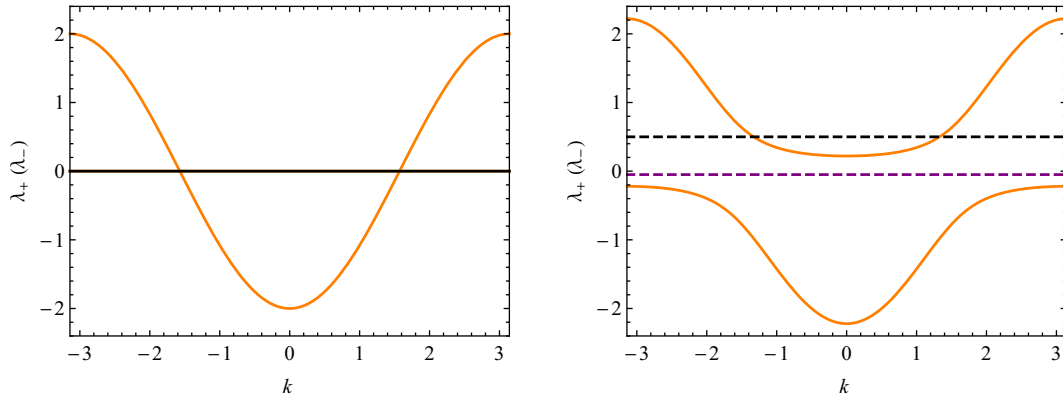
Figure 1.4: The band structure of PAM for $U_f = 0$, plotted in one dimension for illustration. Left panel: Dispersions, $\lambda_\pm(\mathbf{k})$, without hybridization, $V = 0$. The conduction band (orange) is dispersive and the localized band (black) is completely flat. Right panel: A non-zero V opens a gap. If the chemical potential (black dashed line) lies inside a band (near the top of the lower band or the bottom of the upper band), then the system is a heavy-fermion metal, otherwise (purple dashed line) it is an insulator.

show that this special case of PAM is symmetric under particle-hole transformation, which guarantees the half-filling. For instance, on a hypercubic lattice with nearest-neighbour hopping, this so-called "symmetric" periodic Anderson model can be written as:

$$
\begin{aligned}
\hat{H}_{\mathrm{SPAM}} = & -t \sum_{\mathbf{r},\boldsymbol{\delta}} \sum_{s=\uparrow,\downarrow} \hat{c}^\dagger_{\mathbf{r},s} \hat{c}_{\mathbf{r}+\boldsymbol{\delta},s} - V \sum_{\mathbf{r}} \sum_{s=\uparrow,\downarrow} \left(\hat{c}^\dagger_{\mathbf{r},s} \hat{f}_{\mathbf{r},s} + \mathrm{h.c.} \right) \\
& + U_f \sum_{\mathbf{r}} \left[n^f_{\mathbf{r},\uparrow} n^f_{\mathbf{r},\downarrow} - \frac{1}{2} \left(n^f_{\mathbf{r},\uparrow} + n^f_{\mathbf{r},\downarrow} \right) \right]
\end{aligned}
\tag{1.8}
$$

where $\boldsymbol{\delta}$ is summed over the nearest neighbours of $\mathbf{r}$. The symmetric periodic Anderson model (SPAM) has been variously studied to understand the basic properties of Kondo insulators [19, 25, 3]. Here, we will study it to understand magnetic quantum oscillations in Kondo insulators.

1.2 The de Haas-van Alphen Oscillations

The de Haas-van Alphen (dHvA) effect refers to the oscillations of magnetization, M, with respect to magnetic field, B. It was discovered in 1930 by Wander Johannes de Haas and P. M. van Alphen in a single crystal of Bi at liquid hydrogen

temperatures [5, 26]. The dHvA oscillations are periodic in $1/B$, and are understood to occur due to Landau quantization of electronic orbits in magnetic field. Hence, they are also called quantum oscillations, or more specifically, magnetic quantum oscillations. Historically, the dHvA effect is considered to be a hallmark of the metallic response.
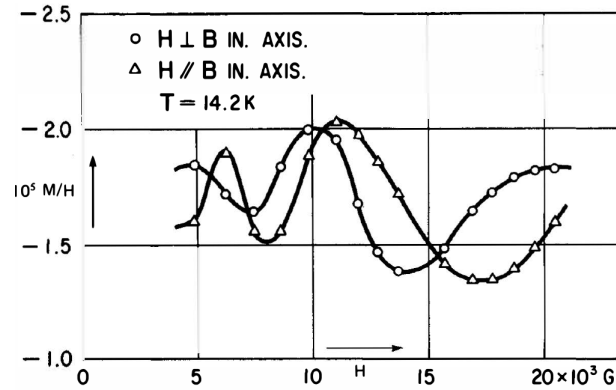
Figure 1.5: The oscillations of magnetization with magnetic field, as found by de Haas and van Alphen, in Bi at temperature, $T = 14.2$K. This figure is taken from Ref. [26].

Classically, an electron traverses in the orbits caused by the Lorentz force. Quantum mechanics quantizes these orbits in the plane perpendicular to magnetic field. The area of these orbits in real space decreases upon increasing B, which implies that the corresponding area in the momentum space would increase with B. Therefore, when an orbit crosses the extremal cross-sectional area of the Fermi surface in a metal, it shows a peak in the density of state, $\mathcal{D}$. The peak in $\mathcal{D}$ appears periodically as B increases. Therefore, all the physical quantities that depend on $\mathcal{D}$ show an oscillatory behaviour with respect to B. For instance, like M, the resistivity also exhibits such oscillations, which is known as Shubnikov-de Haas effect. Interestingly, the oscillation frequency, f, can be related to the extremal area, F, (perpendicular to magnetic field) on the Fermi surface through the following relation due to Onsager [27].

$$f = \frac{\hbar}{2\pi e} F \tag{1.9}$$

Here, $\hbar = h/2\pi$ is the Planck's constant, and e is magnitude of the charge of electron. Notably, the proportionality constant between f and F in Eq. (1.9) depends only on two fundamental quantities.

1.2.1 Landau quantization and dHvA effect in metals

To understand the microscopic basis of the dHvA effect, let us consider the Landau quantization for free electrons in a cubical box of sides L_x, L_y, L_z, in the presence of a uniform magnetic field, B (say, along z-axis). The Hamiltonian of a free electron of mass m and charge $-e$ travelling in a magnetic field can be written as:

$$\hat{H} = \frac{(\mathbf{p} + e\mathbf{A})^2}{2m} \tag{1.10}$$

where, $\mathbf{p} = -i\hbar\nabla$ is canonical momentum operator. Since the magnetic field $\mathbf{B} = B\hat{z}$, therefore, we can choose the vector potential to be $\mathbf{A} = -By\hat{x}$, which satisfies the relation $\mathbf{B} = \nabla \times \mathbf{A}$. It is called the Landau gauge. So, in the Landau gauge, Eq. (1.10) reads as:

$$\hat{H} = \frac{1}{2m}\left(-i\hbar\frac{\partial}{\partial x} - eBy\right)^2 - \frac{\hbar^2}{2m}\left(\frac{\partial^2}{\partial y^2} + \frac{\partial^2}{\partial z^2}\right). \tag{1.11}$$

Note that the momentum operators p_x and p_z are conserved in the above Hamiltonian. That is, $[p_x, \hat{H}] = 0$ and $[p_z, \hat{H}] = 0$. So, we can write the wavefunction as:

$$\psi(x, y, z) = \chi(y)e^{i(k_x x + k_z z)} \tag{1.12}$$

and then the Schrödinger equation $\hat{H}\psi = E\psi$ reads as:

$$\left[E - \frac{\hbar^2 k_z^2}{2m} - \frac{1}{2}m\omega_c^2(y - y_0)^2\right]\chi + \frac{\hbar^2}{2m}\frac{\partial^2\chi}{\partial y^2} = 0 \tag{1.13}$$

where $\omega_c = eB/m$ is the cyclotron frequency. Here, we see that the electron's motion is free along z direction, while in the xy-plane, it behaves as a harmonic oscillator along y centred at $y_0 = \frac{\hbar k_x}{m\omega_c}$. Equation (1.13) is a standard problem in quantum mechanics, whose energy eigenvalues, given by the wavenumber, k_z, and an integer $n \geq 0$, can be written as follows:

$$E_{n,k_z} = \frac{\hbar^2 k_z^2}{2m} + \left(n + \frac{1}{2}\right)\hbar\omega_c \tag{1.14}$$

This is the *Landau quantization* of a free electron in uniform magnetic field.

Equation (1.14) is quite remarkable. We can see that the energy $\hbar^2 k_z^2/2m$ coming from the motion along z direction remains the same even after turning

on B, because the Lorentz force does not act along the magnetic field direction (z-axis). However, the energy of the motion in the plane perpendicular to $\mathbf{B}$ is quantized in the steps of $\hbar\omega_c$. That is, the cyclotron motion in the x-y plane gets quantized according to the following (semiclassical) condition:

$$\frac{\hbar^2}{2m}(k_x^2 + k_y^2) = \left(n + \frac{1}{2}\right)\hbar\omega_c \tag{1.15}$$

We note that the energy in Eq. (1.14) does not depend on quantum number k_x, which can take any value of $k_x = \frac{2\pi N}{L_x}$ (N is integer). So, each level is highly degenerate. The set of all eigenstates [of Eq. (1.13)] for a given n (and arbitrary k_z) is referred to as the nth *Landau level*. Since $0 < y_0 < L_y$, we get the following condition on N:

$$0 < \frac{\hbar k_x}{m\omega_c} < L_y$$
$$\Rightarrow \quad 0 < N < \frac{eB}{h}L_x L_y = \frac{\Phi}{\Phi_0}$$

where $\Phi = BL_x L_y$ is magnetic flux passing through the sample and $\Phi_0 = h/e$ is the quantum flux. Hence, the total number of eigenstates per Landau level is $2\Phi/\Phi_0$, where the factor of 2 is due to spin degeneracy for electrons.

Origin of quantum oscillations: Semiclassical approach

We use the semiclassical approach to understand the origin of quantum oscillations in metals [6, 5, 28]. An electron moving in magnetic field has momentum, $\mathbf{p} = \hbar\mathbf{k} - e\mathbf{A}$, where the first term is its kinetic momentum and the second is due to the magnetic field. Assuming that the orbit is closed, the Bohr-Sommerfeld condition quantizes the orbital motion of electron in the magnetic field as:

$$\oint \mathbf{p} \cdot d\mathbf{r} = (n + \theta)2\pi\hbar \tag{1.16}$$

where n is a non-negative integer and θ, the phase correction, is $1/2$ for parabolic dispersion and 0 for graphene-like linear dispersion. The semiclassical equation of motion of an electron in magnetic field can be written as follows:

$$\hbar\frac{d\mathbf{k}}{dt} = -e\frac{d\mathbf{r}}{dt} \times \mathbf{B} \tag{1.17}$$

By integrating it with respect to t, we get $\hbar\mathbf{k} = -e\mathbf{r} \times \mathbf{B}$ plus a constant, which does not contribute to the final result. We use this and Stoke's theorem to find

$$
\begin{aligned}
\oint \mathbf{p} \cdot d\mathbf{r} &= \oint \hbar\mathbf{k} \cdot d\mathbf{r} - e\oint \mathbf{A} \cdot d\mathbf{r} = -e\oint \mathbf{r} \times \mathbf{B} \cdot d\mathbf{r} - e\oint \nabla \times \mathbf{A} \cdot d\boldsymbol{\sigma} \\
&= e\mathbf{B} \cdot \oint \mathbf{r} \times d\mathbf{r} - e\oint \mathbf{B} \cdot d\boldsymbol{\sigma} = e(2\Phi) - e\Phi = e\Phi \\
\Rightarrow \quad &\Phi = (n+\theta)2\pi\hbar/e
\end{aligned}
\tag{1.18}
$$

where $d\boldsymbol{\sigma}$ is the area element in real space. Here, we have also used the fact that $\oint \mathbf{r} \times d\mathbf{r} = 2 \times$ *the area enclosed by the close orbit*. From the above result for Φ, we get the following quantization rule for the area, S, of the cyclotron orbit in real space.

$$
S_n = (n+\theta)\frac{2\pi\hbar}{eB}
\tag{1.19}
$$

Since the line element $\Delta\mathbf{r}$ in the plane normal to magnetic field $\mathbf{B}$ is related to the line element $\Delta\mathbf{k}$ in $\mathbf{k}$-space as $|\Delta\mathbf{r}| = (\hbar/eB)|\Delta\mathbf{k}|$. Therefore, the area, S_n, in real space corresponds to the area, F_n, in $\mathbf{k}$-space as: $S_n = (\hbar/eB)^2 F_n$. From Eq. (1.19) for S_n, we get the following expression for F_n.

$$
F_n = (n+\theta)\frac{2\pi eB}{\hbar}.
\tag{1.20}
$$

Note that, for $\theta = 1/2$, Eq. (1.20) is same as Eq. (1.15) for the free electron.

Most low-temperature electronic properties of metals depend upon the density of states at the Fermi energy. For a non-zero B, the free electron states reorganize into Landau levels whose degeneracy grows with B. Therefore, as B increases or decreases, the Landau levels repeatedly cross the Fermi level leading to an oscillatory behaviour of various physical quantities. The period of this oscillation is determined by the crossing of successive Landau levels ($\sim$ semiclassical quantized orbits in $\mathbf{k}$-space) across those cross-sections on the Fermi surface that enclose an extremal area perpendicular to magnetic field. Let such an extremal area be F, and the nth closed orbit attain this area for the field strength, B_n. Then, the periodicity criteria, $F_n = F_{n+1} = F$, and the quantization condition of Eq. (1.20), together give

$$
\text{the period of oscillation} = \left| \frac{1}{B_{n+1}} - \frac{1}{B_n} \right| = \frac{2\pi e}{\hbar F}.
\tag{1.21}
$$

This explains, for instance, why dHvA oscillations are periodic in $1/B$. Finally, the frequency, f, of such quantum oscillations is given by the following relation:

$$f = \left| \frac{1}{B_{n+1}} - \frac{1}{B_n} \right|^{-1} = \frac{\hbar}{2\pi e} F \tag{1.22}$$

This celebrated equation provides the basis for directly measuring the Fermi surfaces in metals by doing quantum oscillation measurements.

1.2.2 Curious case of SmB$_6$: dHvA effect in insulators?

In the previous subsection, we learnt about the dHvA effect, which has always been considered to be a characteristic of metals, and was never expected to occur in insulators. But this conventional view changed recently, when SmB$_6$, a Kondo insulator, showed magnetic quantum oscillations at low temperatures [11, 12].
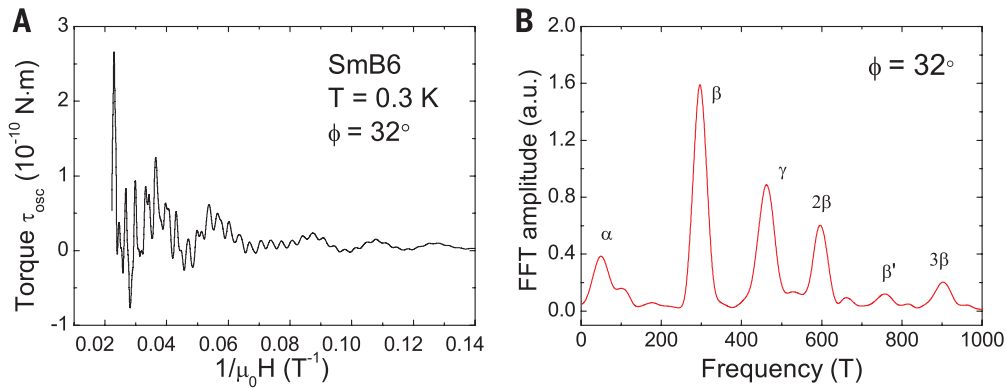
Figure 1.6: Quantum oscillations in SmB$_6$ from Ref. [11]. (**A**) Magnetic torque vs. inverse magnetic field. (**B**) Fourier transform of the oscillation data showing frequencies that are claimed to correspond to the two-dimensional Fermi surface of the conducting surface states.

Some years ago, SmB$_6$ had been theoretically predicted to be a topological Kondo insulator having conducting surface states with an insulating bulk [29, 30]. It motivated experiments that eventually found dHvA oscillations in SmB$_6$. The experiments by Li. et al. [11] claimed to have seen the two-dimensional Fermi surface of the conducting surface states through quantum oscillation measurements. Figure 1.6 shows some data from Ref. [11]. However, in contrast to this, no quantum oscillations have been observed in the resistivity measurements on surface [31].

In separate experiments, Tan et al. also observed magnetic quantum oscillations in SmB_6 [12]. But they claim these oscillations to come from a three-dimensional "Fermi surface". In fact, the high oscillation frequencies in their data are claimed to correspond to the half of the bulk Brillouin zone. Figure 1.7 shows some data from Ref. [12]. This is very puzzling, because the conducting surface states can not account for it, and the bulk is insulating! As there are no free electrons in the bulk, there is no Fermi surface (as we conventionally understand it). So what surface, and of which quasiparticles, these oscillations are actually measuring?

(a)   (b)
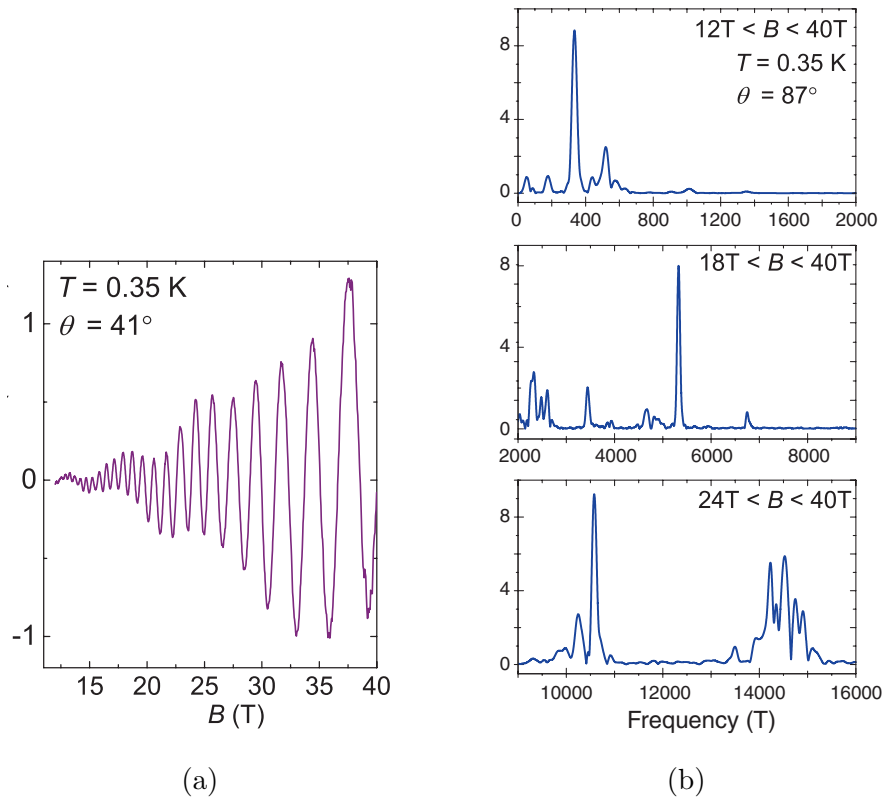
Figure 1.7: (a) Magnetic quantum oscillations in SmB_6. (b) Fourier transform. Notably, the oscillation frequencies $\gtrsim 10,000$ T are claimed to correspond approximately to the half of the bulk Brillouin zone. These figures are taken from Ref. [12].

These findings pose a difficult question of principle on the occurrence of dHvA oscillations, not only in SmB_6, but more generally in any insulator (correlated or otherwise). This has led some to propose exotic neutral quasiparticles giving rise to unconventional Fermi surface in Kondo insulators [32, 33, 34], while others have tried to find answers within more conventional framework [35, 36, 37, 38]. Very

recently, even disorder has been proposed as a possible cause of bulk quantum oscillations in insulators [39, 40]. It is clearly a hotly debated and actively pursued problem of great interest. Interestingly, another Kondo insulator, YbB_{12}, has also been reported recently to show magnetic quantum oscillations [41]. Thus, SmB_6 is not a lonely case anymore, and this list may grow further.

1.3 Brief Outline of the Thesis

Motivated by the situation presented by SmB_6, we too investigated the problem of dHvA oscillations in Kondo insulators, and made some novel contributions to its understanding [42]. Given that the quantum oscillation measurements on SmB_6 observe a bulk Fermi surface (which the surface states obviously can not account for), we believe that it must be so due to some intrinsic property of the Kondo insulating bulk, regardless of its being topological or not. With this point of view, we look *afresh* at the properties of the (non-topological) Kondo insulators by doing calculations on the standard half-filled Kondo lattice and symmetric periodic Anderson models. From these calculations, we discover a novel quasiparticle band inversion that we show to have a direct bearing on the occurrence of dHvA oscillations in Kondo insulators. In fact, the quantum oscillations we get from our calculations on square and simple cubic lattices correspond precisely to the half of the bulk Brillouin zone. Notably, In our computation of dHvA oscillations, we properly take into account the Kondo interaction, which is uncommon. In this thesis, we present our theory of magnetic quantum oscillations in Kondo insulators. Below we give an overview of the work presented in different chapters of this thesis.

1.3.1 Studies on the half-filled Kondo lattice model

In Chapter 2, we investigate the orbital response to uniform magnetic field in the ground state of the KLM (Kondo lattice model) of localized spin-1/2's coupled to the spins of the conduction electrons via an antiferromagnetic exchange coupling, $J > 0$, at half-filling on square and simple cubic lattices. The conduction electron hopping is taken to be nearest-neighbour only, with an amplitude t. It ensures

particle-hole symmetry of the KLM on bipartite lattices, which in turn guarantees half-filling. We formulate a novel self-consistent theory of the effective charge and spin dynamics of the half-filled KLM by employing a canonical representation of electrons, as invented by Brijesh Kumar [43]. This representation describes the electron operators in terms of the spinless fermion and Pauli operators. It has been used quite fruitfully in studying the problems of correlated electrons.

1.3.1.1 Inversion and dHvA oscillations

The ground state properties of the KLM in the absence of magnetic field are correctly described by our self-consistent theory. For instance, the charge gap in this theory is always non-zero for any value of t/J, which is how it should be for an insulating state. Moreover, for small t/J (i.e., strong Kondo coupling), the effective spin dynamics correctly produces the spin-gapped Kondo singlet phase. Upon increasing t/J, the spin gap is found to continuously vanish, due to which the Kondo singlet phase undergoes a continuous transition to the Néel antiferromagnetic (AFM) phase.

Besides producing the commonly known features, our theory also reveals a novel feature of the Kondo insulators, which is that the charge quasiparticle dispersion undergoes inversion, as t (for a fixed J) increases beyond the inversion point, t_i. A simple consequence of the quasiparticle band inversion is that for strong Kondo couplings, the charge gap comes from the Γ point in the Brillouin zone, while it shifts to the half-Brillouin zone boundary for sufficiently weak Kondo couplings. But a remarkable consequence of this inversion is the realization of dHvA oscillations in the Kondo insulating state [42].

In uniform magnetic field, B, coupled via Peierls phase to electron hopping, the effective charge and spin dynamics in our theory become two Hofstadter-like problems of spinless fermions and hard-core bosons, respectively. By numerically diagonalizing them, we calculate magnetization, M, as a function of B in the ground state. The contribution of spin dynamics to M vs. B turns out to be insignificant and not of much consequence. Hence, we focus on the charge dynamics. But even the charge dynamics does not show any quantum oscillations for strong Kondo couplings. However, after the inversion ($t > t_i$) has taken place, we begin

to see magnetic quantum oscillations from the charge dynamics. In fact, these oscillations become more and more pronounced as the Kondo coupling goes from moderate to weak. We do further analysis to clearly establish that the quasiparticle band inversion is the key to dHvA oscillations in Kondo insulators. This is why, in our calculations, the absence or appearance of dHvA oscillations depends on t/J, because t/J controls the inversion.

By Fourier transforming the magnetization data, we find the dominant frequency of dHvA oscillations to correspond to the half of the bulk Brillouin zone. This is like what the experiments suggest. More precisely, these oscillations here measure the surface of the effective chemical potential of the charge quasiparticles, which plays the same role as the Fermi surface in metals.

As noted above, the dHvA oscillations grow stronger as t/J increases into the Néel phase. On a careful reflection, it reveals to us a possibility of dHvA oscillations occurring in the weak-coupling spin-density wave (SDW) insulators. To support this insight, we do the same calculation also for the half-filled Hubbard model. In Chapter 5, we do this again in the standard formulation of the SDW problem.

1.3.1.2 Investigations on Hubbard-Kondo lattice model

The KLM is a minimal physical model of the HF systems, where the local moments are coupled to the 'non-interacting' conduction electrons. But there are materials like $Nd_{2-x}Ce_xCuO_4$ [44], and some Ce-based HF compounds [45], where the interaction between the conduction electrons plays an important role in determining the properties of the system. Therefore, in Chapter 3, we investigate the half-filled KLM but with an additional Hubbard repulsion, $U > 0$, for the conduction electrons. We call it the Hubbard-Kondo lattice model (H-KLM).

By employing the theory developed for KLM in Chapter 2, we study the effect of U on the properties of H-KLM at half-filling. We generate a quantum phase diagram, that has Kondo singlet to Néel AFM phases separated by a critical line. This is in good qualitative agreement with VCA (variational cluster approximation) [46] and QMC (quantum monte carlo) [47] calculations. We find and understand that the main effect of repulsion, U, in H-KLM is to enhance the Kondo coupling, J. Like KLM, the H-KLM also exhibits inversion, and hence dHvA oscillations

with the same frequency. Upon increasing U, these oscillations get suppressed. Here, too, the appearance of quantum oscillations is intimately connected with the inversion.

1.3.2 Studies on symmetric periodic Anderson model

In Chapter 4, we investigate SPAM (symmetric periodic Anderson model) as a model of Kondo insulators, which is more microscopic than KLM. We study SPAM on square and simple cubic lattices using the theory of Kondo insulators that we developed for KLM. It works fine, and produces consistent results. For instance, here too, we get inversion and dHvA oscillations. We also study quantum phase transition from Kondo singlet to Néel phase in the U_f-V plane [for $t = 1$; see Eq. (1.8) for notations]. Here, U_f helps the Néel order, because upon increasing U_f, the effective Kondo exchange ($\sim V^2/U_f$) weakens. The hybridization, V, supports the Kondo singlet.

Interestingly, by decreasing V for a fixed U_f, here we get two inversion transitions, one each for the two kinds of quasiparticle dispersions (one narrow and one broad). In the presence of magnetic field, we get dHvA oscillations, only when the quasiparticle bands have appropriately inverted. The oscillation frequency measures the same extremal area, as for KLM, on the effective chemical-potential surface of the charge quasiparticles. Thus, our theory of Kondo insulators produces consistent results for KLM and SPAM.

1.3.3 Quantum oscillations in spin-density wave insulators

Guided by the insight we had in Chapter 2 on weak-coupling insulators, in Chapter 5, we investigate dHvA oscillations in the Néel SDW state of the half-filled Hubbard model. Here, we do standard spin-density wave mean-field theory directly in terms of the electron operators on square and simple cubic lattices, and obtain the anticipated quantum oscillations. We also do a similar calculation for the half-filled KLM. These simple calculations suggest that the dHvA oscillations can possibly occur in many different kinds of insulators (correlated or otherwise).

● ● ● ● ●

Chapter2

The Half-Filled Kondo Lattice

Typically realized in rare-earth compounds, the Kondo insulators are dense arrays of local moments interacting with the conduction electrons at half-filling [3, 2, 48]. They exhibit insulating behaviour at low temperatures due to singlet formation between the local moments and the conduction electrons. Recent observations of de Haas-van Alphen oscillations in SmB_6 has greatly renewed the interest in Kondo insulators [11, 12]. Very recently, the dHvA effect has also been reported to occur in another Kondo insulator, YbB_{12} [41].

The de Haas-van Alphen (dHvA) effect refers to the quantum oscillations of magnetization as a function of the (inverse) magnetic field. It is considered a hallmark of the metallic response, and a direct probe of the Fermi surface (FS) [5, 28, 27]. The dHvA oscillations are a manifestation of the Landau quantization of electronic states in uniform magnetic field. An insulator is not expected to show dHvA oscillations. But the case of SmB_6 presents a counterexample to this conventional view, and poses a question of principle on the occurrence of dHvA oscillations in the insulators. This question has been given some attention recently, with some studies getting the hitherto unexpected dHvA oscillations in mostly the band-theoretic models of insulators [35, 36, 37, 32, 49, 38]. But the situation in a Kondo insulator (KI) is more precarious, where the electrons are correlated and localized, and one is not quite sure which quasiparticles, if any, exhibit dHvA oscillations, and what surface, Fermi or otherwise, is being measured. It is a hotly debated current problem.

Topologically protected conducting surface states in a topological Kondo insulator with an insulating bulk could in principle give quantum oscillations [50, 49]. But certain high frequency quantum oscillations in SmB_6 imply the FS to correspond to the half of its bulk Brillouin zone (BZ) [12]. This can not be accounted for by the surface states, and calls for an understanding of the dHvA oscillations within the bulk insulating behaviour of the KI's. Another scenario treats the Kondo insulating state on bipartite lattice (SmB_6 has a simple cubic structure) at half-filling as a scalar Majorana Fermi sea spread over half of the bulk BZ [32]. While it may look agreeable on the size of the observed FS, it has gapless quasiparticles, and this gapless Majorana sea can not describe an insulator [1]. A recent experiment also rules this out [51].

Motivated by the curious case of SmB_6, in this chapter, we do a theory of the basic Kondo lattice model using a canonical representation of electrons [43] that appropriately describes the Kondo insulating ground state, and gives the magnetic quantum oscillations corresponding to half Brillouin zone as a general bulk property for the Kondo coupling ranging from intermediate to weak.

---

[1] The Fermi sea of non-interacting electrons on bipartite lattice, which is a conducting state, consists of four such independent gapless Majorana Fermi seas.

2.1 Kondo Lattice Model

To understand the dHvA oscillations in Kondo insulators, we study the orbital response to uniform magnetic field in the ground state of the Kondo lattice model (KLM) of localized spin-1/2 moments coupled via antiferromagnetic exchange, $J > 0$, to the conduction electrons at half-filling with nearest-neighbour hopping, $t > 0$, on square and simple cubic lattices. The Hamiltonian, $\hat{H}$, of this problem reads as follows:

$$\hat{H} = -t \sum_{\mathbf{r},\boldsymbol{\delta}} \sum_s e^{i\frac{e}{\hbar} \int_{\mathbf{r}}^{\mathbf{r}+\boldsymbol{\delta}} \mathbf{A} \cdot d\mathbf{r}} \, \hat{c}_{\mathbf{r},s}^\dagger \hat{c}_{\mathbf{r}+\boldsymbol{\delta},s} + \frac{J}{2} \sum_{\mathbf{r}} \mathbf{S}_{\mathbf{r}} \cdot \boldsymbol{\tau}_{\mathbf{r}} \qquad (2.1)$$

Here, $\mathbf{r}$ runs over the lattice sites, $\boldsymbol{\delta}$ is summed over the nearest neighbours of $\mathbf{r}$, and $s = \uparrow, \downarrow$ is the spin label. The $\hat{c}_{\mathbf{r},s}$ ($\hat{c}_{\mathbf{r},s}^\dagger$), are the annihilation (creation) operators of the conduction electrons, whose spin operators are denoted as $\mathbf{S}_{\mathbf{r}}$. The Pauli operators, $\boldsymbol{\tau}_{\mathbf{r}} = (\tau_{\mathbf{r}}^x, \tau_{\mathbf{r}}^y, \tau_{\mathbf{r}}^z)$, denote the local moments. The uniform external magnetic field, $B\hat{z}$, is coupled here to the electronic motion via Peierls phase in terms of the vector potential, $\mathbf{A} = -By\hat{x}$.

To control the number of conduction electrons, in general, one would also add to Eq. (2.1) the chemical potential term, $-\mu \sum_{\mathbf{r},s} \hat{c}_{\mathbf{r},s}^\dagger \hat{c}_{\mathbf{r},s}$. But our immediate interest is in the Kondo insulating state which is realized at half-filling, and on bipartite lattices, the half-filling of conduction electrons is exactly realized for $\mu = 0$. Therefore, we do not include this term in Hamiltonian, $\hat{H}$, of Eq. (2.1).

A canonical representation of electrons, invented by Kumar [43], in terms of spinless fermions and Pauli operators has been found to be very fruitful in describing the strongly correlated electron problems [52, 53]. Recently, this representation has also been used by others to study quantum quenching [54] and finite-temperature dynamics [55] in one-dimensional Hubbard model. Similar representations have also been constructed independently by a few others, but the two that bear closer resemblance with the Kumar's representation are given in Refs. [56, 57]. However, the way in which it was constructed and put into creative use by Kumar is particularly elegant and novel. Hence, we employ the Kumar's representation to investigate the KLM at half-filling. Interestingly, it reveals for us some beautiful physics of Kondo insulators. Before going into the details of our
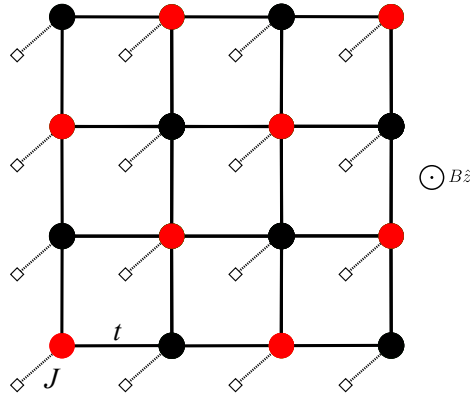
Figure 2.1: A pictorial depiction of the Kondo lattice model on square lattice (with red filled-circles representing $\mathcal{A}$-sublattice, and black ones, the $\mathcal{B}$-sublattice). The conduction electrons hop between the nearest-neighbour sites, and are coupled to the localized moments (empty squares) at each site via an exchange interaction (dotted links).

(a) Bipartite Simple Cubic

(b) Brillouin Zone

$$\vec{a_1} = a(\hat{x} + \hat{y})$$
$$\vec{a_2} = a(\hat{x} + \hat{z})$$
$$\vec{a_3} = a(\hat{y} + \hat{z})$$

$$\vec{b_1} = \frac{\pi}{a}(\hat{x} + \hat{y} - \hat{z})$$
$$\vec{b_2} = \frac{\pi}{a}(\hat{x} - \hat{y} + \hat{z})$$
$$\vec{b_3} = \frac{\pi}{a}(-\hat{x} + \hat{y} + \hat{z})$$
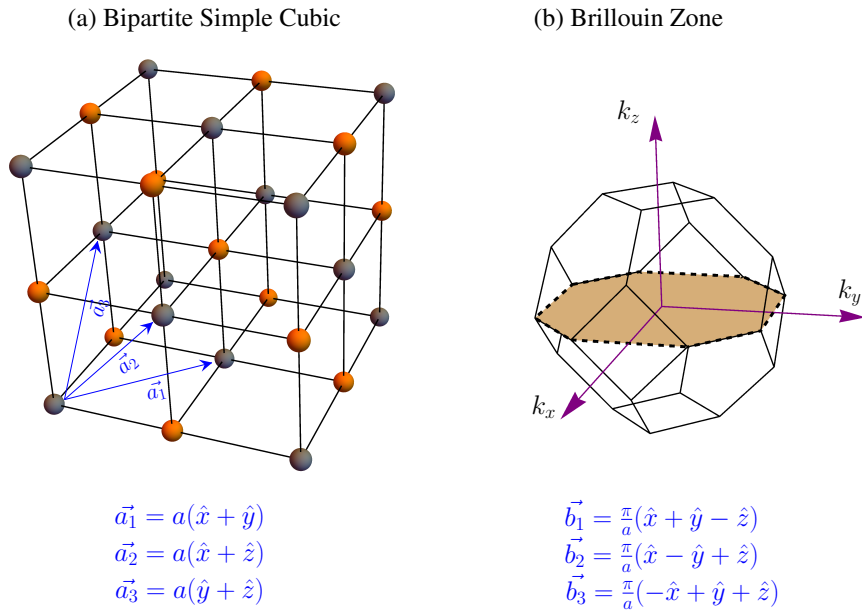
Figure 2.2: (a) The bipartite simple cubic lattice with primitive vectors, $\vec{a}_1$, $\vec{a}_2$, and $\vec{a}_3$. Here, a is the nearest-neighbour distance. (b) The corresponding Brillouin zone (which is the half-Brillouin zone of the simple cubic lattice), and reciprocal lattice vectors, $\vec{b}_1$, $\vec{b}_2$, and $\vec{b}_3$. The orange-coloured octagonal region is the $k_z = 0$ plane inside the Brillouin zone.

calculations and findings, let us briefly describe this representation.

2.2 Kumar's Representation of Electrons

According to Ref. [43], we can write the conduction electron operators, $\hat{c}^{\dagger}_{\mathbf{r}\uparrow}$ and $\hat{c}^{\dagger}_{\mathbf{r}\downarrow}$, at site $\mathbf{r}$, in terms of the spinless fermion and Pauli operators as follows:

$$\hat{c}^{\dagger}_{\mathbf{r}\uparrow} = \hat{\phi}_{a,\mathbf{r}}\sigma^{+}_{\mathbf{r}} \tag{2.2a}$$

$$\hat{c}^{\dagger}_{\mathbf{r}\downarrow} = \frac{1}{2}(i\hat{\psi}_{a,\mathbf{r}} - \hat{\phi}_{a,\mathbf{r}}\sigma^{z}_{\mathbf{r}}) \tag{2.2b}$$

where $\sigma^{z}_{\mathbf{r}}$ and $\sigma^{\pm}_{\mathbf{r}}$ are the Pauli operators, and $\hat{\phi}_{a,\mathbf{r}} = \hat{a}^{\dagger}_{\mathbf{r}} + \hat{a}_{\mathbf{r}}$ and $i\hat{\psi}_{a,\mathbf{r}} = \hat{a}^{\dagger}_{\mathbf{r}} - \hat{a}_{\mathbf{r}}$ are the Majorana fermion operators. These Majorana operators, given in terms of the spinless fermion creation (annihilation) operators, $\hat{a}^{\dagger}_{\mathbf{r}}$ ($\hat{a}_{\mathbf{r}}$), are Hermitian. They mutually anticommute, $\{\hat{\phi}_{a,\mathbf{r}}, \hat{\psi}_{a,\mathbf{r}}\} = 0$, and $\hat{\phi}^{2}_{a,\mathbf{r}} = \hat{\psi}^{2}_{a,\mathbf{r}} = 1$.

This representation is based on a one-to-one mapping between the local Hilbert space of the physical electron and that of the spinless fermion and Pauli operators combined. The mapping given by the following table leads to the representation given in Eqs. (2.2).

$$\begin{array}{c|cc} \otimes & |-\rangle & |+\rangle \\ \hline |o\rangle & |0\rangle & |\uparrow\downarrow\rangle \\ |1\rangle & |\downarrow\rangle & |\uparrow\rangle \end{array} \tag{2.3}$$

Here, $\{|o\rangle, |1\rangle = \hat{a}^{\dagger}_{\mathbf{r}}|o\rangle\}$ and $\{|-\rangle, |+\rangle\}$ are the basis states of spinless fermion and Pauli operators, respectively, at site $\mathbf{r}$. The local Hilbert space of the physical electrons is spanned by the states, $\{|0\rangle, |\downarrow\rangle = \hat{c}^{\dagger}_{\mathbf{r}\downarrow}|0\rangle, |\uparrow\rangle = \hat{c}^{\dagger}_{\mathbf{r}\uparrow}|0\rangle, |\uparrow\downarrow\rangle = \hat{c}^{\dagger}_{\mathbf{r}\uparrow}\hat{c}^{\dagger}_{\mathbf{r}\downarrow}|0\rangle\}$. This table is to be read as: $|0\rangle = |o\rangle \otimes |-\rangle$, $|\downarrow\rangle = |1\rangle \otimes |-\rangle$, and so on. The representation is canonical as it satisfies the necessary anticommutation algebra for the electron operators. It is also invertible, as the mapping is one-to-one. In the inverse picture, the spinless fermion physically describes a Gutzwiller type correlated electron [43].

On bipartite lattices, we can use two slightly different forms of this representation on the two sublattices, which gives an elegant form to the hopping. Say, on $\mathcal{A}$ sublattice, we use Eq. (2.2), but on $\mathcal{B}$ sublattice, we use the form as given below [43],

$$\hat{c}^{\dagger}_{\mathbf{r}\uparrow} = i\hat{\psi}_{b,\mathbf{r}}\sigma^{+}_{\mathbf{r}} \tag{2.4a}$$

$$\hat{c}_{\mathbf{r}\downarrow}^{\dagger} \;\; = \;\; \frac{1}{2}(\hat{\phi}_{b,\mathbf{r}} - i\hat{\psi}_{b,\mathbf{r}}\sigma_{\mathbf{r}}^{z}) \tag{2.4b}$$

Here, $\hat{b}_{\mathbf{r}}$ is the spinless fermion operator on $\mathcal{B}$ sublattice.

In this representation, the electronic spin operator is written as: $\mathbf{S}_{\mathbf{r}} = \frac{1}{2}\hat{n}_{a,\mathbf{r}}\boldsymbol{\sigma}_{\mathbf{r}}$ on $\mathcal{A}$ sublattice and $\mathbf{S}_{\mathbf{r}} = \frac{1}{2}\hat{n}_{b,\mathbf{r}}\boldsymbol{\sigma}_{\mathbf{r}}$ on $\mathcal{B}$ sublattice, where $\hat{n}_{a,\mathbf{r}} = \hat{a}_{\mathbf{r}}^{\dagger}\hat{a}_{\mathbf{r}}$ and $\hat{n}_{b,\mathbf{r}} = \hat{b}_{\mathbf{r}}^{\dagger}\hat{b}_{\mathbf{r}}$. Moreover, the number operator for total number of $\uparrow$ and $\downarrow$ electrons on a site $\mathbf{r} \in \mathcal{A}(\mathcal{B})$ is: $1 + \sigma_{\mathbf{r}}^{z}(1 - \hat{n}_{a(b),\mathbf{r}})$.

2.3 Properties in the Absence of Magnetic Field

To set up our scheme of calculation, we first discuss the KLM without magnetic field. It is given by the following Hamiltonian, which is Eq. (2.1) for $B = 0$,

$$\hat{H} = -t\sum_{\mathbf{r},\boldsymbol{\delta}}\sum_{s}\hat{c}_{\mathbf{r},s}^{\dagger}\hat{c}_{\mathbf{r}+\boldsymbol{\delta},s} + \frac{J}{2}\sum_{\mathbf{r}}\mathbf{S}_{\mathbf{r}}\cdot\boldsymbol{\tau}_{\mathbf{r}} \tag{2.5}$$

In the representation given by Eqs. (2.2) and (2.4), the KLM reads as:

$$\begin{aligned}
\hat{H} \;\; = \;\; & -\frac{it}{2}\sum_{\mathbf{r}\in\mathcal{A}}\sum_{\boldsymbol{\delta}}\left[\hat{\psi}_{a,\mathbf{r}}\hat{\phi}_{b,\mathbf{r}+\boldsymbol{\delta}} + \hat{\psi}_{b,\mathbf{r}+\boldsymbol{\delta}}\hat{\phi}_{a,\mathbf{r}}\left(\boldsymbol{\sigma}_{\mathbf{r}}\cdot\boldsymbol{\sigma}_{\mathbf{r}+\boldsymbol{\delta}}\right)\right] \\
& +\frac{J}{4}\left[\sum_{\mathbf{r}\in\mathcal{A}}\hat{n}_{a,\mathbf{r}}(\boldsymbol{\sigma}_{\mathbf{r}}\cdot\boldsymbol{\tau}_{\mathbf{r}}) + \sum_{\mathbf{r}\in\mathcal{B}}\hat{n}_{b,\mathbf{r}}(\boldsymbol{\sigma}_{\mathbf{r}}\cdot\boldsymbol{\tau}_{\mathbf{r}})\right]
\end{aligned} \tag{2.6}$$

The form of Eq. (2.6) clearly suggests that, if $J \gg t$, then $\boldsymbol{\sigma}_{\mathbf{r}}$ and $\boldsymbol{\tau}_{\mathbf{r}}$ would locally form a singlet, $|s\rangle = (|+\rangle| \Downarrow\rangle - |-\rangle| \Uparrow\rangle)/\sqrt{2}$, on each lattice site. Here, the thick arrows refer to the states of the local spin-1/2 moment. The 'spin' part of the ground state in this limit is the direct product, $\prod_{\mathbf{r}}\otimes|s\rangle_{\mathbf{r}}$, of the local Kondo singlets, while the residual charge dynamics is given by the following Hamiltonian of the spinless fermions:

$$\hat{H}_{0} = -\frac{it}{2}\sum_{\mathbf{r}\in\mathcal{A}}\sum_{\boldsymbol{\delta}}\hat{\psi}_{a,\mathbf{r}}\hat{\phi}_{b,\mathbf{r}+\boldsymbol{\delta}} - \frac{3J}{4}\left[\sum_{\mathbf{r}\in\mathcal{A}}\hat{n}_{a,\mathbf{r}} + \sum_{\mathbf{r}\in\mathcal{B}}\hat{n}_{b,\mathbf{r}}\right] \tag{2.7}$$

It has a charge gap, $\Delta_{c} = \sqrt{(3J/4)^{2} + (\mathsf{z}t/2)^{2}} - \mathsf{z}t/2$ [2]. Here, z is the nearest neighbour coordination. This singlet state also has a spin gap, $\Delta_{s} = J$, and keeps

---

[2]The term corresponding to t in $\hat{H}_{0}$ is the so-called scalar Majorana Fermi sea of Ref. [32]. But here it occurs with an additional term due to J that opens the charge gap.

the local occupancy at one electron per site. We will see that, for $B \neq 0$, this idealized model of strong-coupling KI will not show quantum oscillations. Hence, we improve it by correcting the local singlets for the exchange interaction caused by hopping, and also correcting in return the charge dynamics self-consistently.

To this end, we decouple the Pauli operators from the spinless fermions in Eq. (2.6), and write an approximate version of the KLM: $\hat{H} \approx \hat{H}_c + \hat{H}_s + e_1 L$, where

$$\hat{H}_c = -\frac{it}{2} \sum_{\mathbf{r} \in \mathcal{A}} \sum_{\boldsymbol{\delta}} \left[\hat{\psi}_{a,\mathbf{r}} \hat{\phi}_{b,\mathbf{r}+\boldsymbol{\delta}} + \rho_1 \hat{\psi}_{b,\mathbf{r}+\boldsymbol{\delta}} \hat{\phi}_{a,\mathbf{r}} \right] + \frac{J\rho_0}{4} \left[\sum_{\mathbf{r} \in \mathcal{A}} \hat{n}_{a,\mathbf{r}} + \sum_{\mathbf{r} \in \mathcal{B}} \hat{n}_{b,\mathbf{r}} \right] \quad (2.8a)$$

$$\hat{H}_s = \frac{t\zeta}{4} \sum_{\mathbf{r},\boldsymbol{\delta}} \boldsymbol{\sigma}_\mathbf{r} \cdot \boldsymbol{\sigma}_{\mathbf{r}+\boldsymbol{\delta}} + \frac{J\bar{n}}{4} \sum_\mathbf{r} \boldsymbol{\sigma}_\mathbf{r} \cdot \boldsymbol{\tau}_\mathbf{r}, \quad (2.8b)$$

and $e_1 = -(\mathsf{z}t\zeta\rho_1 + J\bar{n}\rho_0)/4$. Here, L is the total number of lattice sites, and the mean-field parameters are defined as follows:

$$\rho_0 = \frac{1}{L} \sum_\mathbf{r} \langle \boldsymbol{\sigma}_\mathbf{r} \cdot \boldsymbol{\tau}_\mathbf{r} \rangle \quad (2.9a)$$

$$\rho_1 = \frac{1}{\mathsf{z}L} \sum_{\mathbf{r},\boldsymbol{\delta}} \langle \boldsymbol{\sigma}_\mathbf{r} \cdot \boldsymbol{\sigma}_{\mathbf{r}+\boldsymbol{\delta}} \rangle \quad (2.9b)$$

$$\bar{n} = \frac{1}{L} \langle \sum_{\mathbf{r} \in \mathcal{A}} \hat{n}_{a,\mathbf{r}} + \sum_{\mathbf{r} \in \mathcal{B}} \hat{n}_{b,\mathbf{r}} \rangle \quad (2.9c)$$

$$\zeta = \frac{2i}{\mathsf{z}L} \sum_{\mathbf{r} \in \mathcal{A}} \sum_{\boldsymbol{\delta}} \langle \hat{\phi}_{a,\mathbf{r}} \hat{\psi}_{b,\mathbf{r}+\boldsymbol{\delta}} \rangle \quad (2.9d)$$

Here, $\bar{n}$ is the density of spinless fermions. These mean-field parameters, ρ_0, ρ_1, ζ and $\bar{n}$, are determined self-consistently by solving $\hat{H}_c$ and $\hat{H}_s$ [3].

2.3.1 Effective charge dynamics

The charge part of the self-consistent dynamics is given by the effective Hamiltonian $\hat{H}_c$ of Eq. (2.8a). We rewrite the Majorana operator terms as

$$i\hat{\psi}_{a,\mathbf{r}} \hat{\phi}_{b,\mathbf{r}+\boldsymbol{\delta}} = (\hat{a}_\mathbf{r}^\dagger \hat{b}_{\mathbf{r}+\boldsymbol{\delta}} + h.c.) + (\hat{a}_\mathbf{r}^\dagger \hat{b}_{\mathbf{r}+\boldsymbol{\delta}}^\dagger + h.c.)$$

$$i\hat{\phi}_{a,\mathbf{r}} \hat{\psi}_{b,\mathbf{r}+\boldsymbol{\delta}} = -(\hat{a}_\mathbf{r}^\dagger \hat{b}_{\mathbf{r}+\boldsymbol{\delta}} + h.c.) + (\hat{a}_\mathbf{r}^\dagger \hat{b}_{\mathbf{r}+\boldsymbol{\delta}}^\dagger + h.c.)$$

---

[3]The $\hat{H}_s$ resembles the Kondo necklace model [58]. Here, it describes the magnetic properties of the Kondo insulator.

which leads to the following bilinear form of $\hat{H}_c$ in terms of the spinless fermions:

$$
\begin{aligned}
\hat{H}_c &= -\frac{t}{2} \sum_{\mathbf{r} \in \mathcal{A}} \sum_{\boldsymbol{\delta}} \left[(1 + \rho_1)(\hat{a}_r^\dagger \hat{b}_{\mathbf{r}+\boldsymbol{\delta}} + h.c.) + (1 - \rho_1)(\hat{a}_r^\dagger \hat{b}_{\mathbf{r}+\boldsymbol{\delta}}^\dagger + h.c.) \right] \\
&\quad + \frac{J\rho_0}{4} \left[\sum_{\mathbf{r} \in \mathcal{A}} \hat{n}_{a,\mathbf{r}} + \sum_{\mathbf{r} \in \mathcal{B}} \hat{n}_{b,\mathbf{r}} \right]
\end{aligned}
\tag{2.10}
$$

We diagonalize $\hat{H}_c$ by successively applying Fourier and Bogoliubov transformations. The Fourier transformation of $\hat{a}_{\mathbf{r}}$ and $\hat{b}_{\mathbf{r}}$ is given by the relations

$$
\hat{a}_{\mathbf{r}} = \sqrt{\frac{2}{L}} \sum_{\mathbf{k}} e^{i\mathbf{k} \cdot \mathbf{r}} \, \hat{a}_{\mathbf{k}} \quad \text{and} \quad \hat{b}_{\mathbf{r}} = \sqrt{\frac{2}{L}} \sum_{\mathbf{k}} e^{i\mathbf{k} \cdot \mathbf{r}} \, \hat{b}_{\mathbf{k}},
$$

where the wave-vector $\mathbf{k}$ is summed over the half-Brillouin zone, because $\hat{a}_{\mathbf{r}}$ and $\hat{b}_{\mathbf{r}}$ live on separate sublattices. The operators $\hat{a}_{\mathbf{k}}$ and $\hat{b}_{\mathbf{k}}$ are two canonical spinless fermions in the reciprocal space. Applying this transformation to $\hat{H}_c$ leads to the following form:

$$
\begin{aligned}
\hat{H}_c &= -\frac{t}{2} \sum_{\mathbf{k}} \left[(1 + \rho_1)(\gamma_{\mathbf{k}} \hat{a}_{\mathbf{k}}^\dagger \hat{b}_{\mathbf{k}} + h.c.) + (1 - \rho_1)(\hat{a}_{\mathbf{k}}^\dagger \hat{b}_{-\mathbf{k}}^\dagger + h.c.) \right] \\
&\quad + \frac{J\rho_0}{4} \sum_{\mathbf{k}} (\hat{n}_{a,\mathbf{k}} + \hat{n}_{b,\mathbf{k}}),
\end{aligned}
\tag{2.11}
$$

where $\gamma_{\mathbf{k}} = \sum_{\boldsymbol{\delta}} e^{i\mathbf{k} \cdot \boldsymbol{\delta}}$. Under the Bogoliubov transformation given by [4]

$$
\begin{aligned}
\hat{a}_{\mathbf{k}} &= \frac{1}{\sqrt{2}} \left[\cos\theta_{\mathbf{k}} \, \hat{\eta}_+(\mathbf{k}) - \sin\theta_{\mathbf{k}} \, \hat{\eta}_+^\dagger(-\mathbf{k}) - \cos\theta_{\mathbf{k}} \, \hat{\eta}_-(\mathbf{k}) - \sin\theta_{\mathbf{k}} \, \hat{\eta}_-^\dagger(-\mathbf{k}) \right] \\
\hat{b}_{\mathbf{k}} &= \frac{1}{\sqrt{2}} \left[\cos\theta_{\mathbf{k}} \, \hat{\eta}_+(\mathbf{k}) + \sin\theta_{\mathbf{k}} \, \hat{\eta}_+^\dagger(-\mathbf{k}) + \cos\theta_{\mathbf{k}} \, \hat{\eta}_-(\mathbf{k}) - \sin\theta_{\mathbf{k}} \, \hat{\eta}_-^\dagger(-\mathbf{k}) \right]
\end{aligned}
$$

for

$$
\tan 2\theta_{\mathbf{k}} = \left[\frac{-t(1 - \rho_1)|\gamma_{\mathbf{k}}|/2}{E_{\mathbf{k}}} \right]
$$

the $\hat{H}_c$ of Eq. (2.11) becomes diagonal in terms of the new fermion operators, $\hat{\eta}_\pm(\mathbf{k})$.

In the diagonal form, the $\hat{H}_c$ reads as

$$
\hat{H}_c = J\rho_0 L/8 + \sum_{\mathbf{k}} \sum_{\nu=\pm} E_{\mathbf{k}\nu} \left[\hat{\eta}_\nu^\dagger(\mathbf{k}) \hat{\eta}_\nu(\mathbf{k}) - \frac{1}{2} \right]
\tag{2.12}
$$

---

[4]The γ_k is a real function of $\mathbf{k}$ on square and simple cubic lattices. But on other bipartite lattices, it could be complex. For instance, on honeycomb lattice, it is complex. For such cases, we can write $\gamma_{\mathbf{k}} = |\gamma_{\mathbf{k}}| \, e^{i\chi_{\mathbf{k}}}$, and do a gauge transformation, $\hat{a}_{\mathbf{k}} \to \hat{a}_{\mathbf{k}} e^{i\chi_{\mathbf{k}}}$, before doing the Bogoliubov rotation.

where $\mathbf{k} \in$ the half-BZ, and

$$E_{\mathbf{k}\pm} = E_{\mathbf{k}} \pm \frac{1}{2}t(1 + \rho_1)|\gamma_{\mathbf{k}}| > 0 \qquad (2.13)$$

with $E_{\mathbf{k}} = \sqrt{(J\rho_0/4)^2 + [t(1 - \rho_1)|\gamma_{\mathbf{k}}|/2]^2}$ are the charge quasiparticle dispersions. The ground state of $\hat{H}_c$ is given by the vacuum of the $\hat{\eta}_\pm(\mathbf{k})$ quasiparticles, and the ground state energy per site is given by the following equation:

$$e_{g,c} = \frac{J\rho_0}{8} - \frac{1}{2L}\sum_{\mathbf{k}}\sum_{\nu=\pm} E_{\mathbf{k}\nu} \qquad (2.14)$$

The self-consistent equations for $\bar{n}$ and ζ, in the ground state of $\hat{H}_c$, are

$$\bar{n} = \frac{1}{2} - \frac{J\rho_0}{4L}\sum_{\mathbf{k}}\frac{1}{E_{\mathbf{k}}} \quad \text{and} \quad \zeta = \frac{t(1 - \rho_1)}{zL}\sum_{\mathbf{k}}\frac{|\gamma_{\mathbf{k}}|^2}{E_{\mathbf{k}}}. \qquad (2.15)$$

2.3.2 Effective spin dynamics

We study the effective spin Hamiltonian, $\hat{H}_s$ of Eq. (2.8b), using the bond-operator representation [59] for $\boldsymbol{\sigma}_{\mathbf{r}}$ and $\boldsymbol{\tau}_{\mathbf{r}}$, according to which

$$\boldsymbol{\sigma}_{\mathbf{r}}^\alpha = (\hat{s}_{\mathbf{r}}^\dagger \hat{t}_{\mathbf{r}\alpha} + h.c.) - i\epsilon_{\alpha\beta\gamma}\hat{t}_{\mathbf{r}\beta}^\dagger \hat{t}_{\mathbf{r}\gamma} \qquad (2.16a)$$

$$\boldsymbol{\tau}_{\mathbf{r}}^\alpha = -(\hat{s}_{\mathbf{r}}^\dagger \hat{t}_{\mathbf{r}\alpha} + h.c.) - i\epsilon_{\alpha\beta\gamma}\hat{t}_{\mathbf{r}\beta}^\dagger \hat{t}_{\mathbf{r}\gamma}. \qquad (2.16b)$$

Here, $\alpha, \beta, \gamma = x, y, z$ denote the three components of Pauli operators, and $\hat{s}_{\mathbf{r}}$ and $\hat{t}_{\mathbf{r}\alpha}$ are the so-called bond-operators corresponding to the local singlet and triplet states at site $\mathbf{r}$. These bond-operators are taken to be bosonic. For every pair of $\boldsymbol{\sigma}_{\mathbf{r}}$ and $\boldsymbol{\tau}_{\mathbf{r}}$, they are defined as follows:

$$|s\rangle = \frac{1}{\sqrt{2}}(|+\rangle|\Downarrow\rangle - |-\rangle|\Uparrow\rangle) := \hat{s}^\dagger|0\rangle \qquad (2.17a)$$

$$|t_x\rangle = \frac{1}{\sqrt{2}}(|-\rangle|\Downarrow\rangle - |+\rangle|\Uparrow\rangle) := \hat{t}_x^\dagger|0\rangle \qquad (2.17b)$$

$$|t_y\rangle = \frac{i}{\sqrt{2}}(|-\rangle|\Downarrow\rangle + |+\rangle|\Uparrow\rangle) := \hat{t}_y^\dagger|0\rangle \qquad (2.17c)$$

$$|t_z\rangle = \frac{1}{\sqrt{2}}(|+\rangle|\Downarrow\rangle + |-\rangle|\Uparrow\rangle) := \hat{t}_z^\dagger|0\rangle \qquad (2.17d)$$

The completeness of the local spin Hilbert space on every site, $\mathbf{r}$, puts the following local constraint on the bond-operators:

$$\hat{s}_{\mathbf{r}}^\dagger \hat{s}_{\mathbf{r}} + \sum_\alpha \hat{t}_{\mathbf{r}\alpha}^\dagger \hat{t}_{\mathbf{r}\alpha} = 1. \qquad (2.18)$$

We make three standard simplifying approximations [59, 60] to discuss the basic physics of $\hat{H}_s$ using bond-operator representation. Firstly, we treat $\hat{s}_{\mathbf{r}}$ as mean singlet amplitude, $\bar{s}$, which is physically relevant for the present model. Secondly, we ignore the terms bilinear in triplet operators in Eqs. (2.16). It amounts to neglecting the interaction between the triplet excitations. With these two approximations, we can write $\sigma_{\mathbf{r}\alpha} \approx \bar{s}(\hat{t}_{\mathbf{r}\alpha}^{\dagger} + \hat{t}_{\mathbf{r}\alpha})$ and $\tau_{\mathbf{r}\alpha} \approx -\bar{s}(\hat{t}_{\mathbf{r}\alpha}^{\dagger} + \hat{t}_{\mathbf{r}\alpha})$. Thirdly, we treat the local constraint given in Eq. (2.18) only on average using Lagrange multiplier, λ. Under these approximations, the effective spin Hamiltonian, $\hat{H}_s$, takes the following form

$$
\begin{aligned}
\hat{H}_s \approx & \frac{t\zeta\bar{s}^2}{4} \sum_{\mathbf{r},\alpha} \sum_{\boldsymbol{\delta}} \left[\left(\hat{t}_{\mathbf{r},\alpha}^{\dagger} + \hat{t}_{\mathbf{r},\alpha} \right) \left(\hat{t}_{\mathbf{r}+\boldsymbol{\delta},\alpha}^{\dagger} + \hat{t}_{\mathbf{r}+\boldsymbol{\delta},\alpha} \right) \right] \\
& + \frac{J\bar{n}}{4} \sum_{\mathbf{r}} \left[-3\bar{s}^2 + \sum_{\alpha} \hat{t}_{\mathbf{r},\alpha}^{\dagger} \hat{t}_{\mathbf{r},\alpha} \right] - \lambda \sum_{\mathbf{r}} \left[\bar{s}^2 + \sum_{\alpha} \hat{t}_{\mathbf{r},\alpha}^{\dagger} \hat{t}_{\mathbf{r},\alpha} - 1 \right] \ (2.19)
\end{aligned}
$$

It presents the minimal dynamics of triplet fluctuations with respect to mean Kondo singlet background. The corresponding Hamiltonian in $\mathbf{k}$-space is obtained by doing the Fourier transformation, $t_{\mathbf{r}\alpha} = \sqrt{\frac{1}{L}} \sum_{\mathbf{k}} e^{i\mathbf{k}\cdot\mathbf{r}} t_{\mathbf{k}\alpha}$, where $\mathbf{k}$ lies in the full Brillouin zone. The resulting mean-field Hamiltonian reads as:

$$
\begin{aligned}
\hat{H}_s = & \frac{1}{2} \sum_{\mathbf{k},\alpha} \left\{ \left[\lambda + \frac{1}{2} t\zeta\bar{s}^2 \gamma_{\mathbf{k}} \right] \left(\hat{t}_{\mathbf{k}\alpha}^{\dagger} \hat{t}_{\mathbf{k}\alpha} + \hat{t}_{-\mathbf{k}\alpha} \hat{t}_{-\mathbf{k}\alpha}^{\dagger} \right) + \frac{1}{2} t\zeta\bar{s}^2 \gamma_{\mathbf{k}} \left(\hat{t}_{\mathbf{k}\alpha}^{\dagger} \hat{t}_{-\mathbf{k}\alpha}^{\dagger} + \hat{t}_{-\mathbf{k}\alpha} \hat{t}_{\mathbf{k}\alpha} \right) \right\} \\
& + L \left[\lambda\bar{s}^2 - \frac{5}{2}\lambda + J\bar{n}(\bar{s}^2 - 1/4) \right]
\end{aligned}
$$
(2.20)

where L is the total number of sites, $\lambda \rightarrow (J\bar{n}/4 - \lambda)$ is the effective chemical potential, and $\gamma_{\mathbf{k}} = \sum_{\boldsymbol{\delta}} e^{i\mathbf{k}\cdot\boldsymbol{\delta}}$. It can be diagonalized by applying the following Bogoliubov transformation

$$
\hat{t}_{\mathbf{k}\alpha} = \tilde{t}_{\mathbf{k}\alpha} \cosh\tilde{\theta}_{\mathbf{k}} + \tilde{t}_{-\mathbf{k}\alpha}^{\dagger} \sinh\tilde{\theta}_{\mathbf{k}} \tag{2.21}
$$

Here, $\tilde{t}_{\mathbf{k}\alpha}$ are the new bosonic operators describing triplon quasiparticles, and

$$
\tanh 2\tilde{\theta}_{\mathbf{k}} = -\frac{\frac{1}{2} t\zeta\bar{s}^2 \gamma_{\mathbf{k}}}{(\lambda + \frac{1}{2} t\zeta\bar{s}^2 \gamma_{\mathbf{k}})} \tag{2.22}
$$

The $\hat{H}_s$ in the diagonal form reads as:

$$
\hat{H}_s \approx L[\lambda\bar{s}^2 - 5\lambda/2 - J\bar{n}(\bar{s}^2 - 1/4)] + \sum_{\mathbf{k}} \sum_{\alpha=x,y,z} \varepsilon_{\mathbf{k}} \left[\tilde{t}_{\mathbf{k}\alpha}^{\dagger} \tilde{t}_{\mathbf{k}\alpha} + \frac{1}{2} \right] \tag{2.23}
$$

where the bosonic operators $\tilde{t}_{\mathbf{k}\alpha}$ defined in Eq. (4.29) describe the triplon excitations with respect to the mean Kondo singlet given by $\bar{s}$, $\varepsilon_{\mathbf{k}} = \sqrt{\lambda(\lambda + t\zeta\bar{s}^2\gamma_{\mathbf{k}})}$ is the triplon dispersion, and $\mathbf{k} \in$ the full BZ. The ground state energy per site of $\hat{H}_s$ is given as:

$$e_{g,s} = \left[\lambda\bar{s}^2 - 5\lambda/2 - J\bar{n}(\bar{s}^2 - 1/4)\right] + \frac{3}{2L}\sum_{\mathbf{k}}\varepsilon_{\mathbf{k}} \tag{2.24}$$

and the corresponding self-consistent parameters [defined in Eq. (2.9)] for the spin part are given as: $\rho_0 = 1 - 4\bar{s}^2$ and $\rho_1 = 4\bar{s}^2(J\bar{n} - \lambda)/zt\zeta$, where

$$\bar{s}^2 = \frac{5}{2} - \frac{3}{4L}\sum_{\mathbf{k}}\frac{2\lambda + t\zeta\bar{s}^2\gamma_{\mathbf{k}}}{\varepsilon_{\mathbf{k}}}, \text{ and} \tag{2.25a}$$

$$\lambda = J\bar{n} - \frac{3\lambda t\zeta}{4L}\sum_{\mathbf{k}}\frac{\gamma_{\mathbf{k}}}{\varepsilon_{\mathbf{k}}}. \tag{2.25b}$$
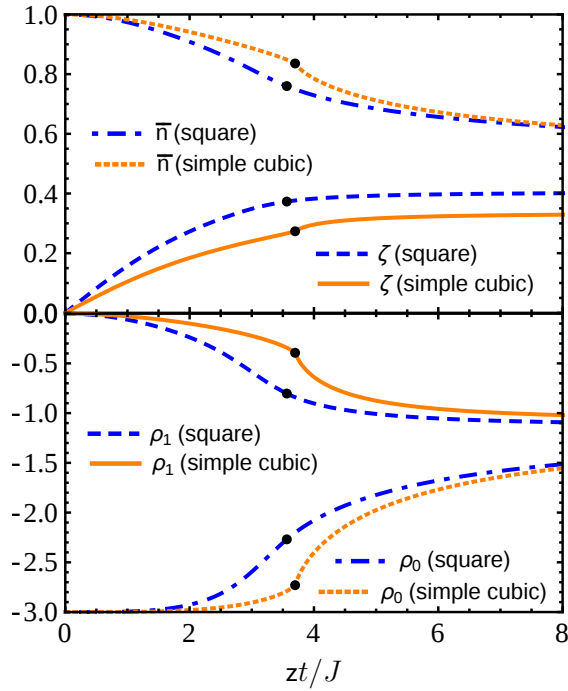

Figure 2.3: Mean-field parameters of the effective charge and spin dynamics as a function of t/J on square and simple cubic lattices. The black dots indicate the critical hopping, t_c, below which the insulating ground state is a Kondo singlet, and above which, it is antiferromagnetically ordered [see Fig. 2.4 for the spin and charge gaps].

2.3.3 Insulating ground state: Kondo singlet vs. Néel order

We compute the parameters, $\bar{n}$, ζ, ρ_0 and ρ_1, by self-consistently solving the Eqs. (2.15) and (2.25) for different value of t/J. In our calculations, we take $J = 1$.

Kondo singlet phase

At $t = 0$, the exact values of these mean-field parameters are: $\rho_0 = -3$, $\rho_1 = 0$, $\bar{n} = 1$, and $\zeta = 0$, which simply means that the local Kondo singlets are perfectly formed. For $t > 0$, we get $-3 < \rho_0 \lesssim \rho_1 < 0$, and $0 < \zeta < 0.5 < \bar{n} < 1$ from the self-consistent calculation, as shown in Fig. 2.3. From our calculations, we correctly find the $\hat{H}_c$ to have a non-zero charge gap, Δ_c, for all values of t, which makes it an insulator. For smaller values of t, the $\hat{H}_s$ also has a gap, Δ_s, to the spin excitations. See Fig. 2.4 for the charge and spin gaps on square lattice. This singlet phase with a non-zero spin gap is called the Kondo singlet (KS) phase.

However, as t increases, Δ_s decreases and eventually vanishes at the critical point, $t = t_c$. Equation (2.29) shows the values of t_c for square and simple cubic lattices. The closing of the spin gap at t_c marks a quantum phase transition from the quantum paramagnetic KS phase to a magnetically ordered phase. The wave-vector $\mathbf{Q}$ at which the gap vanishes, that is $\varepsilon_{\mathbf{Q}} = 0$, determines the nature of magnetic order. In our calculation, we find the KS phase is slightly overestimated as compared to the other methods [61, 62, 63]. See Table 2.1 for a comparison of the values of t_c obtained from different methods.[5]

Antiferromagnetically ordered phase

The gaplessness, $\varepsilon_{\mathbf{Q}} = 0$, fixes the Lagrange multiplier to $\lambda = \mathsf{z}t\zeta\bar{s}^2$. It also makes the $\mathbf{k} = \mathbf{Q}$ terms in Eqs. (2.25) singular, which causes Bose condensation of triplons that leads to magnetic ordering with ordering wave-vector $\mathbf{Q}$ [64]. Corresponding to the singularity at $\mathbf{Q}$, we introduce triplon condensate density, $n_c := \frac{1}{L}\langle \hat{t}^{\dagger}_{\mathbf{Q}\alpha} \hat{t}_{\mathbf{Q}\alpha} \rangle$.

---

[5]VMC$\equiv$ variational monte carlo, BO-MFT$\equiv$ bond operator mean-field theory [C. Jurecka and W. Brenig, Phys. Rev. B. 64.092406 (2001)]

KLM	square lattice(t_c)	simple cubic lattice(t_c)
Our theory	0.89	0.62
QMC[61]	0.69	–
VCA[46]	0.49	–
Series-expansion[62]	0.70	0.50
VMC[63]	0.71	–
BO-MFT[47]	0.67	0.55

Table 2.1: For the Kondo lattice model (KLM), the critical value of hopping, t_c, (for magnetic phase transition from Kondo singlet to Néel antiferromagnetic phase) obtained from different methods are compared from our theory.

Hence, in this gapless ordered phase, the mean-field equations for the spin part read as follows:

$$\lambda = \mathsf{z}t\zeta\bar{s}^2, \tag{2.26a}$$

$$\bar{s}^2 = \frac{5}{2} - n_c - \frac{3}{4L}\sum_{\mathbf{k}\neq\mathbf{Q}}\frac{2\lambda + t\zeta\bar{s}^2\gamma_{\mathbf{k}}}{\varepsilon_{\mathbf{k}}}, \text{ and} \tag{2.26b}$$

$$n_c = \frac{1}{\mathsf{z}t\zeta}\left(\lambda - J\bar{n} + \frac{3\lambda t\zeta}{4L}\sum_{\mathbf{k}\neq\mathbf{Q}}\frac{2\lambda + t\zeta\bar{s}^2\gamma_{\mathbf{k}}}{\varepsilon_{\mathbf{k}}}\right). \tag{2.26c}$$

Together with Eqs. (2.15) for the charge part, the self-consistent solution of Eqs. (2.26), determines the properties of the phase with zero spin gap.

From our calculations, we find the triplon dispersion to become gapless for $t > t_c$ at $\mathbf{Q} = (\pi, \pi)$ on square lattice and $\mathbf{Q} = (\pi, \pi, \pi)$ on simple cubic lattice. See Fig. 2.5 for triplon dispersion. Hence, we get Néel antiferromagnetic order in the insulating ground state of the half-filled KLM for $t > t_c$.

2.3.4 Inversion of the charge quasiparticle dispersion

A special feature of the Kondo insulating state, that we discover here, is the "inversion" of charge quasiparticle dispersion, which has a direct bearing on quantum oscillations (as we will see later). Note that the dispersions $E_{\mathbf{k}+}$ and $E_{\mathbf{k}-}$, of the charge quasiparticles given in Eq. (2.13) always touch each other at $|\gamma_{\mathbf{k}}| = 0$, at a
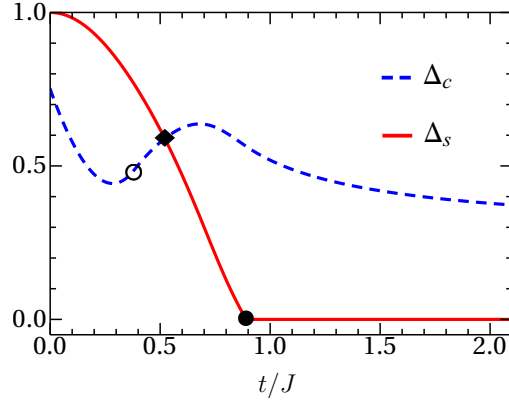
Figure 2.4: The charge (Δ_c) and spin (Δ_s) gaps vs. t/J for square lattice at half-filling of KLM obtained in ground state of Eq. (4.16) and (4.34).
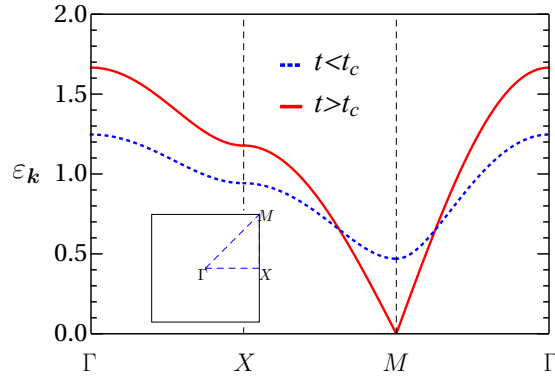
Figure 2.5: Triplon dispersion, $\varepsilon_{\mathbf{k}}$, of $\hat{H}_s$. It is gapped (Kondo singlet) for $t < t_c$ and gapless (Néel antiferromagnetic) for $t > t_c$. See Eq. (2.29) for t_c.

value of $J|\rho_0|/4$, which is the chemical potential of the spinless fermions in $\hat{H}_c$. See Eq. (2.10) for the number operator terms. For small t/J, $E_{\mathbf{k}-(+)}$ is lowest (highest) at $\mathbf{k} = 0$, and highest (lowest) at $|\gamma_{\mathbf{k}}| = 0$. But for t greater than a particular value t_i (we term it as the inversion point), the $\mathbf{k} = 0$ becomes a point of local maxima of $E_{\mathbf{k}-}$, whose lowest value (the charge gap, Δ_c) now lies not at $\mathbf{k} = 0$,[6] but on a contour whose equation is given as:

$$|\gamma_{\mathbf{k}}| = J|\rho_0|(1 - |\rho_1|)/\{4t(1 + |\rho_1|)\sqrt{|\rho_1|}\}. \tag{2.27}$$

See Fig. 2.6 for the evolution of $E_{\mathbf{k}-}$ with t. Thus, for $t > t_i$, $E_{\mathbf{k}-}$ undergoes inversion, while $E_{\mathbf{k}+}$ is always maximum at $\mathbf{k} = 0$ [7]. We further find that, for

---

[6] A shift in the band minimum at a similar value of t as our t_i has also been noted in Ref. [65].

[7] We see no such inversion to occur for the triplon dispersion, $\varepsilon_{\mathbf{k}}$.
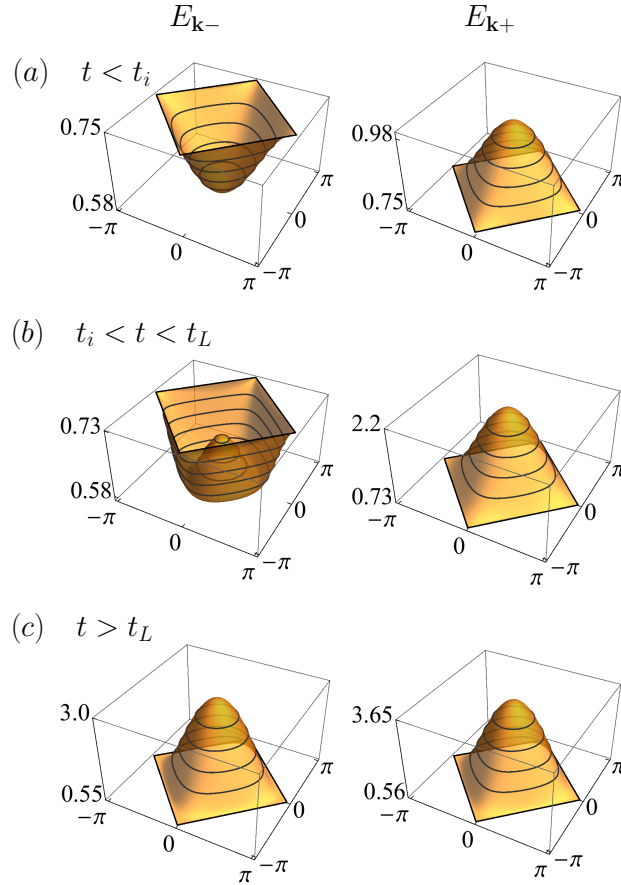
Figure 2.6: Behaviour of charge quasiparticle dispersions, $E_{\mathbf{k}\pm}$, of $\hat{H}_c$ for different t's. The Dispersion, $E_{\mathbf{k}-}$ undergoes *inversion* for $t > t_i$ however $E_{\mathbf{k}+}$ remains uninverted. See Eq. (2.29) for t_i and t_L.

$t > t_L > t_i$, the $\mathbf{k} = 0$ becomes the global maxima of $E_{\mathbf{k}-}$, which leads to a second branch of the *chemical-potential surface* (CPS) given by

$$|\gamma_{\mathbf{k}}| = J|\rho_0|(1 - |\rho_1|)/\{4t|\rho_1|\} \tag{2.28}$$

in addition to $|\gamma_{\mathbf{k}}| = 0$ [see Figs. 2.7 and 2.10(c-d)]. This is akin to Lifshitz transition [66], but in a Kondo insulator! We will see that, for dHvA oscillations, the CPS in KI plays the role of Fermi surface in metals. Sufficiently above t_L, the $E_{\mathbf{k}-}$ nearly fully inverts and looks similar to $E_{\mathbf{k}+}$. This inversion of $E_{\mathbf{k}-}$, shown in Fig. 2.6 for square lattice, is generic to Kondo insulators, at least on bipartite lattices. Having obtained this novel and other expected features of the KI's using
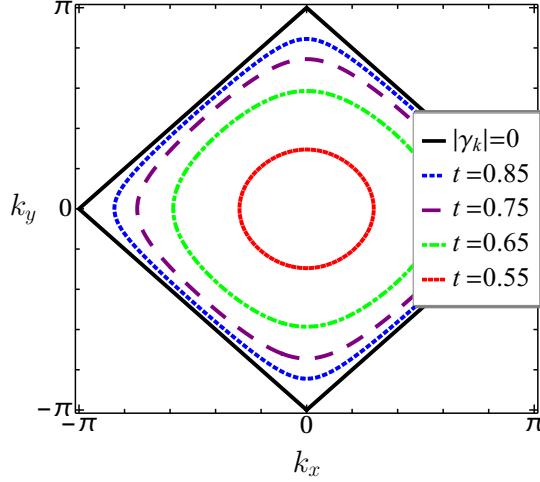
Figure 2.7: The *chemical-potential* surface (CPS), $E_{\mathbf{k}-} = J|\rho_0|/4$, for $t > t_L$, where t_L is the point of *Lifshitz*-like transition, below which $|\gamma_{\mathbf{k}}| = 0$ is the CPS, and above t_L, the CPS has a second t dependent branch that approaches $|\gamma_{\mathbf{k}}| = 0$ with increasing t. We find the dHvA oscillations to measure CPS. See Eq. (2.29) for t_i and t_L.

$\hat{H}_c + \hat{H}_s$, we now study this minimal approximate model in uniform magnetic field.

$$
\begin{array}{c|ccc}
 & t_i & t_L & t_c \\
\hline
\text{square lattice} & 0.38 & 0.52 & 0.89 \\
\hline
\text{simple cubic lattice} & 0.33 & 0.48 & 0.62
\end{array}
\tag{2.29}
$$

2.4 Magnetic Quantum Oscillations

We now rewrite the KLM of Eq. (2.1) for $B \neq 0$, in a manner similar to Eq. (2.6), by keeping only those terms that couple to $\bar{n}$, ζ, ρ_0 and ρ_1. In this way, we derive the following magnetic field dependent minimal models of charge and spin dynamics of a Kondo insulator:

$$
\hat{H}_c^{[B]} = -\frac{it}{2} \sum_{\mathbf{r} \in \mathcal{A}} \sum_{\boldsymbol{\delta}} \cos\left(2\pi\alpha\, \mathbf{r}_y\, \hat{x} \cdot \hat{\boldsymbol{\delta}}\right) \left[\hat{\psi}_{a,\mathbf{r}} \hat{\phi}_{b,\mathbf{r}+\boldsymbol{\delta}} + \rho_1 \hat{\psi}_{b,\mathbf{r}+\boldsymbol{\delta}} \hat{\phi}_{a,\mathbf{r}}\right]
$$
$$
+ \frac{J\rho_0}{4} \left[\sum_{\mathbf{r} \in \mathcal{A}} \hat{n}_{a,\mathbf{r}} + \sum_{\mathbf{r} \in \mathcal{B}} \hat{n}_{b,\mathbf{r}}\right]
\tag{2.30a}
$$
$$
\hat{H}_s^{[B]} = \frac{t\zeta}{4} \sum_{\mathbf{r},\boldsymbol{\delta}} \cos\left(2\pi\alpha\, \mathbf{r}_y\, \hat{x} \cdot \hat{\boldsymbol{\delta}}\right) \boldsymbol{\sigma}_{\mathbf{r}} \cdot \boldsymbol{\sigma}_{\mathbf{r}+\boldsymbol{\delta}} + \frac{J\bar{n}}{4} \sum_{\mathbf{r}} \boldsymbol{\sigma}_{\mathbf{r}} \cdot \boldsymbol{\tau}_{\mathbf{r}}
\tag{2.30b}
$$

These are Hofstadter [67] type models, but for Majorana fermions and hard-core bosons. Here, $\alpha = eBa^2/h$ is the magnetic flux in units of h/e, a is the lattice constant (nearest-neighbour distance), integer $\mathbf{r}_y$ is the y-coordinate of $\mathbf{r}$, and $\hat{\boldsymbol{\delta}} = \boldsymbol{\delta}/|\boldsymbol{\delta}|$. We put zero-field values of ρ_0, ρ_1, $\bar{n}$ and ζ in Eqs. (2.30), and compute magnetization, M, as a function of $\alpha = p/q$ for integer $p = 1, 2, \ldots q$ with q upto 709 on square lattice, and 401 on simple cubic lattice.[8] The numerical diagonalization of $\hat{H}_c^{[B]}$ and the procedure to calculate the corresponding M is described in detail in Appendix A.
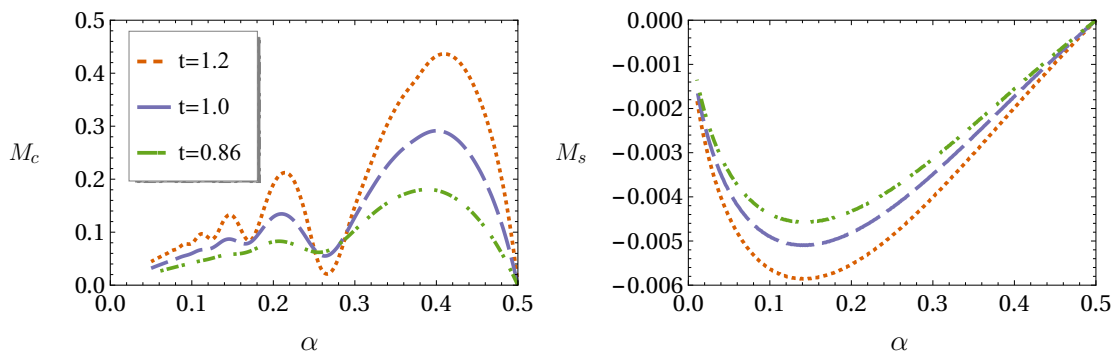
Figure 2.8: The magnetization M_c and M_s as a function of α from $\hat{H}_c$ and $\hat{H}_s$ of Eqs. (2.30) in (a) and (b) for different value of t. We clearly see no oscillations (apart from sinusoidal behaviour) in M_s, and its amplitude is approximately 100 times smaller than M_c.

As the contribution to M from $\hat{H}_s^{[B]}$ happens to be quite (about 100 times) small compared to $\hat{H}_c^{[B]}$, see Fig. 2.8, and we get dHvA oscillations only through charge dynamics, here we discuss the results of our calculations for $\hat{H}_c^{[B]}$ only. While we see no dHvA oscillations for strong Kondo coupling (small t/J), it is very heartening to see clear magnetic quantum oscillations for sufficiently large values of t. Since we know that $E_{\mathbf{k}-}$ undergoes inversion with increasing t, we believe that this inversion has something to do with the appearance of dHvA oscillations in the Kondo insulating ground state. To get a clear insight into this, we resolve the total M into the contributions, M_+ and M_-, coming respectively from $E_{\mathbf{k}+}$ and $E_{\mathbf{k}-}$ bands of quasiparticle states.

---

[8]Unlike the basic Hofstadter model, in our $H_c^{[B]}$ (that has hopping and pairing), the Landau bands are somewhat dispersive with respect to k_x, even for large q. Hence, in our calculations, we have also taken upto 288 k_x-points.
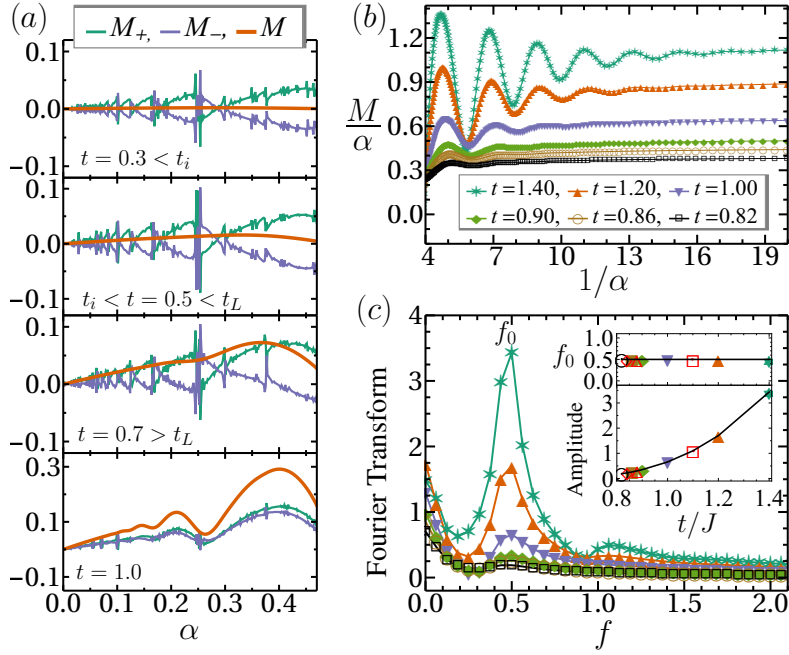
Figure 2.9: The dHvA oscillations from Eq. (2.30a) in the Kondo insulating ground state on square lattice. (a) Magnetization vs. α, where $M_\pm$ are the contributions from the two charge quasiparticle bands, and $M = M_+ + M_-$. (b) M/α vs. $1/\alpha$. (c) Fourier transform of M/α, with an inset showing the dominant frequency of oscillation, f_0, and its amplitude vs. t/J. The $f_0 = 0.5$ is t independent, and it corresponds to the area of the half-BZ enclosed by the $|\gamma_{\mathbf{k}}| = 0$ contour [see Fig. 2.7].

In Fig. 2.9(a), we show the evolution of magnetization behaviour with t on square lattice. For $t < t_i$, we see no oscillations of M with respect to α, except an overall sinusoidal variation of negligible magnitude. This is because the non-trivial oscillatory contribution to M from $E_{\mathbf{k}-}$ states (M_-) cancels that (M_+) from $E_{\mathbf{k}+}$. It is like two opposite cyclotron orbits from two oppositely curved dispersions cancelling each other. This cancellation gets weaker as $E_{\mathbf{k}-}$ starts inverting. But only when t is sufficiently bigger than t_L, with $E_{\mathbf{k}-}$ nearly fully inverted (that is, having the same sense of curvature as $E_{\mathbf{k}+}$), we begin to clearly see the oscillations of M as a function of B in the ground state of $\hat{H}_c^{[B]}$. This analysis neatly reveals the intimate connection between inversion and magnetic quantum oscillations in Kondo insulators.

The amplitude of these oscillations is weak in the Kondo singlet phase for $t \lesssim t_c$, but becomes pronounced when t increases into the Néel phase, as shown in
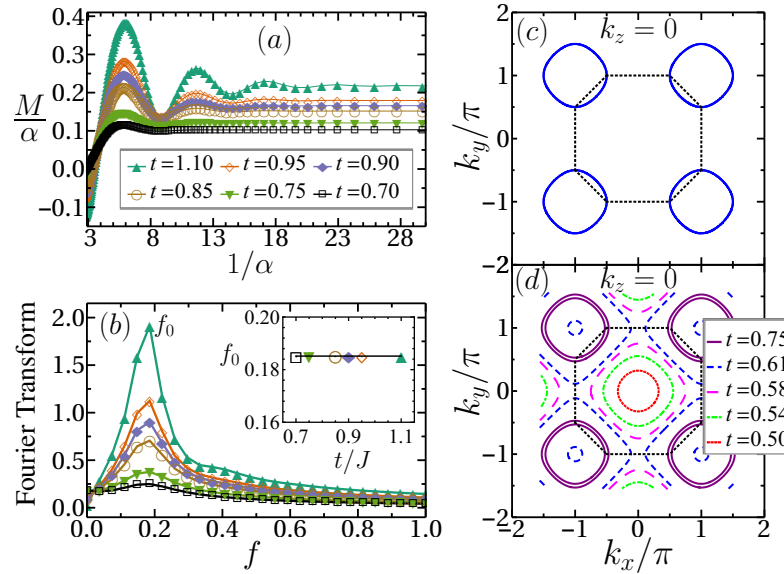
Figure 2.10: (a) M/α vs. $1/\alpha$ in the Kondo insulating ground state on simple cubic lattice. (b) Fourier transform of M/α. The dominant frequency, $f_0 = 0.185$, is same as the area enclosed by the blue orbit in (c). It is a t independent extremal orbit on the $|\gamma_{\mathbf{k}}| = 0$ CPS. (d) The second branch of CPS. It tends to the first one with increasing t. The dotted octagons in (c)-(d) denote the boundary of the half-BZ on $k_z = 0$ plane.

Fig. 2.9(b) by plotting M/α vs. $1/\alpha$ for different t's. Since M/α oscillates with non-zero baseline, therefore to clearly see the non-trivial oscillation frequencies, we subtract the flat background of M/α before performing the Fourier transform. In Appendix C, we have illustrated the procedure to calculate the Fourier transform of any waveform. The Fourier transform of M/α for $4 < 1/\alpha < 20$ is presented in Fig. 2.9(c), where interestingly the dominant Fourier peaks for different t's occur at the same frequency, $f_0 = 0.5$, while their amplitudes grow with t. Empirically, the amplitude of the f_0 peak is found to grow as $(t - t_*)^2$ with $t_* \approx 0.57 \gtrsim t_L$.

The well-known semiclassical relation, $F = (2\pi/a)^2 f$, between the area F of an extremal orbit perpendicular to magnetic field on a constant energy surface in **k**-space and the frequency f (in units of h/ea^2) of dHvA oscillations [27], implies that the $f_0 = 0.5$ corresponds to the area of the half-BZ, which unmistakably points to the $|\gamma_{\mathbf{k}}| = 0$ in Fig. 2.7 as its origin. From this, we infer that these dHvA oscillations measure the CPS of its charge quasiparticles. We think of the CPS as a generalization of the FS to the cases with gapped fermion quasiparticles. In the

gapless Fermi systems, say metals, the CPS would be same as the Fermi surface.

Similarly, we also get magnetic quantum oscillations on simple cubic lattice, as shown in Fig. 2.10(a). Its Fourier transform in Fig. 2.10(b) gives the dominant frequency at $f_0 = 0.185$, which is independent of t/J, and corresponds precisely to the area enclosed by the blue-coloured orbit shown in Fig. 2.10(c). It is an extremal orbit on the $|\gamma_{\mathbf{k}}| = 0$ branch of the CPS on $k_z = 0$ plane. See Fig. 2.2(b) for simple cubic BZ. It is very clear that the dHvA oscillations measure the CPS, in corroboration of what we found on square lattice.

Our study of the half-filled Kondo lattice model unambiguously finds magnetic quantum oscillations corresponding to the half Brillouin zone as a generic bulk phenomenon of Kondo insulators. Moreover, it clearly establishes the role of inversion in realizing these oscillations from moderate to weak Kondo couplings. In experiments, the hopping t can be tuned by applying pressure. Therefore, this finding could in principle be seen in pressure dependent measurements of dHvA oscillations.

We end this section by noting that the effective charge dynamics of the KLM given by $\hat{H}_c$ has an unmistakable likeness to the Hubbard model in Kumar's representation [43], with J acting like the Hubbard interaction, U. It suggests that such quantum oscillations, as we found in the Kondo insulating state, should also occur in the insulating state of the Hubbard model for moderate to weaker strengths of U. We also note that the oscillation amplitude grows in strength as t/J increases. These observations point to a clear possibility of the dHvA oscillations occurring in the weak coupling antiferromagnetic insulators, viz., the spin-density wave (SDW) insulators. In the following section, we make calculations on the half-filled Hubbard model to immediately validate our observation. A study of the dHvA oscillations in SDW insulators is presented separately in Chapter 5 of this thesis.

2.5   Implications for the Half-filled Hubbard Model

The Hubbard model with nearest-neighbour hopping and a chemical potential of $U/2$

$$\hat{H}_H = -t \sum_{\mathbf{r},\boldsymbol{\delta},s} \hat{c}^{\dagger}_{\mathbf{r},s}\hat{c}_{\mathbf{r}+\boldsymbol{\delta},s} + U \sum_{\mathbf{r}} \hat{n}_{\mathbf{r},\uparrow}\hat{n}_{\mathbf{r},\downarrow} - \frac{U}{2}\sum_{\mathbf{r}}(\hat{n}_{\mathbf{r},\uparrow}+\hat{n}_{\mathbf{r},\downarrow}) \tag{2.31}$$

guarantees half-filling on any bipartite lattice. In the canonical representation of Kumar, this half-filled Hubbard model reads as [43]

$$\hat{H}_H = -\frac{it}{2}\sum_{\mathbf{r}\in\mathcal{A}}\sum_{\boldsymbol{\delta}}\left[\hat{\psi}_{a,\mathbf{r}}\hat{\phi}_{b,\mathbf{r}+\boldsymbol{\delta}} + \hat{\psi}_{b,\mathbf{r}+\boldsymbol{\delta}}\hat{\phi}_{a,\mathbf{r}}\left(\boldsymbol{\sigma}_{\mathbf{r}}\cdot\boldsymbol{\sigma}_{\mathbf{r}+\boldsymbol{\delta}}\right)\right] - \frac{U}{2}\left[\sum_{\mathbf{r}\in\mathcal{A}}\hat{n}_{a,\mathbf{r}} + \sum_{\mathbf{r}\in\mathcal{B}}\hat{n}_{b,\mathbf{r}}\right]. \tag{2.32}$$

Under the same decoupling scheme as employed for the KLM, the Hubbard model takes an approximate form: $\hat{H}_H \approx e_0 L + \hat{H}_{H,c} + \hat{H}_{H,s}$, with

$$\hat{H}_{H,c} = -\frac{it}{2}\sum_{\mathbf{r}\in\mathcal{A}}\sum_{\boldsymbol{\delta}}\left[\hat{\psi}_{a,\mathbf{r}}\hat{\phi}_{b,\mathbf{r}+\boldsymbol{\delta}} + \rho_1\hat{\psi}_{b,\mathbf{r}+\boldsymbol{\delta}}\hat{\phi}_{a,\mathbf{r}}\right] - \frac{U}{2}\left[\sum_{\mathbf{r}\in\mathcal{A}}\hat{n}_{a,\mathbf{r}} + \sum_{\mathbf{r}\in\mathcal{B}}\hat{n}_{b,\mathbf{r}}\right] \tag{2.33a}$$

$$\hat{H}_{H,s} = \frac{t\zeta}{4}\sum_{\mathbf{r},\boldsymbol{\delta}}\boldsymbol{\sigma}_{\mathbf{r}}\cdot\boldsymbol{\sigma}_{\mathbf{r}+\boldsymbol{\delta}} \tag{2.33b}$$

where $e_1 = -(\mathsf{z}t\zeta\rho_1)/4$, and the decoupling parameters ρ_1 and ζ are defined in the same way as in Eqs. (2.9b) and (2.9d). Here, the effective spin part, $\hat{H}_{H,s}$, is simply the Heisenberg model, which correctly gives the Néel antiferromagnetic ground state for the half-filled Hubbard model on bipartite lattice. Comparing $\hat{H}_{H,c}$ of Eq. (2.33a) with $\hat{H}_c$ of Eq. (2.8a) clearly suggests that the effective charge dynamics of the half-filled Hubbard and Kondo lattice models are essentially the same, with J and U playing similar roles. That is, their insulating behaviour is governed by the same mechanism.[9]

   This explicit likeness between these two models prompts us to revisit the Hubbard model to see if inversion and magnetic quantum oscillations also arise there. Below we will show that this is indeed the case.

---

[9]Here, we have focused on the ground state properties only. But it would be interesting to also investigate the paramagnetic phase (metal-insulator transition) of Hubbard model at finite temperatures by doing the same self-consistent calculations.

$E_{\mathbf{k}+}$ $E_{\mathbf{k}-}$

(a) $t < t_i$

(b) $t_i < t < t_L$

(c) $t > t_L$
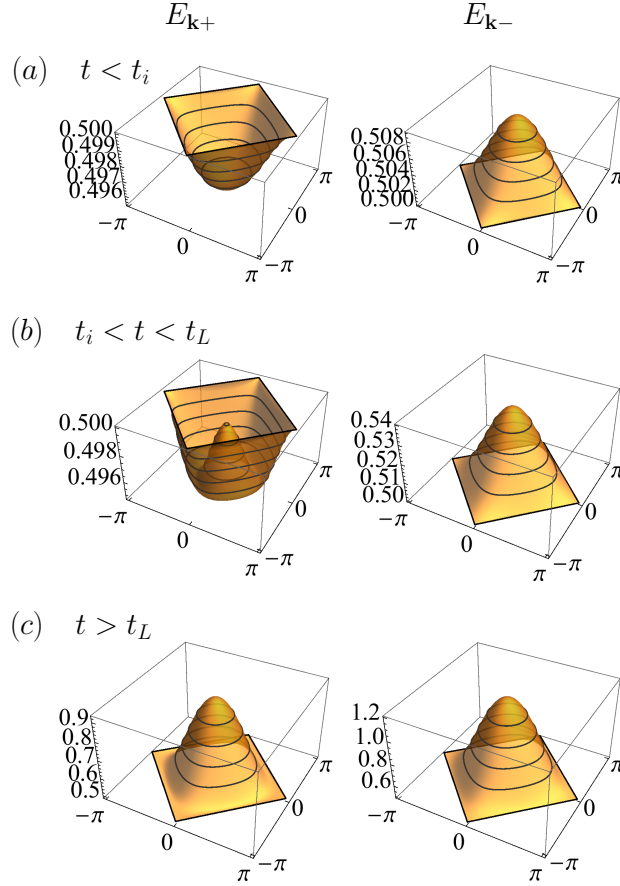
Figure 2.11: The charge quasiparticle dispersions of the Hubbard model. Here, too, we see inversion phenomenon similar to what we saw in the Kondo lattice model.

2.5.1 Inversion

Diagonalization of the effective charge Hamiltonian, $\hat{H}_{H,c}$, for the Hubbard model is done exactly in the same way as for the $\hat{H}_c$ of the KLM. The resulting dispersion for the charge quasiparticles of the Hubbard model is

$$E_{\mathbf{k}\pm} = E_{\mathbf{k}} \pm \frac{1}{2}t(1+\rho_1)|\gamma_{\mathbf{k}}| > 0 \tag{2.34}$$

with $E_{\mathbf{k}} = \sqrt{\left(\frac{U}{2}\right)^2 + [t(1-\rho_1)|\gamma_{\mathbf{k}}|/2]^2}$. To discuss its implications, we assign to ρ_1 (determined by the effective spin dynamics, $\hat{H}_{H,s}$) a numerical value of -1.338 (as known from the quantum monte carlo method [68]) on square lattice, and -1.194 (as known from the spin-wave theory [69]) on simple cubic lattice.

The evolution of the charge quasiparticle dispersion with t/U is presented in Fig. 2.11. For small t (in units of the local repulsion U), the Mott insulating

ground state at half-filling on bipartite lattices is described here by the gapped, oppositely curved dispersions, $E_{\mathbf{k}\pm}$. Here, $E_{\mathbf{k}+}$ undergoes inversion as t increases. On square (simple cubic) lattice, the inversion of $E_{\mathbf{k}+}$ starts at $t_i = 0.016$ (0.007), and the Lifshitz-like transition (crossing of the chemical potential, $U/2$) happens at $t_L \approx 2t_i$.
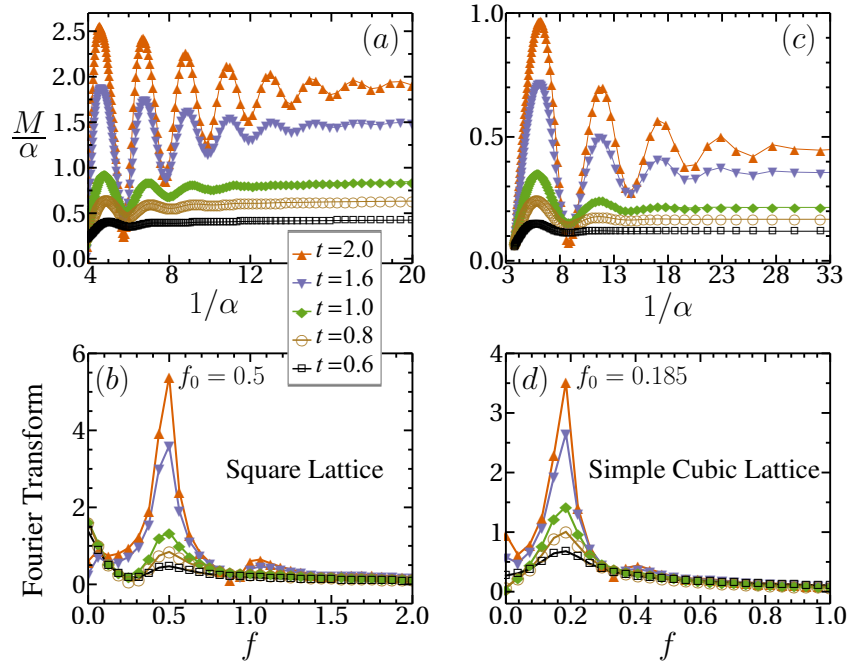
Figure 2.12: The dHvA oscillations in the insulating Néel ground state of the Hubbard model (with $U = 1$) at half-filling on (a) square and (c) simple cubic lattices. Their Fourier amplitudes (divided by t for better visibility at smaller t's) are plotted in (b) and (d). The dominant frequency, f_0, in the two cases here is same as that for the corresponding KI's.

2.5.2 dHvA oscillations

We study the orbital response of electrons in the Hubbard model to magnetic field coupled to electron hopping as: $-t \sum_{\mathbf{r},\boldsymbol{\delta},s} e^{i\frac{e}{\hbar} \int_{\mathbf{r}}^{\mathbf{r}+\boldsymbol{\delta}} \mathbf{A}\cdot\mathbf{dr}} \hat{c}_{\mathbf{r},s}^{\dagger} \hat{c}_{\mathbf{r}+\boldsymbol{\delta},s}$. In the presence of magnetic field, the effective charge Hamiltonian, $\hat{H}_{H,c}$, suitably modifies to an Hofstadter like model as derived in Sec. 2.4, using which we compute M vs B in the insulating Néel ground state of the Hubbard model. For the same $\alpha = p/q$ as taken for the KLM, the data in Fig. 2.12 for the Hubbard model shows clear oscillations

for $t \gtrsim 0.5$, with $f_0 = 0.5$ and 0.185 coming from the $|\gamma_{\mathbf{k}}| = 0$ chemical potential surface on square and simple cubic lattices. Note that the strong U Mott insulating phase does not show magnetic quantum oscillations. This calculation predicts the dHvA oscillations to occur in spin-density wave (SDW) insulators, because the Néel insulating state of the half-filled Hubbard model for such large values of t describes the SDW insulators. Motivated by this, we further investigate the occurrence of dHvA oscillations in weakly correlated SDW insulators in Chapter 5.

2.6 Conclusion

In this chapter, to understand the quantum oscillations of magnetization in Kondo insulators, we have studied the spin-1/2 Kondo lattice model at half-filling on square and simple cubic lattices. The key finding of our study is that the dHvA oscillations corresponding to half Brillouin zone in Kondo insulators occur as a bulk phenomenon, which manifests itself through the inversion of a Hofstadter-quantized dispersion of the gapped charge quasiparticles whose chemical-potential surface these oscillations measure. We have found this through a minimal effective dynamics, in a certain canonical representation of electrons, that appropriately describes the Kondo insulating ground state, and reveals the inversion and Lifshitz-like transition for charge quasiparticles. This approach also gives the same oscillations in the Néel insulating ground state of the half-filled Hubbard model, with an amplitude that grows with hopping. It clearly suggests that the spin-density wave insulators would also exhibit quantum oscillations of magnetization.

• • • • •

Chapter3

Kondo Lattice with Interacting Conduction Electrons

While the Kondo lattice model of localized moments coupled to "non-interacting" conduction electrons (as discussed in the previous chapter) provides the minimal physical description of the heavy-fermion systems, there are materials (such as $Nd_{2-x}Ce_xCuO_4$ [44], $CaCu_3Ru_4O_{12}$, and certain Ce-based compounds [45]) in which the "interaction" between the conduction electrons is known to play an important role. This led to the studies of an extended KLM that includes onsite repulsion, U, between the conduction electrons, in addition to the hopping, t, and the Kondo interaction, J. We call it the Hubbard-Kondo lattice model (H-KLM) [70, 71].

In this chapter, we apply the theory of Kondo insulators, as developed for KLM in the previous chapter, to H-KLM at half-filling. The basic motivation for this study is to understand the influence of U on the Kondo insulating ground state, and how it affects the dHvA oscillations. In the absence of magnetic field, there

have been done a few studies on H-KLM by methods such as QMC (quantum monte carlo), generalized bond-operator mean-field theory, DMRG (density matrix renormalization group) [47, 70]. Our theory, in concert with VCA (variational cluster approximation) calculations [46], not only produces results that are in qualitative agreement with what is known, but also reveals inversion (as in KLM) and provides a neat understanding of the role U plays relative to J. Furthermore, we study dHvA oscillations in the insulating ground state of H-KLM, which was never done before. Our calculations give clear magnetic quantum oscillations for H-KLM. We find these oscillations to become weaker, and eventually disappear, by increasing U or J or both.

$$\Gamma = (0,0) \qquad X = (\pi, 0)$$
$$M = (\pi, \pi) \qquad \Lambda = (\pi/2, \pi/2)$$

(a)   (b)
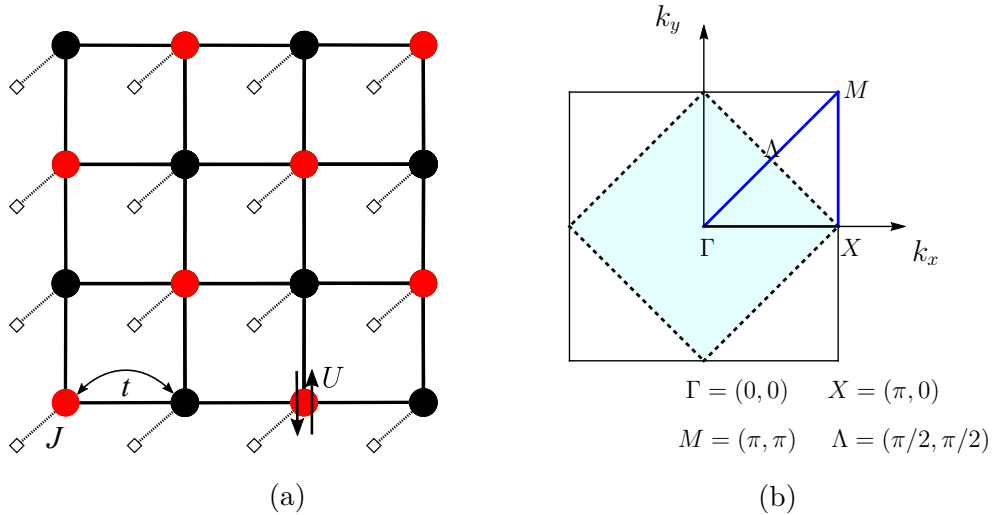
Figure 3.1: (a) A depiction of the Hubbard-Kondo lattice model on square lattice. Here, red solid circles represent $\mathcal{A}$-sublattice, and the black ones denote $\mathcal{B}$-sublattice. The conduction electrons hop between nearest-neighbour sites with an amplitude, t, and the antiferromagnetic exchange interaction, J, couples the conduction electron with the local moment present at each site. In addition, the onsite repulsion, U, acts between the conduction electrons. (b) Brillouin zone (BZ) of the square lattice. Here, the dashed black line (enclosing the faded blue region) indicates magnetic BZ or the half-BZ, and the solid black line represents full BZ. Also shown are the special points Γ, X, M and Λ along various symmetry directions.

3.1 Hubbard-Kondo Lattice Model

The model that we study here is the KLM of Eq. (2.5) with an additional onsite Coulomb repulsion, $U > 0$, between the conduction electrons. It is given by the following Hamiltonian (in the same notation as used in the previous chapter),

$$\hat{H} = -t \sum_{\mathbf{r},\boldsymbol{\delta},s} \hat{c}^{\dagger}_{\mathbf{r},s} \hat{c}_{\mathbf{r}+\boldsymbol{\delta},s} + \frac{J}{2} \sum_{\mathbf{r}} \mathbf{S}_{\mathbf{r}} \cdot \boldsymbol{\tau}_{\mathbf{r}} + U \sum_{\mathbf{r}} \hat{n}_{\mathbf{r},\uparrow} \hat{n}_{\mathbf{r},\downarrow} - \frac{U}{2} \sum_{\mathbf{r},s} \hat{n}_{\mathbf{r},s} \qquad (3.1)$$

Here, in the last term, the chemical potential of the conduction electrons is set to $U/2$, which on bipartite lattices exactly fixes the conduction electron filling to half. That is, the average number of electrons per site is equal to 1. In the canonical representation described in Sec. 2.2, the H-KLM given by Eq. (3.1) on bipartite lattice reads as:

$$\hat{H} = -\frac{it}{2} \sum_{\mathbf{r}\in\mathcal{A}} \sum_{\boldsymbol{\delta}} \left[\hat{\psi}_{a,\mathbf{r}} \hat{\phi}_{b,\mathbf{r}+\boldsymbol{\delta}} + \hat{\psi}_{b,\mathbf{r}+\boldsymbol{\delta}} \hat{\phi}_{a,\mathbf{r}} \left(\boldsymbol{\sigma}_{\mathbf{r}} \cdot \boldsymbol{\sigma}_{\mathbf{r}+\boldsymbol{\delta}} \right) \right]$$
$$+ \frac{J}{4} \left[\sum_{\mathbf{r}\in\mathcal{A}} \hat{n}_{a,\mathbf{r}}(\boldsymbol{\sigma}_{\mathbf{r}} \cdot \boldsymbol{\tau}_{\mathbf{r}}) + \sum_{\mathbf{r}\in\mathcal{B}} \hat{n}_{b,\mathbf{r}}(\boldsymbol{\sigma}_{\mathbf{r}} \cdot \boldsymbol{\tau}_{\mathbf{r}}) \right] - \frac{U}{2} \left[\sum_{\mathbf{r}\in\mathcal{A}} \hat{n}_{a,\mathbf{r}} + \sum_{\mathbf{r}\in\mathcal{B}} \hat{n}_{b,\mathbf{r}} \right] \quad (3.2)$$

Following the procedure worked out in Sec. 2.3, we derive the effective spin and charge dynamics of the half-filled H-KLM. Under this procedure, Eq. (3.2) becomes: $\hat{H} \approx \hat{H}_c + \hat{H}_s + e_1 L$, where $e_1 = -(\mathsf{z}t\zeta\rho_1 + J\bar{n}\rho_0)/4$,

$$\hat{H}_s = \frac{t\zeta}{4} \sum_{\mathbf{r},\boldsymbol{\delta}} \boldsymbol{\sigma}_{\mathbf{r}} \cdot \boldsymbol{\sigma}_{\mathbf{r}+\boldsymbol{\delta}} + \frac{J\bar{n}}{4} \sum_{\mathbf{r}} \boldsymbol{\sigma}_{\mathbf{r}} \cdot \boldsymbol{\tau}_{\mathbf{r}}, \text{ and} \qquad (3.3a)$$

$$\hat{H}_c = -\frac{it}{2} \sum_{\mathbf{r}\in\mathcal{A}} \sum_{\boldsymbol{\delta}} \left[\hat{\psi}_{a,\mathbf{r}} \hat{\phi}_{b,\mathbf{r}+\boldsymbol{\delta}} + \rho_1 \hat{\psi}_{b,\mathbf{r}+\boldsymbol{\delta}} \hat{\phi}_{a,\mathbf{r}} \right] + \left(\frac{J\rho_0}{4} - \frac{U}{2} \right) \left[\sum_{\mathbf{r}\in\mathcal{A}} \hat{n}_{a,\mathbf{r}} + \sum_{\mathbf{r}\in\mathcal{B}} \hat{n}_{b,\mathbf{r}} \right]$$
$$(3.3b)$$

Here, the parameters, $\bar{n}$, ζ, ρ_0 and ρ_1, are defined exactly in the same way as for the KLM in Eqs. (2.9) of Chapter 2. Since ρ_0 (the local Kondo singlet correlation) is always negative, we note that the Hubbard repulsion, U, adds to the Kondo interaction, J, in the charge dynamics given by Eq. (3.3b). Thus, a non-zero U clearly strengthens the Kondo coupling.

By comparing Eq. (2.8a) with Eq. (3.3b), we can immediately derive the charge quasiparticle dispersions for H-KLM by replacing J in $E_{\mathbf{k}\pm}$ of Eq. (2.13) by

$\left(J - \frac{2U}{\rho_0}\right)$. Thus, the charge dynamics of H-KLM is essentially like that of KLM, in which U just adds on to J. The effective spin dynamics of H-KLM is governed in fact by the same $\hat{H}_s$ as for KLM, with no explicit dependence on U. However, it doesn't mean that U has no influence on its magnetic nature. In fact, implicitly through $\bar{n}$ and ζ, the spin dynamics given by Eq. (3.3a) does depend on U.

The equations that determine these parameters for the charge part are:

$$\bar{n} = \frac{1}{2} - \frac{1}{L}\left(\frac{J\rho_0}{4} - \frac{U}{2}\right)\sum_{\mathbf{k}}\frac{1}{E_{\mathbf{k}}} \quad \text{and} \quad \zeta = \frac{t(1-\rho_1)}{zL}\sum_{\mathbf{k}}\frac{|\gamma_{\mathbf{k}}|^2}{E_{\mathbf{k}}}. \tag{3.4}$$

and those for the spin part are: $\rho_0 = 1 - 4\bar{s}^2$, and $\rho_1 = 4\bar{s}^2(J\bar{n} - \lambda)/zt\zeta$, where

$$\bar{s}^2 = \frac{5}{2} - \frac{3}{4L}\sum_{\mathbf{k}}\frac{2\lambda + t\zeta\bar{s}^2\gamma_{\mathbf{k}}}{\varepsilon_{\mathbf{k}}}, \quad \text{and} \tag{3.5a}$$

$$\lambda = J\bar{n} - \frac{3\lambda t\zeta}{4L}\sum_{\mathbf{k}}\frac{\gamma_{\mathbf{k}}}{\varepsilon_{\mathbf{k}}}. \tag{3.5b}$$

These parameters are determined by solving the above equations iteratively in the ground state of Eq. (3.3). Figures 3.2 and 3.3 show their values obtained from the self-consistent calculation on square lattice. In the calculations here, we specify J and U in units of t. That is, we have put $t = 1$.
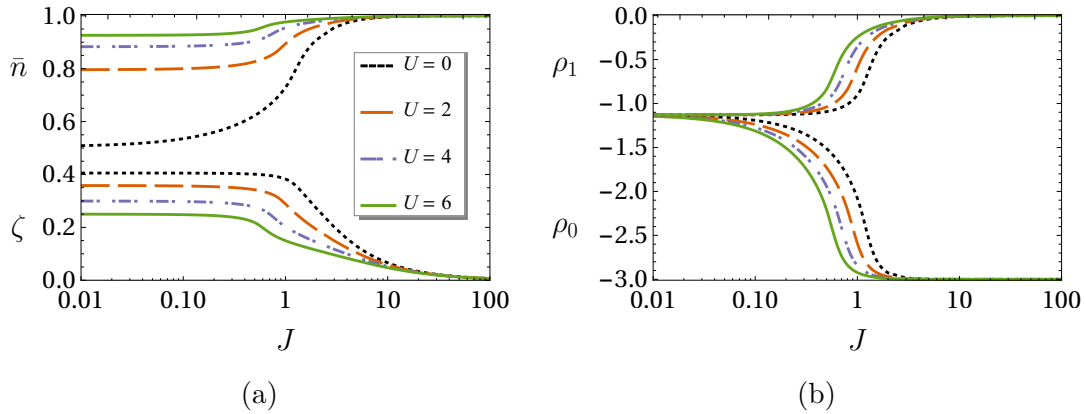

(a)

(b)

Figure 3.2: The self-consistent parameters as a function of J for different values of U on square lattice. (a) The $\bar{n}$ and ζ for the charge part. (b) The parameters ρ_0 and ρ_1 for the spin part. In extreme limit of J, all these parameters saturate to a specific value for any U.
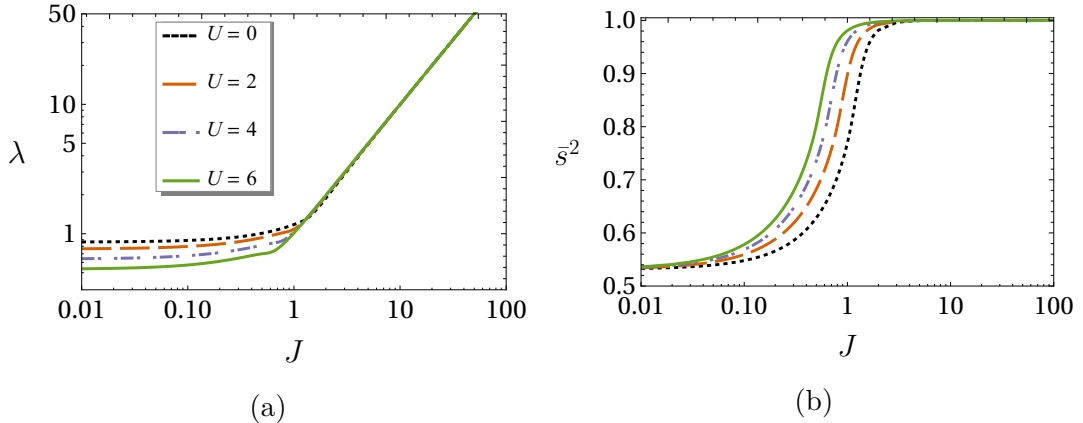
Figure 3.3: The mean-field parameters, λ and $\bar{s}^2$, of the bond-operator theory of $\hat{H}_s$, plotted as a function of J for different values of U on square lattice.

3.2 Ground State Properties

In Fig. 3.2, we see that for any value of U, when J is large enough, the mean-field parameters saturates at, $\bar{n} = 1$, $\zeta = 0$, $\rho_0 = -3$ and $\rho_1 = 0$. In this limit, the Kondo exchange dominates, forming perfect local singlets between the electron spin and the local moment with spin gap, $\Delta_s = J$. In this case, the charge dynamics is governed by the strong coupling model (similar to KLM): $\hat{H}_{0c} = -\frac{it}{2} \sum_{\mathbf{r} \in \mathcal{A}} \sum_{\boldsymbol{\delta}} \hat{\psi}_{a,\mathbf{r}} \hat{\phi}_{b,\mathbf{r}+\boldsymbol{\delta}} - \left(\frac{3J}{4} + \frac{U}{2} \right) \left(\sum_{\mathbf{r} \in \mathcal{A}} \hat{n}_{a,\mathbf{r}} + \sum_{\mathbf{r} \in \mathcal{B}} \hat{n}_{b,\mathbf{r}} \right)$, with charge gap, $\Delta_c = \sqrt{(3J/4 + U/2)^2 + (\mathsf{z}t/2)^2} - \mathsf{z}t/2$. In this extreme J limit, the ground state of H-KLM is a Kondo singlet insulator for any U. As we lower the value of J, the values of the self-consistent parameters renormalize strongly and depend on U, the physical consequences of which are discussed in the following sections.

3.2.1 Quantum phase diagram

We know that in KLM (the $U = 0$ case of H-KLM), by decreasing J below a critical value, J_c, a continuous phase transition occurs from the Kondo singlet to Néel ordered phase in the insulating ground state on square and simple cubic lattices.[1] Therefore, it is natural to ask how a non-zero U affects this quantum

---

[1]Note that, on one-dimensional lattice, there is no antiferromagnetic order, but only the Kondo singlet phase.

phase transition. To this end, we obtain the quantum phase diagram in the J-U plane by tracking the quasiparticle gaps of the effective spin and charge dynamics.

(a)   (b)
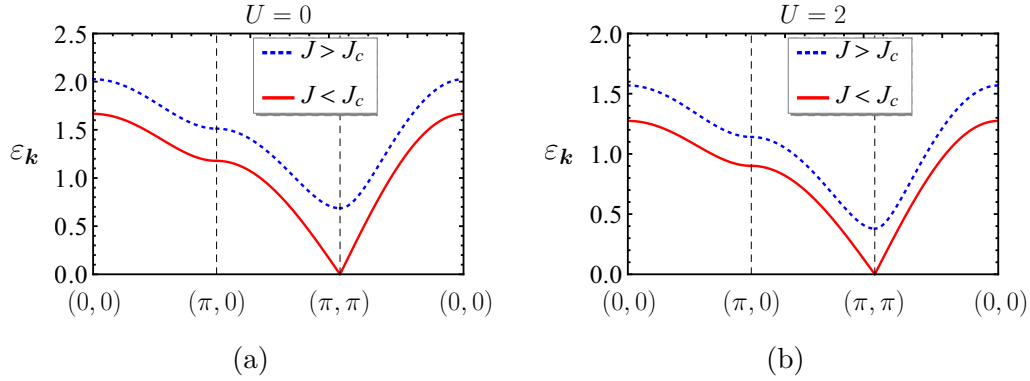
Figure 3.4: The triplon dispersion, $\varepsilon_{\mathbf{k}}$, for $U = 0$ and 2 on square lattice, plotted along the symmetric directions in the Brillouin zone (see Fig. 3.1). We find that for $J > J_c$, it is always gapped. But when $J \leq J_c$, we find the gap closes at (π, π) for all U's.

(a)   (b)
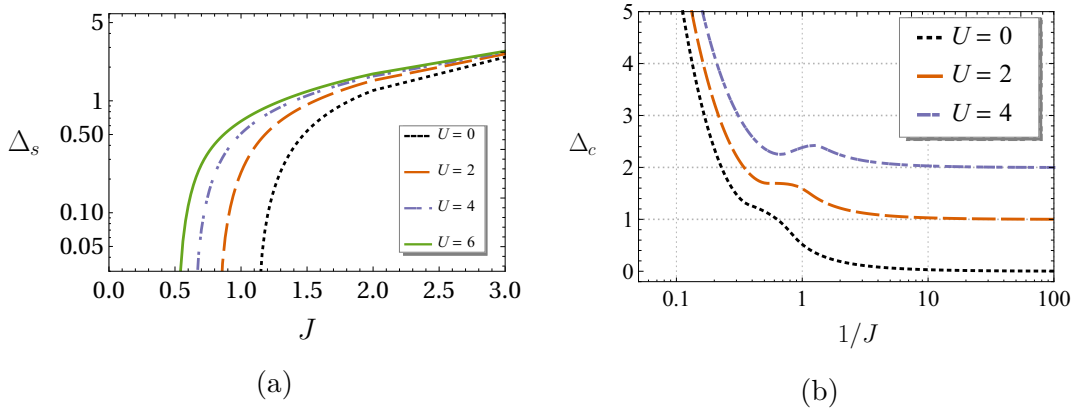
Figure 3.5: Square lattice. (a) Spin gap, Δ_s vs. J at $U = 0, 2, 4, 6$. It clearly shows that J_c decreases with an increase in U. This means, U helps J in forming the Kondo singlet. (b) Charge gap, Δ_c is always non-zero, and increases with U.

Look at the triplon dispersion, $\varepsilon_{\mathbf{k}}$, plotted in Fig. 3.4 for two different U's on square lattice. It is found to be gapped for $J > J_c$, and gapless at $\mathbf{Q} = (\pi, \pi)$ [on simple cubic lattice, $\mathbf{Q} = (\pi, \pi, \pi)$] for $J < J_c$, where J_c is the point at which Δ_s (spin gap) vanishes. See Figs. 3.5a and 3.6a for Δ_s vs. J for different U's on square and simple cubic lattices. From this figure, it is quite clear that J_c decreases with increasing U. While the spin gap closes below J_c, the charge gap,
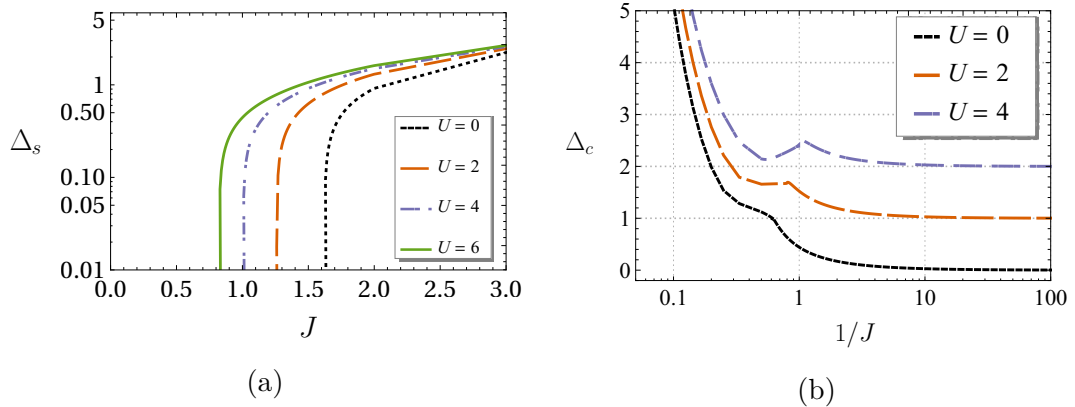
Figure 3.6: Simple cubic lattice. (a) Spin gap, Δ_s vs. J for $U = 0, 2, 4, 6$. (b) Charge gap, Δ_c vs. $1/J$ for $U = 0, 2, 4$.

Δ_c is found to be always non-zero, as shown in Figs. 3.5b and 3.6b. This describes an insulating ground state. Notably, as shown in Fig. 3.7, both spin and charge gaps are always non-vanishing on a chain, resulting in the absence of any transition to a magnetically ordered phase in the insulating ground state. Our theory, thus, also captures the correct dimensional dependence of the properties of the Kondo insulators.

On square and simple cubic lattice, where the quantum phase transition occurs, we obtain the phase boundary between the Kondo singlet and Néel phase by the condition, $\varepsilon_{\mathbf{Q}} = 0$, of the Goldstone mode, which fixes λ as: $\lambda = zt\zeta\bar{s}^2$. After a few steps of manipulations, it gives the following equation of the boundary separating the Néel phase from the Kondo singlet phase:

$$J_c = t\left(\frac{5}{2} - 3x + 3y\right)\frac{\zeta}{\bar{n}} \qquad (3.6)$$

where x and y are two constants[2]. Notably, $\rho_0 = 3(4x - 3)$ and $\rho_1 = 6(5 - 6x)y$ are also constants on the phase boundary. Thus, only through the parameter, $\zeta/\bar{n}$, of the charge dynamics, the J_c depends on U. Figure 3.12 shows the resulting quantum phase diagram of the half-filled H-KLM on square and simple cubic lattices. From this phase diagram, it is very clear that U, like J, favours the Kondo singlet state.

By taking a simplistic constant density of states for the summations over $\mathbf{k}$ in

---

[2]Here, $x = \frac{1}{4L}\sum_{\mathbf{k}}\frac{2 + (\gamma_{\mathbf{k}}/z)}{\sqrt{1 + (\gamma_{\mathbf{k}}/z)}}$ and $y = \frac{1}{4L}\sum_{\mathbf{k}}\frac{(\gamma_{\mathbf{k}}/z)}{\sqrt{1 + (\gamma_{\mathbf{k}}/z)}}$.

(a)   (b)
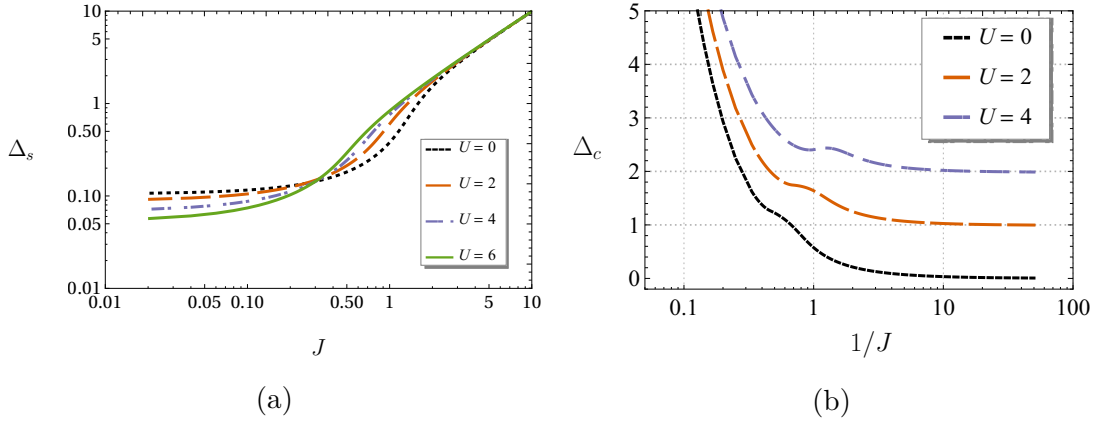
Figure 3.7: One-dimensional Kondo lattice. (a) Spin gap, Δ_s, vs. J for $U = 0, 2, 4, 6$. Note that Δ_s never vanishes for any $J > 0$. (b) Charge gap, Δ_c, vs. $1/J$ for $U = 0, 2, 4$. It is always non-zero. Hence, the insulating ground state in one dimension is always the Kondo singlet, which is qualitatively consistent with DMRG and other numerical and analytical studies [72, 70, 73, 74, 75, 65].

Eqs. (3.4) for $\bar{n}$ and ζ, we can analytically derive the following explicit expression for the quantum phase boundary given by Eq. (3.6)

$$J_c(J_c + aU_c) = \sum_{m=0}^{\infty} \frac{b_m}{(J_c + aU_c)^{2m}} \tag{3.7}$$

Here, a is a positive constant, and b_m's are the constant coefficients of the power series in $\frac{1}{(J_c + aU_c)^2}$. At the leading order, it reads as: $J_c(J_c + aU_c) = b_0$, where b_0 is also a positive constant. This leading order equation is a parabola in the J-UJ plane. Hence, in Fig. 3.8, we present the phase diagrams for square and simple cubic lattices in the J-UJ plane, which indeed look pretty much like a parabola.

3.2.1.1   Comparison with VCA and QMC

We compare the findings of our theory with the numerical results from a recent VCA (variational cluster approximation) calculation by our collaborators [46], and a QMC (quantum monte carlo) calculation [47], both on square lattice.

In Fig. 3.9, we show the quantum phase diagram obtained from our theory together with that from the VCA calculation, in the J-UJ plane. Although quantitatively they differ, but there is good agreement in the qualitative behaviour of the two. The VCA phase boundary nicely fits to the equation of the critical line,
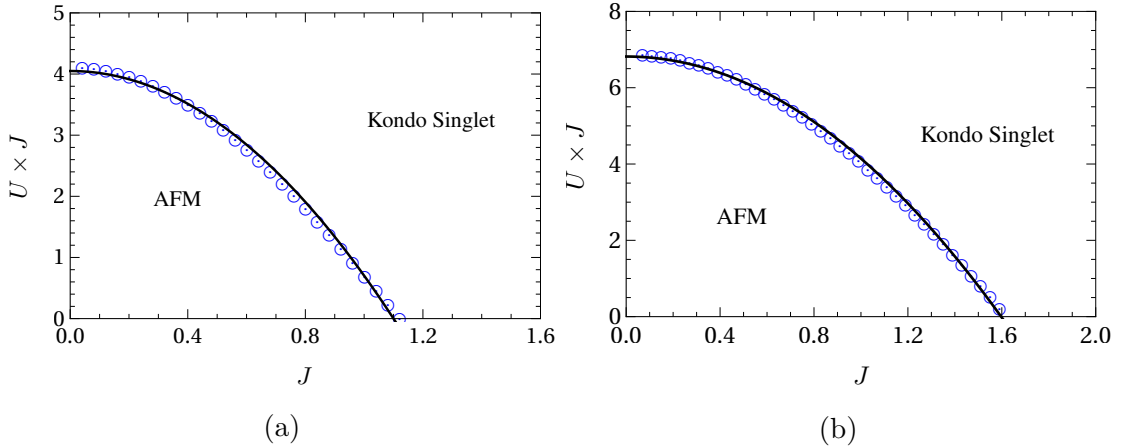
Figure 3.8: Quantum phase diagram of the Hubbard-Kondo lattice model in the J-UJ plane (for $t = 1$). (a) Square lattice. (b) Simple cubic lattice.

Eq. (3.7), from our theory. In fact, this fitting is quite remarkable already at the level of the leading order parabolic equation, $J_c(J_c + aU_c) = b_0$, with $a \approx 0.58$ and $b_0 \approx 4.26$ for the VCA data.

The QMC data in Fig. 3.10b, taken from Ref. [47], is also in qualitative agreement with our theory plotted in Fig. 3.10a. Quantitatively, however, the VCA overestimates the antiferromagnetic phase, while our theory slightly overestimates the Kondo singlet phase, in comparison to QMC. We can see that for $U = 0$ the critical point from QMC is $J_c = 1.45 \pm 0.05$, but our theory gives $J_c = 1.12$ and it is 2.05 from VCA. The J_c from our theory is lower because, in making the bond-operator calculations of the effective spin dynamics, we assume an average Kondo singlet per site and then consider triplet fluctuations on top of it, while in VCA the magnetic order is assumed and determined self-consistently. So, our theory and VCA approach the critical line from the opposite phases, which overestimates one or the other phase. However, our theory is quantitatively still closer to the QMC. Moreover, the size of the cluster in VCA is finite and small (4 sites), due to which it is not expected to meet close quantitative agreement. But it is the qualitative agreement that is notably good.
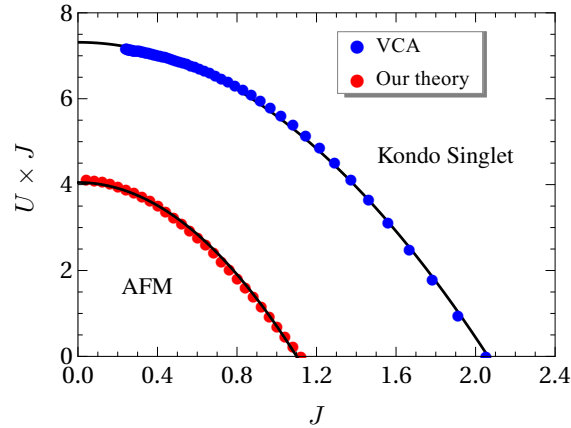
Figure 3.9: Quantum phase diagram of the half-filled H-KLM on square lattice from the VCA (blue filled circles) and from our theory (red empty circles). Since, for small J, the critical value of U goes as $1/J$, we have plotted the data in the J-UJ plane. The black line is the fit to the leading order equation, $J_\perp(J_\perp + aU) = b_0$, of the critical line from our theory. For the VCA data, $a \approx 0.58$ and $b_0 \approx 4.26$. In spite of the quantitative differences, the VCA phase boundary follows remarkably closely the behaviour obtained by our theory.

(a)

(b)
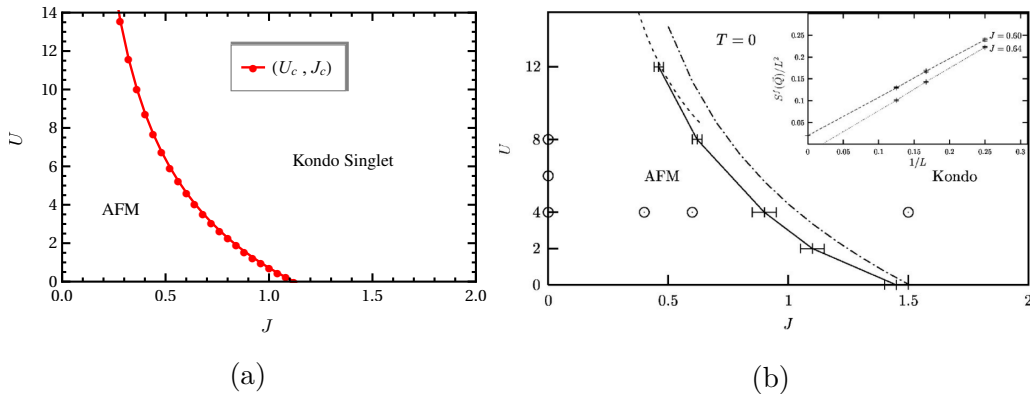
Figure 3.10: Quantum phase diagram of the Hubbard-Kondo lattice model in the J-U plane (for $t = 1$). (a) Our result for square lattice. (b) Quantum phase diagram of the Hubbard-Kondo lattice model at half-filling on square lattice. This figure is taken from Ref. [47]. The solid line: QMC data, dot-dashed line: MF and dashed line is spin Hamiltonian. At $U = 0$, the critical $J_c = 1.45 \pm 0.05$ for QMC however it is approximately $J_c = 1.5$ for MF and close enough to the QMC.

3.2.2   Inversion and Lifshitz-like transitions

In this subsection, we discuss the evolution of the charge quasiparticle dispersions, $E_{\mathbf{k}\pm}$, with J for different fixed values of U. As for the KLM in the previous
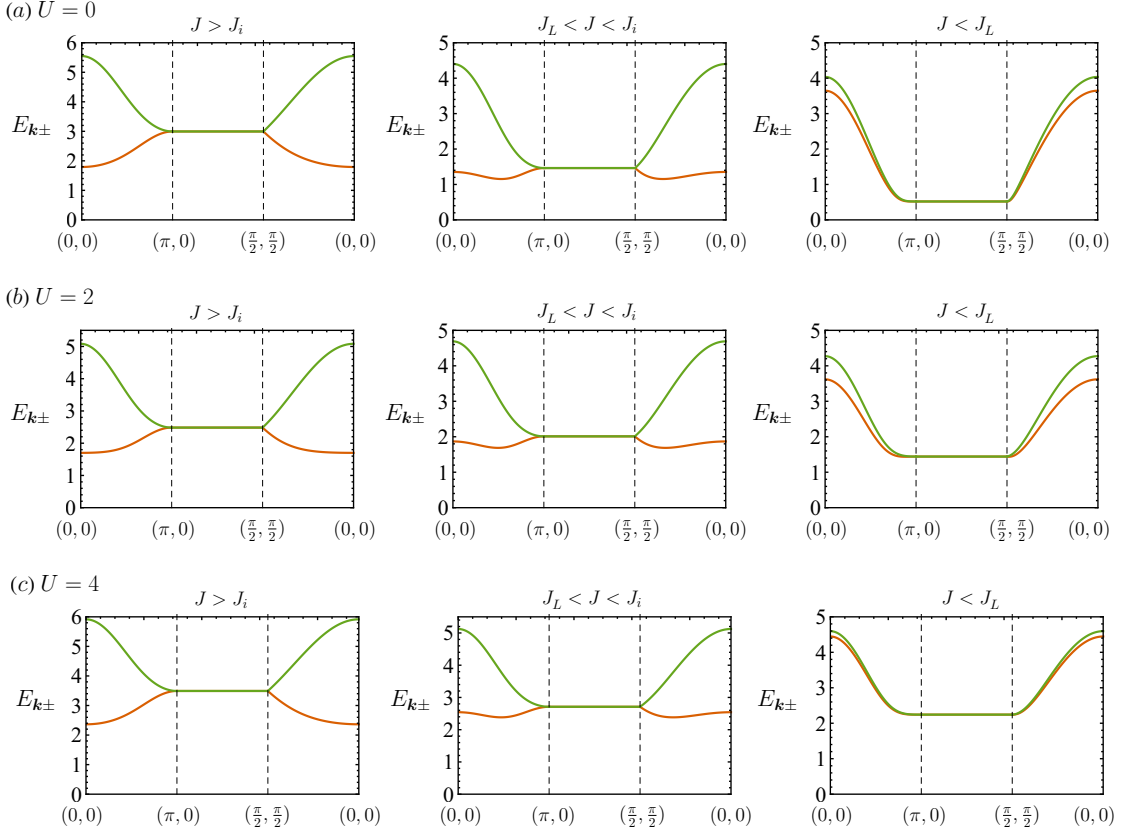
Figure 3.11: Charge quasiparticle dispersions, $E_{\mathbf{k}+}$ (green) and $E_{\mathbf{k}-}$ (orange), along symmetric directions in the Brillouin zone of the square lattice (see Fig. 3.1) for $U = 0, 2, 4$. Similar to KLM, here too, the $E_{\mathbf{k}-}$ undergoes inversion for $J < J_i$.

chapter, here too, the lower charge quasiparticle dispersion, $E_{\mathbf{k}-}$, reveals inversion and Lifshitz like transitions as we decrease the value of J for any U.

We call that value of J at which $E_{\mathbf{k}-}$ starts to invert the inversion point, J_i. For a given U, at large J the minimum (maximum) of $E_{\mathbf{k}-}$ ($E_{\mathbf{k}+}$) occurs at the Γ point, that is $\mathbf{k} = (0,0)$, and the maximum (minimum) is located on the boundary of the half BZ, i.e $|\gamma_{\mathbf{k}}| = 0$. As we lower J below J_i, the Γ point becomes a local maxima, and the minima of $E_{\mathbf{k}-}$ shifts to the points away from Γ (on a contour surrounding the Γ point). See Figs. 3.11. We define this contour as the charge gap contour. By setting $\frac{\partial E_{\mathbf{k}-}}{\partial |\gamma_{\mathbf{k}}|} = 0$, we get the following equation for the charge gap contour:

$$|\gamma_{\mathbf{k}}| = \frac{1}{t\sqrt{|\rho_1|}} \left(\frac{1 - |\rho_1|}{1 + |\rho_1|} \right) \left(\frac{J\rho_0}{4} + \frac{U}{2} \right) \tag{3.8}$$

We calculate an expression for the inversion point, J_i, by expanding $E_{\mathbf{k}-}$ upto

quadratic term in $|\mathbf{k}|$ around the Γ point. As long the coefficient of this quadratic term is positive, the minimum of $E_{\mathbf{k}-}$ stays at the Γ point. But just when the coefficient of the quadratic term changes sign, the Γ point is no more the point of minima. It gives us the following equation whose solution is the J_i.

$$J_i = t\mathsf{z}\sqrt{|\rho_1|}\left(\frac{1+|\rho_1|}{1-|\rho_1|}\right)\frac{1}{\left(\frac{|\rho_0|}{4}+\frac{U}{2J_i}\right)} \tag{3.9}$$

Here, ρ_0 and ρ_1 also depend implicitly on J_i. Hence, for a given U, we iteratively solve Eq. (3.9) for J_i, together with the self-consistent Eqs. (3.4) and (4.36). The result is plotted in Fig. (3.12). We find J_i to become small with increase in U.

When J is further decreased below J_i, at some point, J_L, the $E_{\mathbf{k}-}$ at Γ point crosses the effective chemical potential in Eq. (3.3b). We call it a Lifshitz-like transition, because now in addition to $|\gamma_{\mathbf{k}}| = 0$, there is another contour (or surface) at which $E_{\mathbf{k}-}$ is equal to the effective chemical potential, $\frac{J|\rho_0|}{4}+\frac{U}{2}$, of the spinless fermions. The J_L is obtained by equating $E_{\mathbf{k}}$ (at $|\gamma_{\mathbf{k}}| = 0$) $= E_{\mathbf{k}=0}$, then

$$J_L = \frac{t\mathsf{z}|\rho_1|}{(1-|\rho_1|)\left(\frac{|\rho_0|}{4}+\frac{U}{2J_L}\right)} \tag{3.10}$$

Similar to J_i, we calculate J_L by solving the above equation. Upon increasing the repulsion U, the value of J_L also decreases. See Fig. 3.12 for the inversion and Lifshitz-like transitions, in relation to the phase transition from Kondo singlet to Néel phase.

For the charge gap, Δ_c, as a function of J, calculated for different U, see Fig. 3.13. The Δ_c is always non-zero, and decreases with decrease in J and U. For large J (small $1/J$), it comes from the Γ point. As discussed above, for $J < J_i$, the Δ_c comes from the charge gap contour of Eq. (3.8), which for small J approaches the half-BZ boundary. The overall behaviour of the charge gap from our theory is similar to the spectral gap from VCA [46], as shown in Fig. 3.13(b).

3.3   Magnetic Quantum Oscillations

Since we find the H-KLM to behave pretty much like the KLM, we expect to see dHvA oscillations also in the insulating ground state of H-KLM. Moreover,
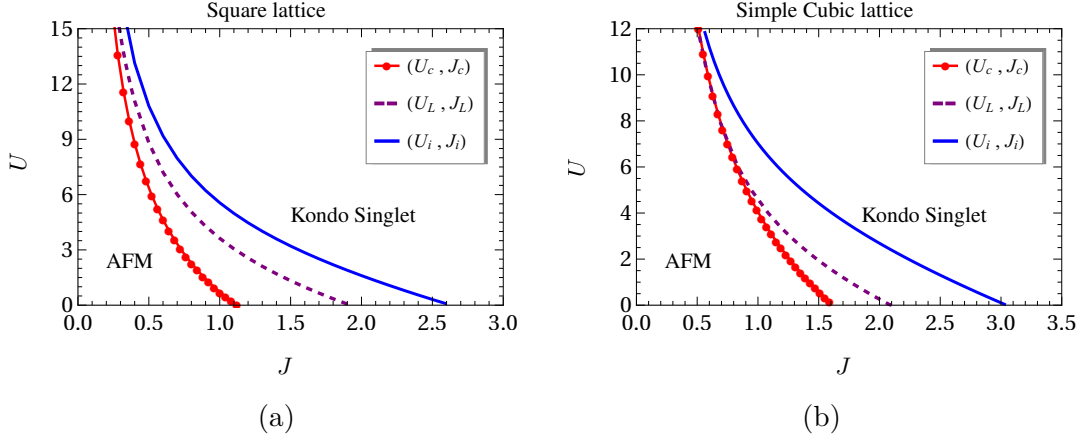
Figure 3.12: Quantum phase, inversion and Lifshitz-like transitions of the Hubbard-Kondo lattice model in the J-U plane (for $t = 1$). (a) Square lattice. (b) Simple cubic lattice.
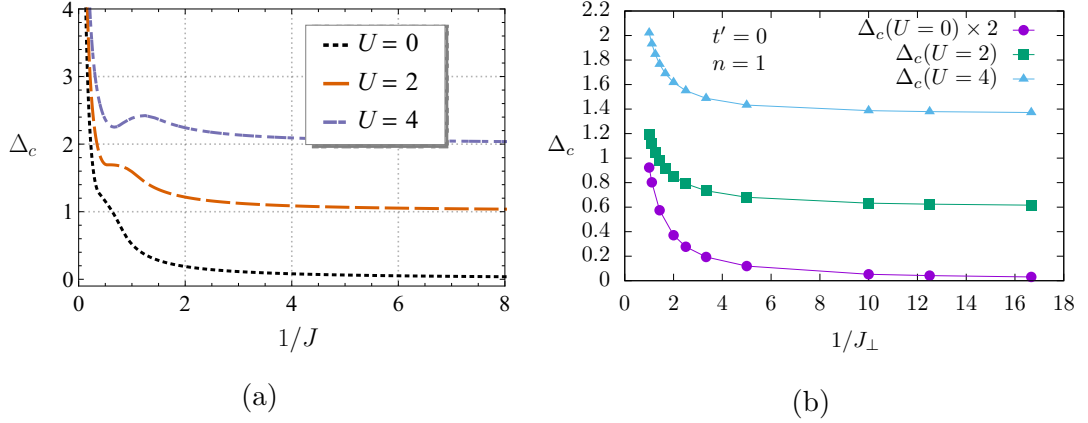
Figure 3.13: On square lattice. (a) Quasiparticle charge gap, Δ_c, vs. $1/J$ for $U = 0, 2, 4$ from our calculations. (b) The spectral gap obtained by VCA, figure from Ref. [46].

since U in H-KLM simply adds onto J in the effective charge dynamics, we expect the increase in U to suppress these oscillations. To check these expectations, we calculate the magnetic response of H-KLM to a uniform magnetic field, exactly the way we did it in Sec. 2.4 for KLM, The effective charge dynamics of H-KLM in the presence of a magnetic field, B, is given by the following Hamiltonian.

$$\hat{H}_c^{[B]} = -\frac{it}{2} \sum_{\mathbf{r} \in \mathcal{A}} \sum_{\boldsymbol{\delta}} \cos\left(2\pi\alpha\mathbf{r}_y\hat{x} \cdot \boldsymbol{\delta}\right) \left[\hat{\psi}_{a,\mathbf{r}}\hat{\phi}_{b,\mathbf{r}+\boldsymbol{\delta}} + \rho_1\hat{\psi}_{b,\mathbf{r}+\boldsymbol{\delta}}\hat{\phi}_{a,\mathbf{r}}\right]$$
$$+ \left(\frac{J\rho_0}{4} - \frac{U}{2}\right)\left[\sum_{\mathbf{r} \in \mathcal{A}} \hat{n}_{a,\mathbf{r}} + \sum_{\mathbf{r} \in \mathcal{B}} \hat{n}_{b,\mathbf{r}}\right] \qquad (3.11)$$

Here, α is magnetic flux defined in terms of B and lattice constant, a, as $\alpha = eBa^2/h$, and integer $\mathbf{r}_y$ is the y-coordinate of $\mathbf{r}$, and $\hat{\boldsymbol{\delta}} = \boldsymbol{\delta}/|\boldsymbol{\delta}|$.
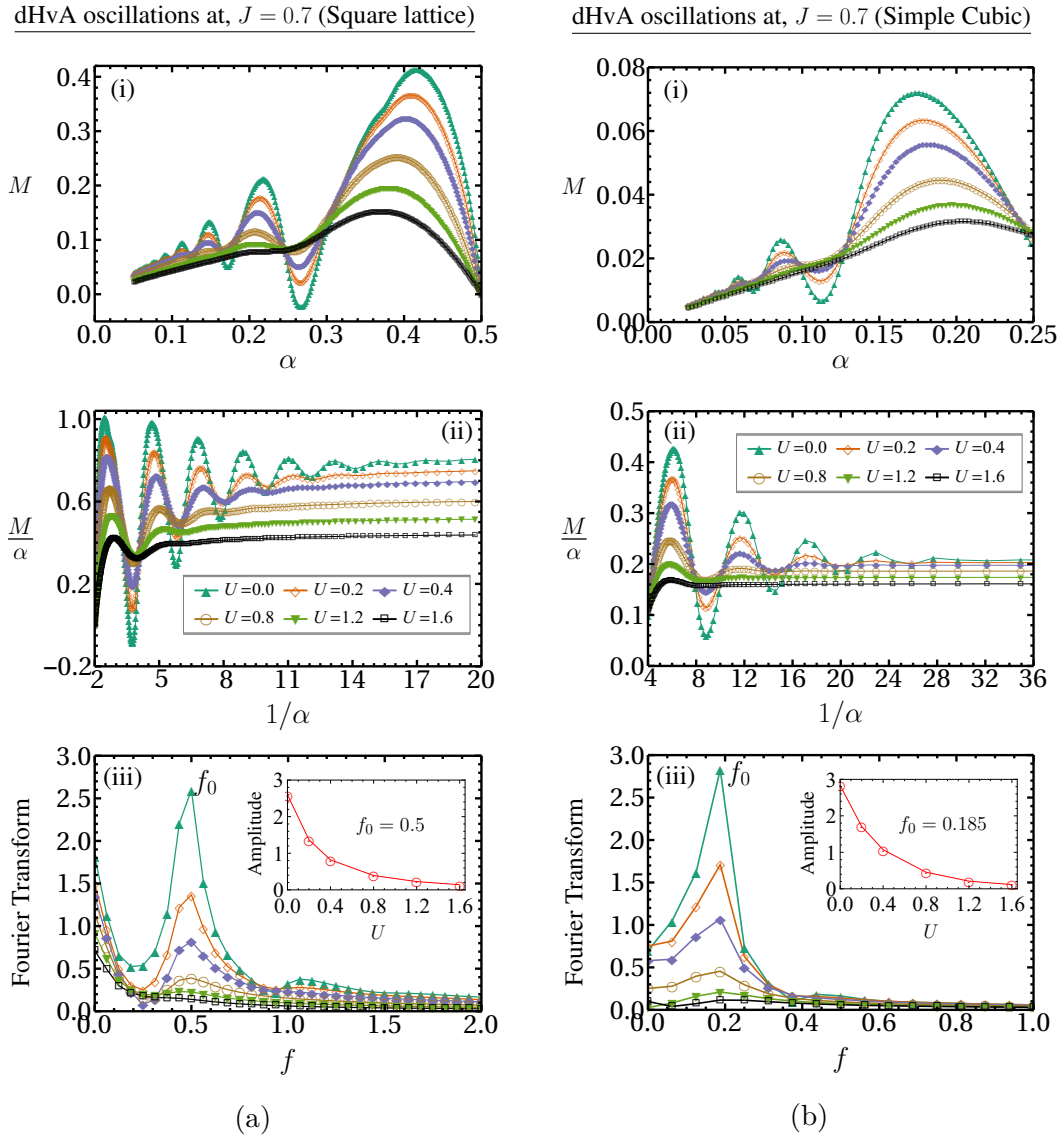
Figure 3.14: The effect of U on dHvA oscillations in the insulating ground state of H-KLM on (a) square lattice, and (b) simple cubic lattice. Here, $J = 0.7$ is fixed, and $U = 0, 0.2, 0.4, 0.8, 1.2, 1.6$. It is clear that U tends to suppress quantum oscillations. See amplitude vs U plots in the insets of the bottom two figures. Also note the dominant frequency, which corresponds the half Brillouin zone.

We know that at $U = 0$ the oscillations occur more prominently for smaller J's sufficiently below J_i. Hence, we fix $J = 0.7$, and do the calculations for different U's. As for the KLM, we put zero field value of the parameters ρ_0 and ρ_1 in

Eq. (3.11), and calculate M as a function of $\alpha = \frac{p}{q}$ for integer $p = 1, 2, \ldots, q$ with $q = 601$ for square lattice. We also do this calculation on simple cubic lattice for $q = 401$. Figure 3.14 shows the behaviour of M with respect to α (magnetic field) for different U's. Expectedly, we see clear dHvA oscillations corresponding to the half Brillouin zone. We also see that, upon increasing U, the amplitude of these oscillations gradually decreases and eventually vanishes.

3.4 Conclusion

In summary, we have studied here the ground state properties of the half-filled Hubbard-Kondo lattice model, given by Eq. (3.1), using the theory that we developed for KLM in Chapter 2. The H-KLM is an extended version of the KLM obtained by adding onsite Coulomb interaction, U, between the conduction electrons. From our theory, we obtain a quantum phase diagram having Kondo singlet and Néel phases, that is in qualitative agreement with what is obtained from VCA [46] and QMC calculations [47]. Moreover, for a 1D chain, we correctly obtain a ground state that is insulating and always a Kondo singlet for all J and U. The fact that a repulsive U helps the Kondo singlet phase in H-KLM is neatly seen in our theory, where a non-zero U essentially amount to enhancing J as: $J \rightarrow J + \frac{2U}{|\rho_0|}$. Like KLM [42], here too, we have found the charge quasiparticle dispersion to undergo inversion, which is important for quantum oscillations. Finally, we have investigated the effect of U on magnetic quantum oscillations in the insulating ground state of H-KLM. We have found that the dHvA oscillations, with frequency corresponding to half-Brillouin zone, do occur for moderate to small values of J, sufficiently below J_i. Moreover, we have found that these oscillations are suppressed upon increasing U.

•••••

Chapter4

Symmetric Periodic Anderson Model

A model of the heavy-fermion systems, that is more microscopic than the KLM, is the periodic Anderson model (PAM). In PAM, the conduction electrons are coupled through hybridization to the localized and correlated f-electrons (having a Hubbard repulsion, U_f) [24]. The KLM can be derived from the PAM [76], in the same way as the t-J model can be derived from the Hubbard model [77]. The PAM has proved to be fruitful in studying the rare-earth and actinide compounds exhibiting phenomena such as valence fluctuation [19, 78], heavy-fermion physics [79, 80], volume collapse [81, 82], and unconventional superconductivity [83].

Like the KLM, the PAM at half-filling too describes a Kondo insulator [84, 25, 85]. On bipartite lattices, such as the square or simple cubic lattice with nearest-

neighbour hopping, the particle-hole symmetric form of the Hubbard interaction exactly guarantees the half-filling. The PAM with this particle-hole symmetric Hubbard repulsion for the localized f-electrons, $U_f \sum_{\mathbf{r}} (\hat{n}^f_{\mathbf{r}\uparrow} - \frac{1}{2})(\hat{n}^f_{\mathbf{r}\downarrow} - \frac{1}{2})$, is called the symmetric periodic Anderson model (SPAM). In this chapter, the SPAM is the object of our study.

Continuing with our investigation of the orbital response of Kondo insulators to magnetic field, we in this chapter investigate the SPAM on square lattice. The theory of Kondo insulators, as worked out in the previous chapters, is applied here to the SPAM. Notably, with this theory of SPAM, we discover two inversions happening once each for the two kinds of charge quasiparticles (with narrow and broad bands), as the hybridization, V, decreases for a fixed U_f. The two inversions occur at two different points along V axis. It also gives us clear dHvA oscillations with frequency corresponding to the half Brillouin zone, like what we got for the half-filled KLM and H-KLM. Thus, we get consistent physics for all the three models of Kondo insulators.

This chapter is arranged in the following way. In Sec. 4.1, we introduce the SPAM. We then rewrite it in terms of the spinless fermions and Pauli operators using Kumar's representation [43], and derive from it the models to describe effective spin and charge dynamics of SPAM. In Sec. 4.2, we show that our canonical theory correctly describes the insulating ground state of SPAM, with a quantum phase transition from the Kondo singlet to AFM phase. In Sec. 4.3, we describe that the charge quasiparticle dispersions (narrow and broad) go through an inversion process as hybridization strength is decreased. Through the effective charge dynamics, we investigate the dHvA oscillations in the insulating ground state of SPAM in Sec. 4.4. We conclude and discuss the important results obtained in this chapter in Sec. 4.5.

4.1 Theory in Kumar Representation

The SPAM includes the nearest-neighbour hopping, t, for the conduction electrons, the hybridization, V, between the conduction and localized electrons, and an onsite repulsion, U_f, between the localized electrons. We denote the conduction and

localized electrons as c and f electrons, respectively. The Hamiltonian of S-PAM can be written as follows:

$$\hat{H} = -t \sum_{\mathbf{r},\boldsymbol{\delta}} \sum_{s=\uparrow,\downarrow} \hat{c}^{\dagger}_{\mathbf{r},s} \hat{c}_{\mathbf{r}+\boldsymbol{\delta},s} - V \sum_{\mathbf{r}} \sum_{s=\uparrow,\downarrow} \left[\hat{c}^{\dagger}_{\mathbf{r},s} \hat{f}_{\mathbf{r},s} + h.c. \right]$$
$$+ U_f \sum_{\mathbf{r}} \left(\hat{n}^f_{\mathbf{r},\uparrow} - \frac{1}{2} \right) \left(\hat{n}^f_{\mathbf{r},\downarrow} - \frac{1}{2} \right) \qquad (4.1)$$

where $\mathbf{r}$ is a lattice site, $\boldsymbol{\delta}$ denotes the nearest-neighbours of $\mathbf{r}$, and $s = \uparrow, \downarrow$ is the spin label. The fermion operators $\hat{c}^{\dagger}_{\mathbf{r},s}(\hat{c}_{\mathbf{r},s})$ create (annihilate) a conduction electron at site $\mathbf{r}$ with spin s, and likewise the operators $\hat{f}^{\dagger}_{\mathbf{r},s}(\hat{f}_{\mathbf{r},s})$ do for the localized electrons. The number of f electrons at site $\mathbf{r}$ with spin $s = \uparrow, \downarrow$ is $\hat{n}^f_{\mathbf{r},s} = f^{\dagger}_{\mathbf{r},s} f_{\mathbf{r},s}$. This model is symmetric under particle-hole transformation on any bipartite lattice. We use the following Kumar representation for c and f electron operators:
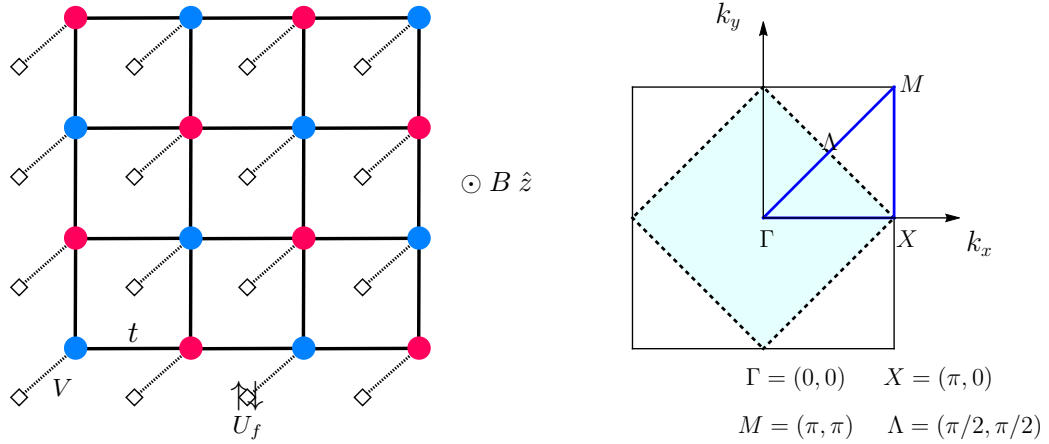
Figure 4.1: Left panel: A pictorial depiction of symmetric periodic Anderson model given in Eq. (4.1) on a bipartite square lattice. The solid circles are lattice sites where c electrons hop from one site to another with strength t, set to $t = 1$ as energy scale. The c electrons hybridize (V) with f electrons (shown as diamond). The f electrons feel repulsion (U_f) when they sit at the same site. An external magnetic field, B, is applied along $\hat{z}$ direction to see the quantum oscillations. Right panel: The full Brillouin zone (BZ) and half-BZ (faded blue region) of the square lattice and corresponding high symmetric lines.

	sublattice $\mathcal{A}$	sublattice $\mathcal{B}$
c-electrons	$\hat{c}_{\mathbf{r}\uparrow}^{\dagger} = \hat{\phi}_{a,\mathbf{r}}\sigma_{\mathbf{r}}^{+}$	$\hat{c}_{\mathbf{r}\uparrow}^{\dagger} = i\hat{\psi}_{b,\mathbf{r}}\sigma_{\mathbf{r}}^{+}$
	$\hat{c}_{\mathbf{r}\downarrow}^{\dagger} = \frac{1}{2}(i\hat{\psi}_{a,\mathbf{r}} - \hat{\phi}_{a,\mathbf{r}}\sigma_{\mathbf{r}}^{z})$	$\hat{c}_{\mathbf{r}\downarrow}^{\dagger} = \frac{1}{2}(\hat{\phi}_{b,\mathbf{r}} - i\hat{\psi}_{b,\mathbf{r}}\sigma_{\mathbf{r}}^{z})$
f-electrons	$\hat{f}_{\mathbf{r}\uparrow}^{\dagger} = i\hat{\eta}_{a,\mathbf{r}}\tau_{\mathbf{r}}^{+}$	$\hat{f}_{\mathbf{r}\uparrow}^{\dagger} = \hat{\chi}_{b,\mathbf{r}}\tau_{\mathbf{r}}^{+}$
	$\hat{f}_{\mathbf{r}\downarrow}^{\dagger} = \frac{1}{2}(\hat{\chi}_{a,\mathbf{r}} - i\hat{\eta}_{a,\mathbf{r}}\tau_{\mathbf{r}}^{z})$	$\hat{f}_{\mathbf{r}\downarrow}^{\dagger} = \frac{1}{2}(i\hat{\eta}_{b,\mathbf{r}} - \hat{\chi}_{b,\mathbf{r}}\tau_{\mathbf{r}}^{z})$

$$(4.2)$$

Here, $\hat{\phi}_{a,\mathbf{r}} = \hat{a}_{c,\mathbf{r}}^{\dagger} + \hat{a}_{c,\mathbf{r}}$, $i\hat{\psi}_{a,\mathbf{r}} = \hat{a}_{c,\mathbf{r}}^{\dagger} - \hat{a}_{c,\mathbf{r}}$ and $\hat{\chi}_{a,\mathbf{r}} = \hat{a}_{f,\mathbf{r}}^{\dagger} + \hat{a}_{f,\mathbf{r}}$, $i\hat{\eta}_{a,\mathbf{r}} = \hat{a}_{f,\mathbf{r}}^{\dagger} - \hat{a}_{f,\mathbf{r}}$ are the Majorana operators corresponding to the spinless fermions $\hat{a}_{c,\mathbf{r}}$ and $\hat{a}_{f,\mathbf{r}}$, respectively, on $\mathcal{A}$ sublattice. Similarly, $\hat{\phi}_{b,\mathbf{r}} = \hat{b}_{c,\mathbf{r}}^{\dagger} + \hat{b}_{c,\mathbf{r}}$, $i\hat{\psi}_{b,\mathbf{r}} = \hat{b}_{c,\mathbf{r}}^{\dagger} - \hat{b}_{c,\mathbf{r}}$ and $\hat{\chi}_{b,\mathbf{r}} = \hat{b}_{f,\mathbf{r}}^{\dagger} + \hat{b}_{f,\mathbf{r}}$, $i\hat{\eta}_{b,\mathbf{r}} = \hat{b}_{f,\mathbf{r}}^{\dagger} - \hat{b}_{f,\mathbf{r}}$ are the Majorana operators corresponding to the spinless fermions $\hat{b}_{c,\mathbf{r}}$ and $\hat{b}_{f,\mathbf{r}}$, respectively, on $\mathcal{B}$ sublattice. However, $\sigma_{\mathbf{r}}^{\pm}$, $\sigma_{\mathbf{r}}^{z}$ and $\tau_{\mathbf{r}}^{\pm}$, $\tau_{\mathbf{r}}^{z}$ are Pauli operators corresponding to the c and f electrons respectively. The Hamiltonian of the SPAM, given by Eq. (4.1), in this representation reads as:

$$
\begin{aligned}
\hat{H} = & -\frac{it}{2}\sum_{\mathbf{r}\in\mathcal{A}}\sum_{\boldsymbol{\delta}}\left[\hat{\psi}_{a,\mathbf{r}}\hat{\phi}_{b,\mathbf{r}+\boldsymbol{\delta}} + \hat{\psi}_{b,\mathbf{r}+\boldsymbol{\delta}}\hat{\phi}_{a,\mathbf{r}}\left(\boldsymbol{\sigma}_{\mathbf{r}}\cdot\boldsymbol{\sigma}_{\mathbf{r}+\boldsymbol{\delta}}\right)\right] \\
& -\frac{iV}{2}\sum_{\mathbf{r}\in\mathcal{A}}\left[\hat{\psi}_{a,\mathbf{r}}\hat{\chi}_{a,\mathbf{r}} + \hat{\eta}_{a,\mathbf{r}}\hat{\phi}_{a,\mathbf{r}}\left(\boldsymbol{\sigma}_{\mathbf{r}}\cdot\boldsymbol{\tau}_{\mathbf{r}}\right)\right] - \frac{iV}{2}\sum_{\mathbf{r}\in\mathcal{B}}\left[\hat{\eta}_{b,\mathbf{r}}\hat{\phi}_{b,\mathbf{r}} + \hat{\psi}_{b,\mathbf{r}}\hat{\chi}_{b,\mathbf{r}}\left(\boldsymbol{\sigma}_{\mathbf{r}}\cdot\boldsymbol{\tau}_{\mathbf{r}}\right)\right] \\
& -\frac{U_f}{2}\left[\sum_{\mathbf{r}\in\mathcal{A}}\hat{a}_{f,\mathbf{r}}^{\dagger}\hat{a}_{f,\mathbf{r}} + \sum_{\mathbf{r}\in\mathcal{B}}\hat{b}_{f,\mathbf{r}}^{\dagger}\hat{b}_{f,\mathbf{r}}\right] + \frac{U_f L}{4}
\end{aligned}
$$

$$(4.3)$$

Following the approach described in Chapter 2, and developed in Ref. [42], we decouple the spinless fermion and Pauli operator terms in Eq. (4.3). In this approximation, the SPAM reads as: $\hat{H} \approx \hat{H}_c + \hat{H}_s + e_0 L$, where $e_0 = -(\mathsf{z}t\zeta_1\rho_1 + 2V\zeta_2\rho_0)/4$,

$$
\begin{aligned}
\hat{H}_c = & -\frac{it}{2}\sum_{\mathbf{r}\in\mathcal{A}}\sum_{\boldsymbol{\delta}}\left[\hat{\psi}_{a,\mathbf{r}}\hat{\phi}_{b,\mathbf{r}+\boldsymbol{\delta}} + \rho_1\hat{\psi}_{b,\mathbf{r}+\boldsymbol{\delta}}\hat{\phi}_{a,\mathbf{r}}\right] - \frac{iV}{2}\sum_{\mathbf{r}\in\mathcal{A}}\left[\hat{\psi}_{a,\mathbf{r}}\hat{\chi}_{a,\mathbf{r}} + \rho_0\ \hat{\eta}_{a,\mathbf{r}}\hat{\phi}_{a,\mathbf{r}}\right] \\
& -\frac{iV}{2}\sum_{\mathbf{r}\in\mathcal{B}}\left[\hat{\eta}_{b,\mathbf{r}}\hat{\phi}_{b,\mathbf{r}} + \rho_0\hat{\psi}_{b,\mathbf{r}}\hat{\chi}_{b,\mathbf{r}}\right] - \frac{U_f}{2}\left[\sum_{\mathbf{r}\in\mathcal{A}}\hat{a}_{f,\mathbf{r}}^{\dagger}\hat{a}_{f,\mathbf{r}} + \sum_{\mathbf{r}\in\mathcal{B}}\hat{b}_{f,\mathbf{r}}^{\dagger}\hat{b}_{f,\mathbf{r}}\right] + \frac{U_f L}{4}
\end{aligned}
$$

$$(4.4)$$

describes the effective charge dynamics of the SPAM, and

$$
\hat{H}_s = \frac{t\zeta_1}{4}\sum_{\mathbf{r},\boldsymbol{\delta}}\boldsymbol{\sigma}_{\mathbf{r}}\cdot\boldsymbol{\sigma}_{\mathbf{r}+\boldsymbol{\delta}} + \frac{V\zeta_2}{2}\sum_{\mathbf{r}}\boldsymbol{\sigma}_{\mathbf{r}}\cdot\boldsymbol{\tau}_{\mathbf{r}}
$$

$$(4.5)$$

is the model of its effective spin dynamics. Here, L is the total number of lattice sites and z is the coordination number. Note that in $\hat{H}_s$, the $\mathbf{r}$ is summed over the

entire lattice, unlike for $\hat{H}_c$ where it is summed either of the sublattice. The $\boldsymbol{\delta}$ in both cases is summed over all the z nearest-neighbours. The mean-field parameters ρ_1, ρ_0, ζ_1, and ζ_2 are defined as follows:

$$\rho_1 = \frac{2}{zL} \sum_{\mathbf{r} \in \mathcal{A}} \sum_{\boldsymbol{\delta}} \langle \boldsymbol{\sigma}_{\mathbf{r}} \cdot \boldsymbol{\sigma}_{\mathbf{r}+\boldsymbol{\delta}} \rangle \tag{4.6a}$$

$$\rho_0 = \frac{1}{L} \sum_{\mathbf{r}} \langle \boldsymbol{\sigma}_{\mathbf{r}} \cdot \boldsymbol{\tau}_{\mathbf{r}} \rangle \tag{4.6b}$$

$$\zeta_1 = \frac{2i}{zL} \sum_{\mathbf{r} \in \mathcal{A}} \sum_{\boldsymbol{\delta}} \langle \hat{\phi}_{a,\mathbf{r}} \hat{\psi}_{b,\mathbf{r}+\boldsymbol{\delta}} \rangle \tag{4.6c}$$

$$\zeta_2 = \frac{i}{L} \langle \sum_{\mathbf{r} \in \mathcal{A}} \hat{\phi}_{a,\mathbf{r}} \hat{\eta}_{a,\mathbf{r}} + \sum_{\mathbf{r} \in \mathcal{B}} \hat{\chi}_{b,\mathbf{r}} \hat{\psi}_{b,\mathbf{r}} \rangle \tag{4.6d}$$

We calculate these parameters self-consistently in ground states of Eqs. (4.4) and (4.5). To find the ground state, we diagonalize the charge part, $\hat{H}_c$, numerically. However the spin dynamics, $\hat{H}_s$, is discussed using bond-operator mean-field theory [86, 60], similar to what we did for the Kondo lattice model [42].

4.1.1 Effective charge dynamics

To diagonalize $\hat{H}_c$ given in Eq. (4.4), we first write it directly in terms of the spinless fermion operators, by using the definition of the corresponding Majorana operators given below Eq. (4.2)

$$\begin{aligned}
\hat{H}_c = &-\frac{t}{2} \sum_{\mathbf{r} \in \mathcal{A}} \sum_{\boldsymbol{\delta}} \left[(1+\rho_1)\{\hat{a}_{c,\mathbf{r}}^\dagger \hat{b}_{c,\mathbf{r}+\boldsymbol{\delta}} + h.c.\} + (1-\rho_1)\{\hat{a}_{c,\mathbf{r}}^\dagger \hat{b}_{c,\mathbf{r}+\boldsymbol{\delta}}^\dagger + h.c.\} \right] \\
&-\frac{V}{2} \sum_{\mathbf{r} \in \mathcal{A}} \left[(1+\rho_0)\{\hat{a}_{c,\mathbf{r}}^\dagger \hat{a}_{f,\mathbf{r}} + h.c.\} + (1-\rho_0)\{\hat{a}_{c,\mathbf{r}}^\dagger \hat{a}_{f,\mathbf{r}}^\dagger + h.c.\} \right] \\
&-\frac{V}{2} \sum_{\mathbf{r} \in \mathcal{A}} \left[(1+\rho_0)\{\hat{b}_{f,\mathbf{r}}^\dagger \hat{b}_{c,\mathbf{r}} + h.c.\} + (1-\rho_0)\{\hat{b}_{f,\mathbf{r}}^\dagger \hat{b}_{c,\mathbf{r}}^\dagger + h.c.\} \right] \\
&-\frac{U_f}{2} \left[\sum_{\mathbf{r} \in \mathcal{A}} \hat{a}_{f,\mathbf{r}}^\dagger \hat{a}_{f,\mathbf{r}} + \sum_{\mathbf{r} \in \mathcal{B}} \hat{b}_{f,\mathbf{r}}^\dagger \hat{b}_{f,\mathbf{r}} \right] + \frac{U_f L}{4}
\end{aligned} \tag{4.7}$$

We use the Fourier transformation

$$\hat{a}_{\vartheta,\mathbf{r}} = \sqrt{\frac{2}{L}} \sum_{\mathbf{k}} e^{i\mathbf{k}\cdot\mathbf{r}} \, \hat{a}_{\vartheta,\mathbf{k}}$$

$$\hat{b}_{\vartheta,\mathbf{r}} = \sqrt{\frac{2}{L}} \sum_{\mathbf{k}} e^{i\mathbf{k}\cdot\mathbf{r}} \, \hat{b}_{\vartheta,\mathbf{k}}, \quad \vartheta = c, f \tag{4.8}$$

to go from the real $\mathbf{r}$-space to momentum $\mathbf{k}$-space. The $\hat{H}_c$ in $\mathbf{k}$-space reads as:

$$
\begin{aligned}
\hat{H}_c = &-\frac{t}{4}\sum_{\mathbf{k}}\Big[(1+\rho_1)|\gamma_{\mathbf{k}}|\Big\{\big(\hat{a}^{\dagger}_{c,\mathbf{k}}\hat{b}_{c,\mathbf{k}} + \hat{b}^{\dagger}_{c,\mathbf{k}}\hat{a}_{c,\mathbf{k}}\big) - \big(\hat{b}_{c,-\mathbf{k}}\hat{a}^{\dagger}_{c,-\mathbf{k}} + \hat{a}_{c,-\mathbf{k}}\hat{b}^{\dagger}_{c,-\mathbf{k}}\big)\Big\} \\
&+ (1-\rho_1)|\gamma_{\mathbf{k}}|\Big\{\big(\hat{a}^{\dagger}_{c,\mathbf{k}}\hat{b}^{\dagger}_{c,-\mathbf{k}} + \hat{b}_{c,-\mathbf{k}}\hat{a}_{c,\mathbf{k}}\big) - \big(\hat{b}^{\dagger}_{c,\mathbf{k}}\hat{a}^{\dagger}_{c,-\mathbf{k}} + \hat{a}_{c,-\mathbf{k}}\hat{b}_{c,\mathbf{k}}\big)\Big\}\Big] \\
&- \frac{V}{4}\sum_{\mathbf{k}}\Big[(1+\rho_0)\Big\{\big(\hat{a}^{\dagger}_{c,\mathbf{k}}\hat{a}_{f,\mathbf{k}} + \hat{a}^{\dagger}_{f,\mathbf{k}}\hat{a}_{c,\mathbf{k}}\big) - \big(\hat{a}_{f,-\mathbf{k}}\hat{a}^{\dagger}_{c,-\mathbf{k}} + \hat{a}_{c,-\mathbf{k}}\hat{a}^{\dagger}_{f,-\mathbf{k}}\big)\Big\} \\
&+ (1-\rho_0)\Big\{\big(\hat{a}^{\dagger}_{c,\mathbf{k}}\hat{a}^{\dagger}_{f,-\mathbf{k}} + \hat{a}_{f,-\mathbf{k}}\hat{a}_{c,\mathbf{k}}\big) - \big(\hat{a}^{\dagger}_{f,\mathbf{k}}\hat{a}^{\dagger}_{c,-\mathbf{k}} + \hat{a}_{c,-\mathbf{k}}\hat{a}_{f,\mathbf{k}}\big)\Big\} \\
&+ (1+\rho_0)\Big\{\big(\hat{b}^{\dagger}_{f,\mathbf{k}}\hat{b}_{c,\mathbf{k}} + \hat{b}^{\dagger}_{c,\mathbf{k}}\hat{b}_{f,\mathbf{k}}\big) - \big(\hat{b}_{c,-\mathbf{k}}\hat{b}^{\dagger}_{f,-\mathbf{k}} + \hat{b}_{f,-\mathbf{k}}\hat{b}^{\dagger}_{c,-\mathbf{k}}\big)\Big\} \\
&+ (1-\rho_0)\Big\{\big(\hat{b}^{\dagger}_{f,\mathbf{k}}\hat{b}^{\dagger}_{c,-\mathbf{k}} + \hat{b}_{c,-\mathbf{k}}\hat{b}_{f,\mathbf{k}}\big) - \big(\hat{b}^{\dagger}_{c,\mathbf{k}}\hat{b}^{\dagger}_{f,-\mathbf{k}} + \hat{b}_{f,-\mathbf{k}}\hat{b}_{c,\mathbf{k}}\big)\Big\}\Big] \\
&- \frac{U_f}{4}\sum_{\mathbf{k}}\Big[\hat{a}^{\dagger}_{f,\mathbf{k}}\hat{a}_{f,\mathbf{k}} + \hat{b}^{\dagger}_{f,\mathbf{k}}\hat{b}_{f,\mathbf{k}} - \hat{a}_{f,-\mathbf{k}}\hat{a}^{\dagger}_{f,-k} - \hat{b}_{f,-\mathbf{k}}\hat{b}^{\dagger}_{f,-\mathbf{k}}\Big] \quad (4.9)
\end{aligned}
$$

where $\mathbf{k} \in$ half-BZ, $\gamma_{\mathbf{k}} = \sum_{\boldsymbol{\delta}} e^{i\mathbf{k}\cdot\mathbf{r}} = |\gamma_{\mathbf{k}}|\, e^{i\varphi_{\mathbf{k}}}$, and a gauge transformation, $\hat{a}^{\dagger}_c(\mathbf{k}) \to e^{-i\varphi_{\mathbf{k}}}\hat{a}^{\dagger}_c(\mathbf{k})$ and $\hat{a}^{\dagger}_f(\mathbf{k}) \to e^{-i\varphi_{\mathbf{k}}}\hat{a}^{\dagger}_f(\mathbf{k})$, has been applied to absorb the phase factor $\phi_{\mathbf{k}}$. To diagonalize Eq. (4.9), we rewrite it in the Nambu basis in the following manner:

$$
\hat{H}_c = \sum_{\mathbf{k}} \Psi^{\dagger}_{\mathbf{k}} \mathcal{H}_{\mathbf{k}} \Psi_{\mathbf{k}} \quad (4.10)
$$

where the Nambu vector, $\Psi^{\dagger}_{\mathbf{k}}$, is an operator row-vector defined as:

$$
\Psi^{\dagger}_{\mathbf{k}} = \begin{bmatrix} \hat{a}^{\dagger}_{c,\mathbf{k}} & \hat{b}^{\dagger}_{c,\mathbf{k}} & \hat{b}^{\dagger}_{f,\mathbf{k}} & \hat{a}^{\dagger}_{f,\mathbf{k}} & \hat{a}_{c,-\mathbf{k}} & \hat{b}_{c,-\mathbf{k}} & \hat{b}_{f,-\mathbf{k}} & \hat{a}_{f,-\mathbf{k}} \end{bmatrix} \quad (4.11)
$$

and $\Psi_{\mathbf{k}} = [\Psi^{\dagger}_{\mathbf{k}}]^{\dagger}$. The $\mathcal{H}_{\mathbf{k}}$ is the following 8×8 matrix:

$$
\mathcal{H}_{\mathbf{k}} = \begin{bmatrix} A & B \\ -B & -A \end{bmatrix} \quad (4.12)
$$

with

$$
A = -\frac{1}{4}\begin{bmatrix} 0 & t|\gamma_{\mathbf{k}}|\rho_{1+} & 0 & V\rho_{0+} \\ t|\gamma_{\mathbf{k}}|\rho_{1+} & 0 & V\rho_{0+} & 0 \\ 0 & V\rho_{0+} & U & 0 \\ V\rho_{0+} & 0 & 0 & U \end{bmatrix} \quad \text{and} \quad (4.13a)
$$

$$B \;=\; -\frac{1}{4} \begin{bmatrix} 0 & t|\gamma_{\mathbf{k}}|\rho_{1-} & 0 & V\rho_{0-} \\ -t|\gamma_{\mathbf{k}}|\rho_{1-} & 0 & -V\rho_{0-} & 0 \\ 0 & V\rho_{0-} & U & 0 \\ -V\rho_{0-} & 0 & 0 & U \end{bmatrix}, \tag{4.13b}$$

where $\rho_{1\pm} = (1 \pm \rho_1)$ and $\rho_{0\pm} = (1 \pm \rho_0)$. We diagonalize Eq. (4.10) by applying Bogoliubov transformation for each $\mathbf{k}$. To do this, define a unitary matrix $\mathcal{U}_{\mathbf{k}}$ as:

$$\mathcal{U}_{\mathbf{k}} = \begin{bmatrix} W & X \\ X^* & W^* \end{bmatrix} \text{ where } W \text{ and } X \text{ are } 4 \times 4 \text{ matrices}, \tag{4.14}$$

such that

$$\mathcal{U}_{\mathbf{k}}^{\dagger} \mathcal{H}_{\mathbf{k}} \mathcal{U}_{\mathbf{k}} = \begin{bmatrix} \Sigma_{4\times4} & 0 \\ 0 & -\Sigma_{4\times4} \end{bmatrix} \text{ with } \Sigma_{4\times4} = \begin{bmatrix} E_1 & 0 & 0 & 0 \\ 0 & E_2 & 0 & 0 \\ 0 & 0 & E_3 & 0 \\ 0 & 0 & 0 & E_4 \end{bmatrix} \tag{4.15}$$

and $\Psi_{\mathbf{k}}^{\dagger} \mathcal{U}_{\mathbf{k}} = \Lambda_{\mathbf{k}}^{\dagger} = \begin{bmatrix} \Lambda_{\mathbf{k},1}^{\dagger} & \Lambda_{\mathbf{k},2}^{\dagger} & \Lambda_{\mathbf{k},3}^{\dagger} & \Lambda_{\mathbf{k},4}^{\dagger} & \Lambda_{-\mathbf{k},1} & \Lambda_{-\mathbf{k},2} & \Lambda_{-\mathbf{k},3} & \Lambda_{-\mathbf{k},4} \end{bmatrix}$ are the new canonical fermions. The fermion operators, $\Lambda_{\mathbf{k},i}$'s, describe the charge quasiparticles. In the diagonal form, in terms of these quasiparticle operators, the $\hat{H}_c$ reads as:

$$\hat{H}_c = \sum_{\mathbf{k}} \sum_{i=1}^{4} E_{\mathbf{k},i} \left(2\Lambda_{\mathbf{k},i}^{\dagger} \Lambda_{\mathbf{k},i} - 1 \right) \tag{4.16}$$

where $E_{\mathbf{k},i} > 0$, $i = 1, 2, 3, 4$ are the dispersions of the charge quasiparticles. The ground state of $\hat{H}_c$ is the vacuum of the $\Lambda_{\mathbf{k},i}$ quasiparticles i.e.

$$|G_c\rangle = \prod_{\mathbf{k}} \otimes \left(\prod_{i} \otimes |0\rangle_{\mathbf{k},i} \right) \tag{4.17}$$

So, in the ground state $\langle G_c|\Lambda_{\mathbf{k},i}^{\dagger}\Lambda_{\mathbf{k},i}|G_c\rangle = 0$ and $\langle G_c|\Lambda_{\mathbf{k},i}\Lambda_{\mathbf{k},i}^{\dagger}|G_c\rangle = 1$. Therefore, the ground state energy per site ($e_{g,c}$) of charge dynamics part is given by

$$e_{g,c} = -\frac{1}{L} \sum_{\mathbf{k}} \sum_{i=1}^{4} E_{\mathbf{k},i} \tag{4.18}$$

To find the mean-field parameters ζ_1 and ζ_2, we rewrite Eqs. (4.6c) and (4.6d) in $\mathbf{k}$-space, apply the Bogoliubov transformation begin by $\mathcal{U}_{\mathbf{k}}$, and then calculate the

expectation values in the vacuum of the charge quasiparticles (that is, the ground state of $\hat{H}_c$). This gives us the following equations for ζ_1 and ζ_2:

$$
\begin{aligned}
\zeta_1 &= \frac{2}{zL}\langle G_c| \sum_{\mathbf{k}} \left[|\gamma_{\mathbf{k}}|\{\left(\hat{a}_c^\dagger(\mathbf{k})\hat{b}_c^\dagger(-\mathbf{k}) - \hat{a}_c^\dagger(\mathbf{k})\hat{b}_c(\mathbf{k})\right) + h.c\}\right]|G_c\rangle \\
&= \frac{1}{zL}\langle G_c| \sum_{\mathbf{k}} \Psi_{\mathbf{k}}^\dagger M_{\zeta_1}(\mathbf{k})\Psi_{\mathbf{k}}|G_c\rangle
\end{aligned}
\tag{4.19}
$$

and,

$$
\begin{aligned}
\zeta_2 &= \frac{1}{L}\langle G_c| \sum_{\mathbf{k}} \left[\{(\hat{a}_c^\dagger(\mathbf{k})\hat{a}_f^\dagger(-\mathbf{k}) + h.c) + (\hat{b}_f^\dagger(\mathbf{k})\hat{b}_c^\dagger(-\mathbf{k}) + h.c)\right. \\
&\quad \left. -(\hat{a}_c^\dagger(\mathbf{k})\hat{a}_f(\mathbf{k}) + h.c) - (\hat{b}_f^\dagger(\mathbf{k})\hat{b}_c(\mathbf{k}) + h.c)\}\right]|G_c\rangle \\
&= \frac{1}{L}\langle G_c| \sum_{\mathbf{k}} \Psi_{\mathbf{k}}^\dagger M_{\zeta_2}(\mathbf{k})\Psi_{\mathbf{k}}|G_c\rangle
\end{aligned}
\tag{4.20}
$$

Here, $M_{\zeta_1}(\mathbf{k})$ and $M_{\zeta_2}(\mathbf{k})$ are 8×8 matrices and they are given as:

$$
M_{\zeta_1}(\mathbf{k}) = \begin{bmatrix}
0 & -|\gamma_{\mathbf{k}}| & 0 & 0 & 0 & |\gamma_k| & 0 & 0 \\
-|\gamma_{\mathbf{k}}| & 0 & 0 & 0 & -|\gamma_k| & 0 & 0 & 0 \\
0 & 0 & 0 & 0 & 0 & 0 & 0 & 0 \\
0 & 0 & 0 & 0 & 0 & 0 & 0 & 0 \\
0 & -|\gamma_{\mathbf{k}}| & 0 & 0 & 0 & |\gamma_k| & 0 & 0 \\
|\gamma_{\mathbf{k}}| & 0 & 0 & 0 & |\gamma_k| & 0 & 0 & 0 \\
0 & 0 & 0 & 0 & 0 & 0 & 0 & 0 \\
0 & 0 & 0 & 0 & 0 & 0 & 0 & 0
\end{bmatrix}
\tag{4.21}
$$

$$
M_{\zeta_2}(\mathbf{k}) = \begin{bmatrix}
0 & 0 & 0 & -1 & 0 & 0 & 0 & 1 \\
0 & 0 & -1 & 0 & 0 & 0 & -1 & 0 \\
0 & -1 & 0 & 0 & 0 & 1 & 0 & 0 \\
-1 & 0 & 0 & 0 & -1 & 0 & 0 & 0 \\
0 & 0 & 0 & -1 & 0 & 0 & 0 & 1 \\
0 & 0 & 1 & 0 & 0 & 0 & 1 & 0 \\
0 & -1 & 0 & 0 & 0 & 1 & 0 & 0 \\
1 & 0 & 0 & 0 & 1 & 0 & 0 & 0
\end{bmatrix}
\tag{4.22}
$$

Since, we know that $\Psi_{\mathbf{k}}^\dagger \mathcal{U}_{\mathbf{k}} = \Lambda_{\mathbf{k}}^\dagger \Rightarrow \Psi_{\mathbf{k}}^\dagger = \Lambda_{\mathbf{k}}^\dagger \mathcal{U}_{\mathbf{k}}^\dagger$ and $\Psi_{\mathbf{k}} = \mathcal{U}_{\mathbf{k}}\Lambda_{\mathbf{k}}$ because $\mathcal{U}_{\mathbf{k}}$ is unitary i.e. $\mathcal{U}_{\mathbf{k}}\mathcal{U}_{\mathbf{k}}^\dagger = \mathcal{U}_{\mathbf{k}}^\dagger\mathcal{U}_{\mathbf{k}} = \mathcal{I}$, where $\mathcal{I}$ is identity matrix. We use these relations

in ζ_1 and ζ_2 and find that

$$
\begin{aligned}
\zeta_1 &= \frac{1}{zL}\langle G_c|\sum_{\mathbf{k}}\Lambda_{\mathbf{k}}^{\dagger}\mathcal{U}_{\mathbf{k}}^{\dagger}M_{\zeta_1}(\mathbf{k})\mathcal{U}_{\mathbf{k}}\Lambda_{\mathbf{k}}|G_c\rangle \\
&= \frac{1}{zL}\langle G_c|\sum_{\mathbf{k}}\Lambda_{\mathbf{k}}^{\dagger}\tilde{M}_{\zeta_1}(\mathbf{k})\Lambda_{\mathbf{k}}|G_c\rangle
\end{aligned}
\tag{4.23}
$$

and

$$
\begin{aligned}
\zeta_2 &= \frac{1}{L}\langle G_c|\sum_{\mathbf{k}}\Lambda_{\mathbf{k}}^{\dagger}\mathcal{U}_{\mathbf{k}}^{\dagger}M_{\zeta_2}(\mathbf{k})\mathcal{U}_{\mathbf{k}}\Lambda_{\mathbf{k}}|G_c\rangle \\
&= \frac{1}{L}\langle G_c|\sum_{\mathbf{k}}\Lambda_{\mathbf{k}}^{\dagger}\tilde{M}_{\zeta_2}(\mathbf{k})\Lambda_{\mathbf{k}}|G_c\rangle
\end{aligned}
\tag{4.24}
$$

where, $\mathcal{U}_{\mathbf{k}}^{\dagger}M_{\zeta_1}(\mathbf{k})\mathcal{U}_{\mathbf{k}} = \tilde{M}_{\zeta_1}(\mathbf{k})$ and $\mathcal{U}_{\mathbf{k}}^{\dagger}M_{\zeta_2}(\mathbf{k})\mathcal{U}_{\mathbf{k}} = \tilde{M}_{\zeta_2}(\mathbf{k})$. Now, exploiting the ground state properties $\langle G_c|\Lambda_{\mathbf{k},i}^{\dagger}\Lambda_{\mathbf{k},j}|G_c\rangle = 0$ and $\langle G_c|\Lambda_{\mathbf{k},i}\Lambda_{\mathbf{k},j}^{\dagger}|G_c\rangle = \delta_{i,j}$ in above equations of ζ_1 and ζ_2, we arrive at the final expressions:

$$
\zeta_1 = \frac{1}{zL}\sum_{\mathbf{k}}\sum_{i=1}^{4}[\tilde{M}_{\zeta_1}(\mathbf{k})]_{i+4,i+4}
\tag{4.25a}
$$

$$
\zeta_2 = \frac{1}{L}\sum_{\mathbf{k}}\sum_{i=1}^{4}[\tilde{M}_{\zeta_2}(\mathbf{k})]_{i+4,i+4}
\tag{4.25b}
$$

4.1.2 Effective spin dynamics

The spin dynamics given by $\hat{H}_s$ of Eq. (4.5) is exactly like Eq. (2.8b) of Chapter 2. We study it by doing the same bond-operator mean-field theory, as we did in the previous two chapters. Taking an average Kondo singlet per site (that is, the local singlet between $\boldsymbol{\sigma}_{\mathbf{r}}$ and $\boldsymbol{\tau}_{\mathbf{r}}$) $\bar{s}$, we write $\boldsymbol{\sigma}_{\mathbf{r}}$ and $\boldsymbol{\tau}_{\mathbf{r}}$ approximately as: $\sigma_{\mathbf{r}}^{\alpha} \approx \bar{s}\left(t_{\alpha} + \hat{t}_{\alpha}^{\dagger}\right) \approx -\tau_{\mathbf{r}}^{\alpha}$, where $\alpha.\beta,\gamma = x,y,z$ denote the three components of Pauli operators and $\hat{t}_{\mathbf{r}\alpha}$ are the bosonic bond-operators representing triplet excitations above the average local singlet. These operators are physically constrained by the condition: $\hat{s}_{\mathbf{r}}^{\dagger}\hat{s}_{\mathbf{r}} + \sum_{\alpha}\hat{t}_{\mathbf{r}\alpha}^{\dagger}\hat{t}_{\mathbf{r}\alpha} = 1$, on every site, which in the mean-field approximation is satisfied only on average by using the same Lagrange multiplier λ for all sites. Refer to Sec. 2.3.2 for more discussion on bond-operator mean-field theory. In this theory, the local interaction between $\boldsymbol{\sigma}_{\mathbf{r}}$ and $\boldsymbol{\tau}_{\mathbf{r}}$, is written as follows:

$$
\boldsymbol{\sigma}_{\mathbf{r}} \cdot \boldsymbol{\tau}_{\mathbf{r}} \approx -3\bar{s}^2 + \sum_{\alpha}\hat{t}_{\mathbf{r}\alpha}^{\dagger}\hat{t}_{\mathbf{r}\alpha}
\tag{4.26}
$$

After making all these approximations, the $\hat{H}_s$ takes the following mean-field form

$$\hat{H}_s = \frac{t\zeta_1 \bar{s}^2}{4} \sum_\alpha \sum_{\mathbf{r},\boldsymbol{\delta}} \left[(\hat{t}^\dagger_{\mathbf{r},\alpha} + \hat{t}_{\mathbf{r},\alpha})(\hat{t}^\dagger_{\mathbf{r}+\boldsymbol{\delta},\alpha} + \hat{t}_{\mathbf{r}+\boldsymbol{\delta},\alpha}) \right] + \frac{V\zeta_2}{2} \sum_\mathbf{r} \left(-3\bar{s}^2 + \sum_\alpha \hat{t}^\dagger_{\mathbf{r},\alpha} \hat{t}_{\mathbf{r},\alpha} \right)$$
$$- \lambda \sum_\mathbf{r} \left(\bar{s}^2 + \sum_\alpha \hat{t}^\dagger_{\mathbf{r},\alpha} \hat{t}_{\mathbf{r},\alpha} - 1 \right). \tag{4.27}$$

In above we only keep upto bilinear terms and ignore the higher terms in triplet operators. The Hamiltonian in $\mathbf{k}$-space is obtained by doing Fourier transformation,

$$\hat{t}_{\mathbf{r}\alpha} = \sqrt{\frac{1}{L}} \sum_\mathbf{k} e^{i\mathbf{k}\cdot\mathbf{r}} \hat{t}_{\mathbf{k}\alpha}$$

where $\mathbf{k} \in$ full BZ. The final mean-field Hamiltonian has the following form

$$\hat{H}_s = L \left[\lambda \bar{s}^2 - \frac{5}{2}\lambda - 2V\zeta_2(\bar{s}^2 - 1/4) \right] + \frac{1}{2} \sum_{\mathbf{k},\alpha} \left\{ \left[\lambda + \frac{1}{2}t\zeta_1 \bar{s}^2 \gamma_\mathbf{k} \right] \right.$$
$$\left. \times \left(\hat{t}^\dagger_{\mathbf{k}\alpha} \hat{t}_{\mathbf{k}\alpha} + \hat{t}_{-\mathbf{k}\alpha} \hat{t}^\dagger_{-\mathbf{k}\alpha} \right) + \frac{1}{4}t\zeta_1 \bar{s}^2 \gamma_\mathbf{k} \left(\hat{t}^\dagger_{\mathbf{k}\alpha} \hat{t}^\dagger_{-\mathbf{k}\alpha} + \hat{t}_{-\mathbf{k}\alpha} \hat{t}_{\mathbf{k}\alpha} \right) \right\} \tag{4.28}$$

Here, L is the total number of sites, $\lambda \to (V\zeta_2/2 - \lambda)$ is the effective chemical potential, and $\gamma_\mathbf{k} = \sum_{\boldsymbol{\delta}} e^{i\mathbf{k}\cdot\boldsymbol{\delta}}$. This mean-field Hamiltonian can be diagonalized by applying the following Bogoliubov transformation:

$$\hat{t}_{\mathbf{k}\alpha} = \beta_{\mathbf{k}\alpha} \cosh\theta_\mathbf{k} + \beta^\dagger_{-\mathbf{k}\alpha} \sinh\theta_\mathbf{k} \tag{4.29}$$

Here, $\beta_{\mathbf{k}\alpha}$ is new bosonic operator (triplon quasiparticles). Under the above transformation, the operators in the mean-field Hamiltonian of Eq. (4.28) become

$$(\hat{t}^\dagger_{\mathbf{k}\alpha} \hat{t}_{\mathbf{k}\alpha} + \hat{t}_{-\mathbf{k}\alpha} \hat{t}^\dagger_{-\mathbf{k}\alpha}) = \cosh 2\theta_\mathbf{k} (\beta^\dagger_{\mathbf{k}\alpha} \beta_{\mathbf{k}\alpha} + \beta_{-\mathbf{k}\alpha} \beta^\dagger_{-\mathbf{k}\alpha})$$
$$+ \sinh 2\theta_\mathbf{k} (\beta^\dagger_{\mathbf{k}\alpha} \beta^\dagger_{-\mathbf{k}\alpha} + \beta_{-\mathbf{k}\alpha} \beta_{\mathbf{k}\alpha}) \tag{4.30a}$$
$$(\hat{t}^\dagger_{\mathbf{k}\alpha} \hat{t}^\dagger_{-\mathbf{k}\alpha} + \hat{t}_{-\mathbf{k}\alpha} \hat{t}_{\mathbf{k}\alpha}) = \sinh 2\theta_\mathbf{k} (\beta^\dagger_{\mathbf{k}\alpha} \beta_{\mathbf{k}\alpha} + \beta_{-\mathbf{k}\alpha} \beta^\dagger_{-\mathbf{k}\alpha})$$
$$+ \cosh 2\theta_\mathbf{k} (\beta^\dagger_{\mathbf{k}\alpha} \beta^\dagger_{-\mathbf{k}\alpha} + \beta_{-\mathbf{k}\alpha} \beta_{\mathbf{k}\alpha}) \tag{4.30b}$$

Substituting Eqs. (4.30a) and (4.30b) into Eq. (4.28) gives the following form of the Hamiltonian:

$$\hat{H}_s = \frac{1}{2} \sum_{\mathbf{k},\alpha} \left\{ \left[\left(\lambda + \frac{1}{2}t\zeta_1 \bar{s}^2 \gamma_\mathbf{k} \right) \cosh 2\theta_\mathbf{k} + \frac{1}{2}t\zeta_1 \bar{s}^2 \gamma_\mathbf{k} \sinh 2\theta_\mathbf{k} \right] \left(\beta^\dagger_{\mathbf{k}\alpha} \beta_{\mathbf{k}\alpha} + \beta_{-\mathbf{k}\alpha} \beta^\dagger_{-\mathbf{k}\alpha} \right) \right.$$

$$+ \left[\left(\lambda + \frac{1}{2} t \zeta_1 \bar{s}^2 \gamma_{\mathbf{k}} \right) \sinh 2\theta_{\mathbf{k}} + \frac{1}{2} t \zeta_1 \bar{s}^2 \gamma_{\mathbf{k}} \cosh 2\theta_{\mathbf{k}} \right] \left(\beta_{\mathbf{k}\alpha}^\dagger \beta_{-\mathbf{k}\alpha}^\dagger + \beta_{-\mathbf{k}\alpha} \beta_{\mathbf{k}\alpha} \right) \Bigg\} + e_0 L$$

$$(4.31)$$

By demanding that the off-diagonal terms in Eq. (4.31) be zero, we fix $\theta_{\mathbf{k}}$ as:

$$\left(\lambda + \frac{1}{2} t \zeta_1 \bar{s}^2 \gamma_{\mathbf{k}} \right) \sinh 2\theta_{\mathbf{k}} + \frac{1}{2} t \zeta_1 \bar{s}^2 \gamma_{\mathbf{k}} \cosh 2\theta_{\mathbf{k}} = 0$$

$$\Rightarrow \tanh 2\theta_{\mathbf{k}} = -\frac{\frac{1}{2} t \zeta_1 \bar{s}^2 \gamma_{\mathbf{k}}}{(\lambda + \frac{1}{2} t \zeta_1 \bar{s}^2 \gamma_{\mathbf{k}})} = \omega_k \qquad (4.32)$$

$$\Rightarrow \cosh 2\theta_{\mathbf{k}} = \frac{1}{\sqrt{1 - \omega_k^2}}, \quad \sinh 2\theta_{\mathbf{k}} = \frac{\omega_k}{\sqrt{1 - \omega_k^2}}. \qquad (4.33)$$

Substituting the values of $\cosh 2\theta_{\mathbf{k}}$ and $\sinh 2\theta_{\mathbf{k}}$ from Eq. (4.33) in Eq. (4.31), we get the following diagonal form for $\hat{H}_s$ in terms of triplons:

$$\hat{H}_s = e_0 L + \sum_{\mathbf{k},\alpha} \varepsilon_{\mathbf{k}} \left(\beta_{\mathbf{k}\alpha}^\dagger \beta_{\mathbf{k}\alpha} + \frac{1}{2} \right) \qquad (4.34)$$

Here, $e_0 = \left[\lambda \bar{s}^2 - \frac{5}{2} \lambda - 2V \zeta_2 (\bar{s}^2 - 1/4) \right]$, and $\varepsilon_{\mathbf{k}} = \sqrt{\lambda(\lambda + t \zeta_1 \bar{s}^2 \gamma_{\mathbf{k}})} \geq 0$ is the triplon dispersion. The ground state energy per site of spin dynamics part is given as:

$$e_{g,s} = e_0 + \frac{3}{2L} \sum_{\mathbf{k}} \varepsilon_{\mathbf{k}} \qquad (4.35)$$

We determine λ and $\bar{s}$ by minimizing $e_{g,s}$. Thus, by demanding that $\partial_\lambda e_{g,s} = 0$ and $\partial_{\bar{s}^2} e_{g,s} = 0$, we get the following equations for λ and $\bar{s}$.

$$\bar{s}^2 = \frac{5}{2} - \frac{3}{4L} \sum_{\mathbf{k}} \frac{2\lambda + t \zeta_1 \bar{s}^2 \gamma_{\mathbf{k}}}{\varepsilon_{\mathbf{k}}}, \text{ and} \qquad (4.36a)$$

$$\lambda = 2V \zeta_2 - \frac{3\lambda t \zeta_1}{4L} \sum_{\mathbf{k}} \frac{\gamma_{\mathbf{k}}}{\varepsilon_{\mathbf{k}}}. \qquad (4.36b)$$

Moreover, the decoupling parameters for the spin part are given as: $\rho_0 = 1 - 4\bar{s}^2$ and $\rho_1 = 4\bar{s}^2 (2V \zeta_2 - \lambda)/zt\zeta_1$.

We can determine ζ_1, ζ_2, ρ_0 and ρ_1, defined in Eqs. (4.6), numerically by solving the Eqs. (4.25) and (4.36) self-consistently through iterative method.
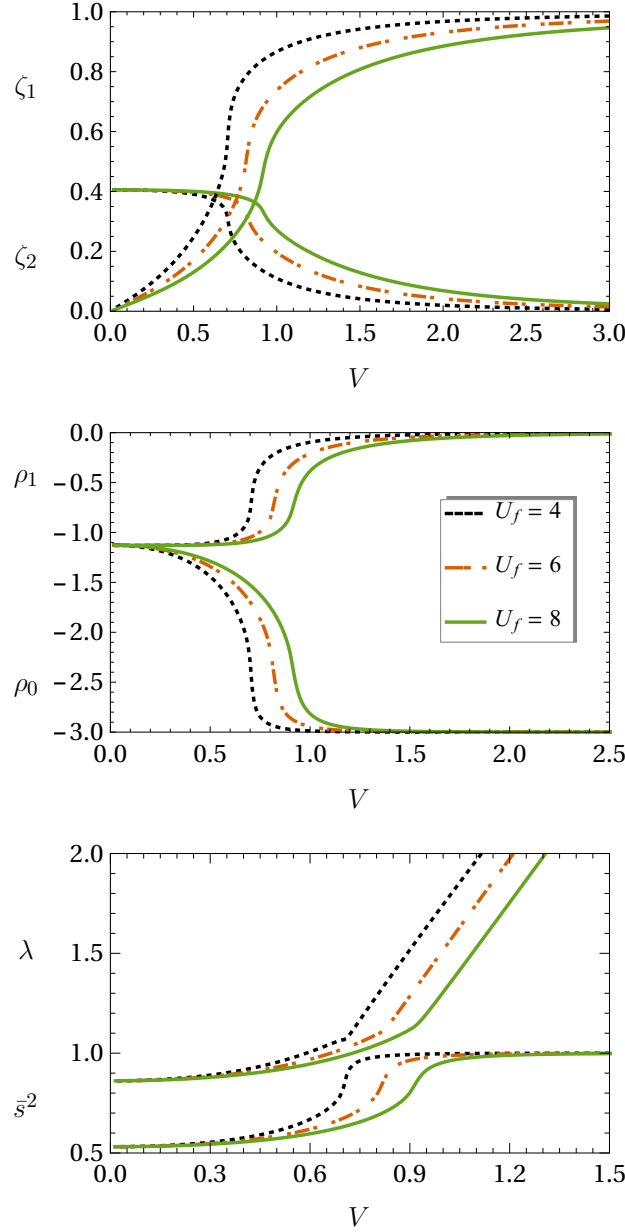
Figure 4.2: The behaviour of the mean-field parameters, ζ_1, ζ_2, ρ_0, ρ_1, λ and $\bar{s}^2$, of the charge and spin dynamics on square lattice, as a function of V for $U_f = 4, 6$, and 8. For large V, the ground is a perfect Kondo singlet with $\bar{s}^2 = 1$ (or $\rho_0 = -3$).

4.2 Magnetic Transition in the Ground State

Now we investigate the ground state properties of SPAM by self-consistently solving the Eqs. (4.25) and (4.36). Here, we put $t = 1$. The computed values of parameters are plotted in Fig. 4.2 as a function of V for different fixed values of U_f

on square lattice. We calculate the triplon dispersion and spin gap to understand the magnetic nature of the ground state. It generates the boundary between the Kondo singlet and antiferromagnetic (AFM) phases. We also compute the charge quasiparticle dispersions. It shows the ground state to be insulating, and notably, reveals two inversion transitions for the charge quasiparticles. But first, let us discuss the magnetic transition in the ground state.

4.2.1 Triplon dispersion and spin gap

We compute the triplon dispersion, $\varepsilon_{\mathbf{k}}$, as given in Eq. (4.34). It is found to show gapped behaviour for large values of V for any U_f. It remains gapped with decreasing V upto a critical value, V_c. Thus, for $V > V_c$, the system is in the spin-gapped Kondo singlet phase. At V_c, however, the $\varepsilon_{\mathbf{k}}$ becomes gapless at $\mathbf{k} = \mathbf{Q} = (\pi, \pi)$, and stays gapless as V is further decreased. The gapless nature of $\varepsilon_{\mathbf{k}}$ at $\mathbf{Q}$ implies Bose condensation for triplons, which in turn implies a phase transition to the Néel ordered AFM phase. This phase transition by decreasing V occurs for any U_f, but at a V_c which depends upon U_f. In Fig. 4.3, we have shown the behaviour of triplon dispersion, $\varepsilon_{\mathbf{k}}$, for two different values of V on both sides of V_c, for $U_f = 4$.
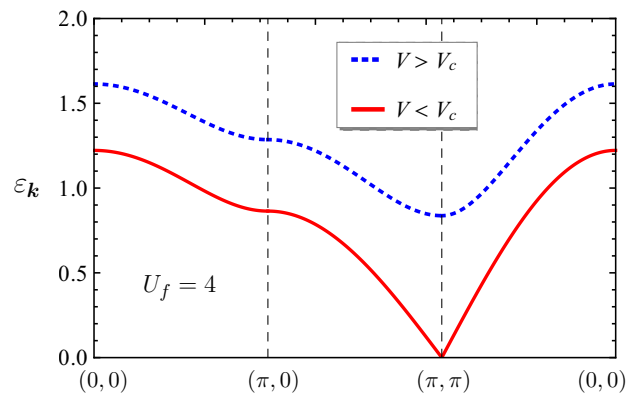
Figure 4.3: Triplon dispersion, $\varepsilon_{\mathbf{k}}$, along the high symmetric lines in full-BZ in Kondo singlet (blue dashed curve) and AFM phase (red solid curve) at $U_f = 4$. This phase transition occurs as V is decreased.

We also calculate the spin gap, Δ_s, as a function of V for different values of U_f. Since, the minima of $\varepsilon_{\mathbf{k}}$ is always at $\mathbf{Q}$, the spin gap is given by equation
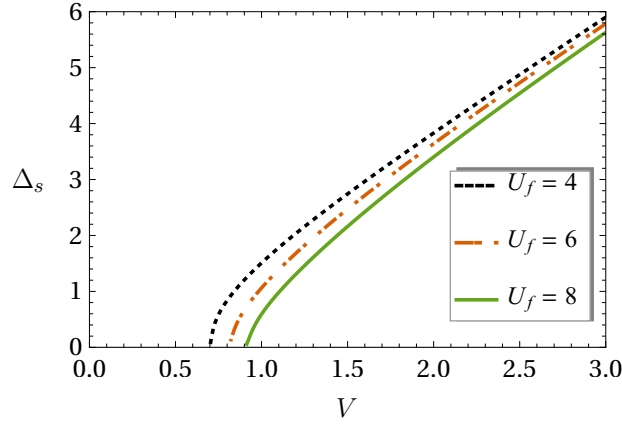
Figure 4.4: The spin gap, Δ_s vs. V for $U_f = 4, 6$ and 8. We can see that when U_f is increased the critical value, V_c, increases which means that U_f hepls to form an order between c and f electrons.

$\varepsilon_{\mathbf{Q}} = \Delta_s$. That is, $\Delta_s = \sqrt{\lambda(\lambda - \mathsf{z}t\zeta_1\bar{s}^2)}$. The calculated Δ_s vs. V is shown in Fig. 4.8, where the spin-gap closes continuously at V_c. We observe that as U_f is increased the critical value, V_c, also increases. Hence, the U_f helps the AFM order in the system.

4.2.2 Phase diagram

We calculate the quantum phase diagram of SPAM in V-U_f phase space. Instead of following the spin-gap by scanning through the entire V-U_f plane to find the critical points, we set up a direct scheme for calculating the phase boundary by imposing the condition, $\varepsilon_{\mathbf{Q}} = 0$, which marks the instability of the Kondo singlet phase towards magnetic ordering by the closing of the spin gap. It fixes λ of the bond-operator theory as: $\lambda = \mathsf{z}t\zeta_1\bar{s}^2$. After a few steps of manipulations of Eqs. (4.36) with this value of λ, we get the following equation for the critical hybridization, V_c, as:

$$V_c = \frac{1}{2}\mathsf{z}t(\bar{s}^2 + 3y)\left(\frac{\zeta_1}{\zeta_2}\right) \tag{4.37}$$

This is similar to Eq. (3.6) in Chapter 3. We find the self-consistent parameters of the spin part to become constants at the phase boundary as given below

$$\rho_0 = 1 - 4\bar{s}^2, \quad \rho_1 = 12\bar{s}^2 y \tag{4.38}$$

where, $\bar{s}^2 = 5/2 - 3x$ with

$$x = \frac{1}{4L} \sum_{\mathbf{k}} \frac{2 + (\gamma_{\mathbf{k}}/\mathsf{z})}{\sqrt{1 + (\gamma_{\mathbf{k}}/\mathsf{z})}}, \text{ and } y = \frac{1}{4L} \sum_{\mathbf{k}} \frac{(\gamma_{\mathbf{k}}/\mathsf{z})}{\sqrt{1 + (\gamma_{\mathbf{k}}/\mathsf{z})}}$$

as two constants. So, the critical hybridization value, V_c, depends implicitly upon
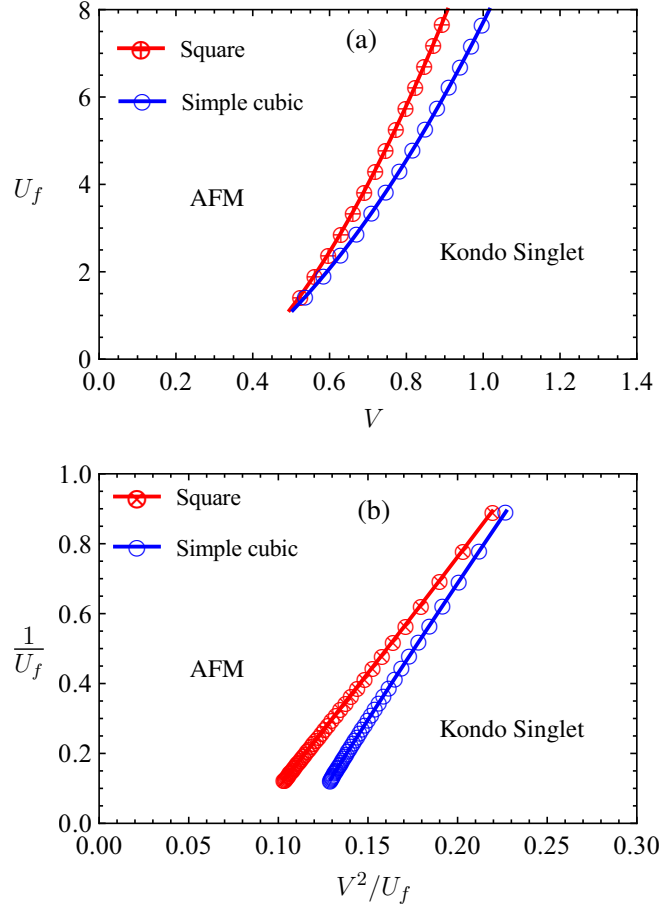
Figure 4.5: The quantum phase diagram of symmetric periodic Anderson model on square and simple cubic lattices, as obtained from Eq. (4.37) of our theory. We have presented it in two different ways: (a) in the V-U_f plane, and (b) in the $\frac{V^2}{U_f}$-$\frac{1}{U_f}$ plane. Here, $t = 1$.

U_f through the parameters ζ_1 and ζ_2 of the charge part.

We calculate V_c as a function of U_f in the ground state by solving the Eqs. (4.37) together with Eqs. (4.25) and (4.36), numerically iteratively. Thus, we obtain the phase boundary between the quantum paramagnetic Kondo singlet phase and the antiferromagnetic Néel phase in the V-U_f plane. The resulting quantum phase diagram, for square and simple cubic lattices, is shown in Fig. 4.5. We see that as

U_f is increased the V_c increases, which means that the AFM order lasts for large values of V for a bigger U_f. This is consistent with the fact that the effective Kondo exchange interaction in SPAM behaves as: $J \sim V^2/U_f$ [76, 87]. So, an increase in U_f reduces the strength of the effective Kondo coupling that allows the AFM order to survive upto the correspondingly larger value of V_c. For moderate to larger values of U, our theory produces a qualitatively correct phase diagram, agreeable with quantum monte carlo calculations [88, 89]. When U_f is small, the spin-density wave theory provides a better description, in which V_c rapidly goes to zero as U_f goes to zero [90, 89].

4.3   Two Inversions for the Charge Quasiparticles

Now let us discuss the nature of charge quasiparticles in our theory of SPAM. To this end, we numerically calculate the dispersions $E_{\mathbf{k},i}$ (for $i = 1, 2, 3, 4$) of the charge quasiparticles, as defined in Eq. (4.16). These $E_{\mathbf{k},i}$'s are the positive eigenvalues of the Hermitian matrix $\mathcal{H}_{\mathbf{k}}$ of Eq. (4.12). The evolution of these dispersions with respect to V, on square lattice, is presented in Fig. 4.6 for $U_f = 4$. Note that, for any non-zero V, the pair of quasiparticle bands, $E_{\mathbf{k},1}$ and $E_{\mathbf{k},2}$, is lower in energy by a finite energy difference than the pair $E_{\mathbf{k},3}$ and $E_{\mathbf{k},4}$. Moreover, the lowest dispersion, $E_{\mathbf{k},1}$, is strictly > 0 for $V \neq 0$. Hence, it describes an insulating state.

The bands $E_{\mathbf{k},1}$ and $E_{\mathbf{k},2}$ touch each other on the contour $|\gamma_{\mathbf{k}}| = 0$, which in the two-dimensional plots in Fig. 4.6 is the middle branch from $(\pi, 0)$ to $(\pi/2, \pi/2)$ lying on the boundary of the half-BZ of square lattice. The higher energy bands, $E_{\mathbf{k},3}$ and $E_{\mathbf{k},4}$, also touch each other exactly in the same way. Note that, for large V, we find that the band $E_{\mathbf{k},1}$ ($E_{\mathbf{k},2}$) has minima (maxima) at $\mathbf{k} = (0,0)$ and maxima (minima) at $|\gamma_{\mathbf{k}}| = 0$. Thus, they are mutually oppositely curved or oriented. Likewise, the dispersions $E_{\mathbf{k},3}$ ($E_{\mathbf{k},4}$) look the same. Notably, $E_{\mathbf{k},3}$ and $E_{\mathbf{k},4}$ are very narrow compared to $E_{\mathbf{k},1}$, and $E_{\mathbf{k},2}$, for large value of V, which however become broader with decreasing V. Eventually, for sufficiently small V's,
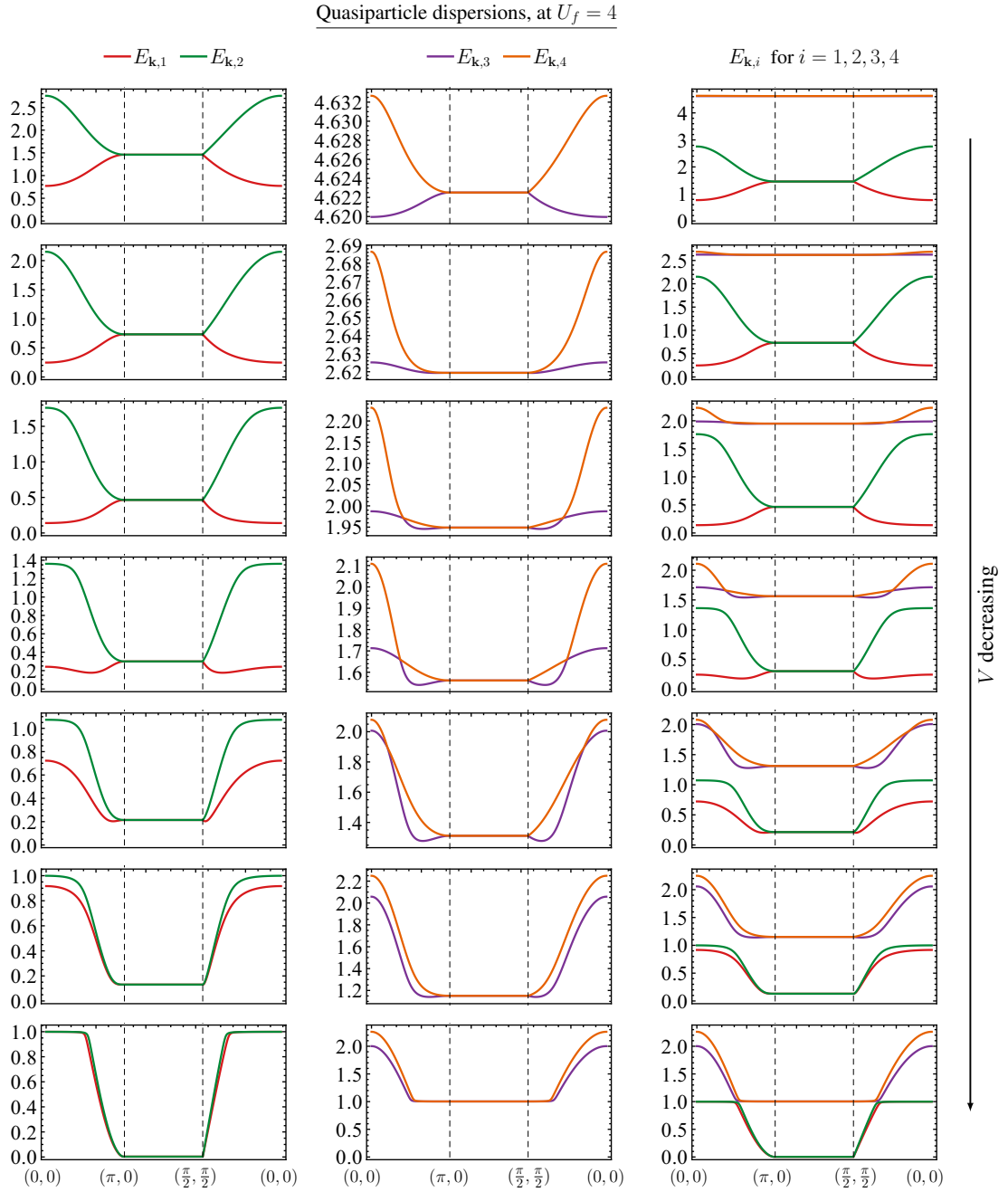
Figure 4.6: Evolution of the charge quasiparticle dispersions, $E_{\mathbf{k},i}$ for $i = 1, 2, 3, 4$, with respect to V along the high symmetric lines in half-BZ. We can clearly see the band inversion happening in $E_{\mathbf{k},1}$ (first column) and $E_{\mathbf{k},3}$ (second column) as V is decreased. In third column, all four bands are plotted together to see overall dispersion. Also note that higher energy narrow bands tend to become broader as V decreases.

they all become of comparable bandwidths.

More importantly, with decrease in V, we see two inversion transitions hap-

Figure 4.7: The charge quasiparticle dispersion $E_{\mathbf{k},1}$ of SPAM undergoes inversion across $V_{i,1}$ line (blue squares), and $E_{\mathbf{k},3}$ across $V_{i,3}$ line (orange up-triangles) in V-U_f plane. Also shown is the critical line (red circle) of transition from Kondo singlet to AFM phase.

pening separately for one narrow and one broad quasiparticle band. We find that for V lower than a characteristic value, $V_{i,3}$, the $\mathbf{k} = (0,0)$ is no more a point of minimum for $E_{\mat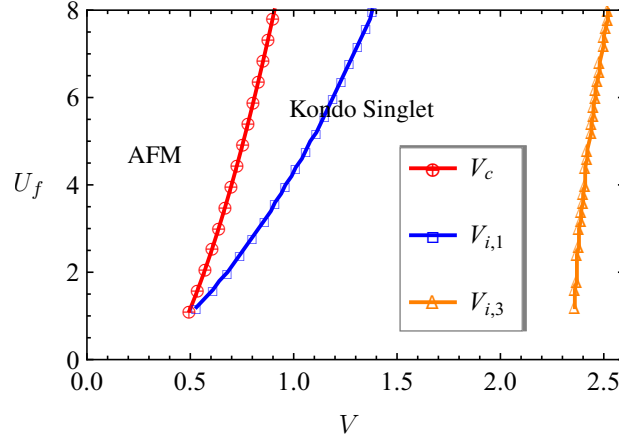hbf{k},3}$. Instead, for $V < V_{i,3}$, the Γ becomes a point of local maxima, and the minimum value of $E_{\mathbf{k},3}$ now shifts onto a contour around it, while the $E_{\mathbf{k},4}$ shows no such change. Neither $E_{\mathbf{k},1}$ and $E_{\mathbf{k},2}$ show any qualitative change across $V_{i,3}$, but only for a while! As we take V further down, there comes a second special point, $V_{i,1}$, below which $E_{\mathbf{k},1}$ (the lowest energy band) undergoes inversion in the same way. Finally, when V is sufficiently below the inversion point, $V_{i,1}$, both $E_{\mathbf{k},1}$ and $E_{\mathbf{k},3}$ get fully inverted and look pretty much like their partner bands, $E_{\mathbf{k},2}$ and $E_{\mathbf{k},4}$, respectively. Hence, like the KLM (and H-KLM), the charge quasiparticle bands of SPAM also undergo inversion transition. But the inversion in SPAM is richer by two! That is, the SPAM exhibits two inversion transitions, first for a narrow band and then for a broad quasiparticle band. This is indeed a novel finding for the symmetric periodic Anderson model. We find the inversion of $E_{\mathbf{k},1}$ and $E_{\mathbf{k},3}$ to occur for any U_f. Figure 4.7 shows the inversion transition lines for $V_{i,1}$ and $V_{i,3}$ in the V-U_f plane, together with the phase boundary between the Kondo singlet and AFM phases.
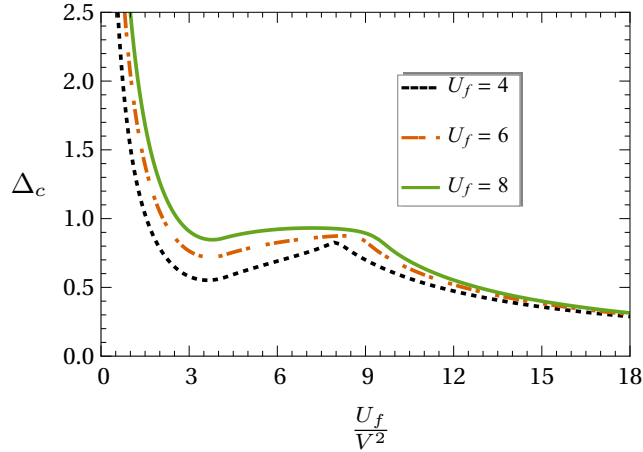
Figure 4.8: The charge gap, Δ_c, vs. $1/V$ for $U_f = 4, 6$ and 8. For large V (strong Kondo coupling), the Δ_c is large, and it come from the Γ point in the Brillouin zone. It decreases as V decreases, and across $V_{i,1}$, it comes from the points away from the Γ point.

Charge gap

In Fig. 4.6, we present the charge gap, Δ_c, calculated as a function of $1/V$ for different U_f. For strong hybridization (i.e., small $1/V$), $\Delta_c = E_{(0,0),1}$, because the Γ point is where the minimum of the lowest band $E_{\mathbf{k},1}$ is. But below $V < V_{i,1}$, due to inversion, the Γ point is no more the point of minima of $E_{\mathbf{k},1}$, and hence the Δ_c now comes from a certain contour around $\mathbf{k} = (0,0)$, which for sufficiently small V tends to the boundary of the half-Brillouin zone. This is qualitatively similar to the behaviour of the charge gaps for KLM and H-KLM (for example, see Fig. 3.13).

4.4 Quantum Oscillations of Magnetization

Our experience with KLM (and H-KLM) shows that after the inversion of the charge quasiparticle band, the dHvA oscillations show up nicely in the insulating ground state. Since we do find inversion happening also for the charge quasiparticles of SPAM, we are confident of seeing magnetic quantum oscillation here too. Thus motivated, we investigate the quantum oscillations of magnetization in the ground state of SPAM. For this purpose, we study the orbital response of SPAM

to uniform magnetic field, B, coupled to the electronic motion via Peierls phase as given below:

$$\hat{H} = -t \sum_{\mathbf{r},\boldsymbol{\delta}} \sum_{s=\uparrow,\downarrow} e^{i\frac{e}{\hbar}\int_{\mathbf{r}}^{\mathbf{r}+\boldsymbol{\delta}} \mathbf{A}\cdot \mathbf{dr}} \hat{c}_{\mathbf{r},s}^\dagger \hat{c}_{\mathbf{r}+\boldsymbol{\delta},s} - V \sum_{\mathbf{r}} \sum_{s=\uparrow,\downarrow} \left[\hat{c}_{\mathbf{r},s}^\dagger f_{\mathbf{r},s} + h.c. \right]$$
$$+ U_f \sum_{\mathbf{r}} \left(n_{\mathbf{r},\uparrow}^f - \frac{1}{2} \right) \left(n_{\mathbf{r},\downarrow}^f - \frac{1}{2} \right) \tag{4.39}$$

We take the vector potential as $\mathbf{A} = -By\hat{x}$, which gives the magnetic field, B, along the $\hat{z}$ direction. As for the KLM in Sec. 2.4, we derive the following field dependent minimal effective model of the charge dynamics from Eq. (4.39).

$$\begin{aligned}
\hat{H}_c^{[B]} &= -\frac{it}{2} \sum_{\mathbf{r}\in\mathcal{A}} \sum_{\boldsymbol{\delta}} \left\{ \left[\hat{\psi}_{a,\mathbf{r}} \hat{\phi}_{b,\mathbf{r}+\boldsymbol{\delta}} + \rho_1 \hat{\psi}_{b,\mathbf{r}+\boldsymbol{\delta}} \hat{\phi}_{a,\mathbf{r}} \right] \cos(2\pi\alpha \mathbf{r}_y \hat{x}\cdot\hat{\boldsymbol{\delta}}) \right\} \\
&\quad - \frac{iV}{2} \sum_{\mathbf{r}\in\mathcal{A}} \left[\hat{\psi}_{a,\mathbf{r}}\hat{\chi}_{b,\mathbf{r}} + \rho_0 \hat{\eta}_{b,\mathbf{r}}\hat{\phi}_{a,\mathbf{r}} \right] - \frac{iV}{2} \sum_{\mathbf{r}\in\mathcal{B}} \left[\hat{\eta}_{a,\mathbf{r}}\hat{\phi}_{b,\mathbf{r}} + \rho_0 \hat{\psi}_{b,\mathbf{r}}\hat{\chi}_{a,\mathbf{r}} \right] \\
&\quad - \frac{U_f}{2} \left[\sum_{\mathbf{r}\in\mathcal{A}} \hat{a}_{f,\mathbf{r}}^\dagger \hat{a}_{f,\mathbf{r}} + \sum_{\mathbf{r}\in\mathcal{B}} \hat{b}_{f,\mathbf{r}}^\dagger \hat{b}_{f,\mathbf{r}} \right] \tag{4.40}
\end{aligned}$$

Here, $\alpha = eBa^2/h$ is the reduced magnetic flux, with a as the lattice constant. The $\mathbf{r}_y$ and $\hat{\boldsymbol{\delta}} = \boldsymbol{\delta}/|\boldsymbol{\delta}|$ are the y coordinate of $\mathbf{r}$ and unit vector for $\boldsymbol{\delta}$, respectively.

To calculate magnetization, M, versus B from this Hofstadter like problem, we (for simplicity) put zero field values of ρ_0 and ρ_1 (calculated in Sec. 4.2) in the $\hat{H}_c^{[B]}$ of Eq. (4.40), and numerically find its ground state energy per site, e_g, as a function of $\alpha = \frac{p}{q}$ for integer $p = 1, 2, \ldots, q$ with $q = 601$ (a prime number) on square lattice. Using the definition $M = -\partial e_g/\partial \alpha$, we calculate M as a function of α. In Fig. 4.9, we present in two different ways the results of this calculation. Three plots on the left-hand side of this figure present the dHvA oscillation data for different values of V for a fixed $U_f = 4$, and on the right side, it is for different values of U_f for a fixed $V = 0.6$. Note that for $U_f = 4$, the critical point for transition from Kondo singlet to AFM phase is $V_c \approx 0.7$. The critical point along U_f axis for a fixed $V = 0.6$ is $U_{f,c} \approx 2.4$. Thus, by keeping one of these two fixed, we are varying the other across the critical point from one phase to another. In both case, we find that the oscillations become more prominent as the Kondo coupling becomes weaker. For a fixed U_f, it happens by decreasing V, and for a

dHvA oscillations at, $U_f = 4$
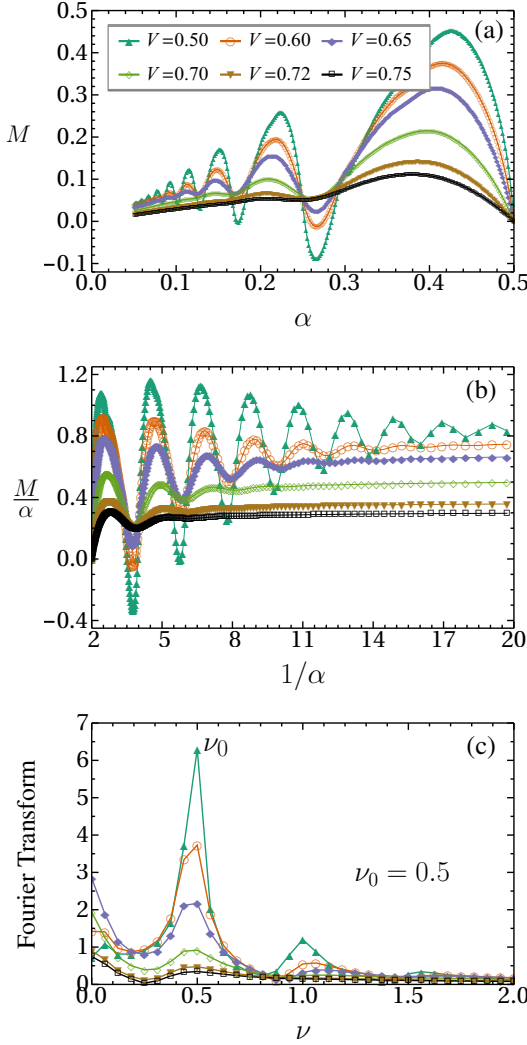
dHvA oscillations at, $V = 0.6$
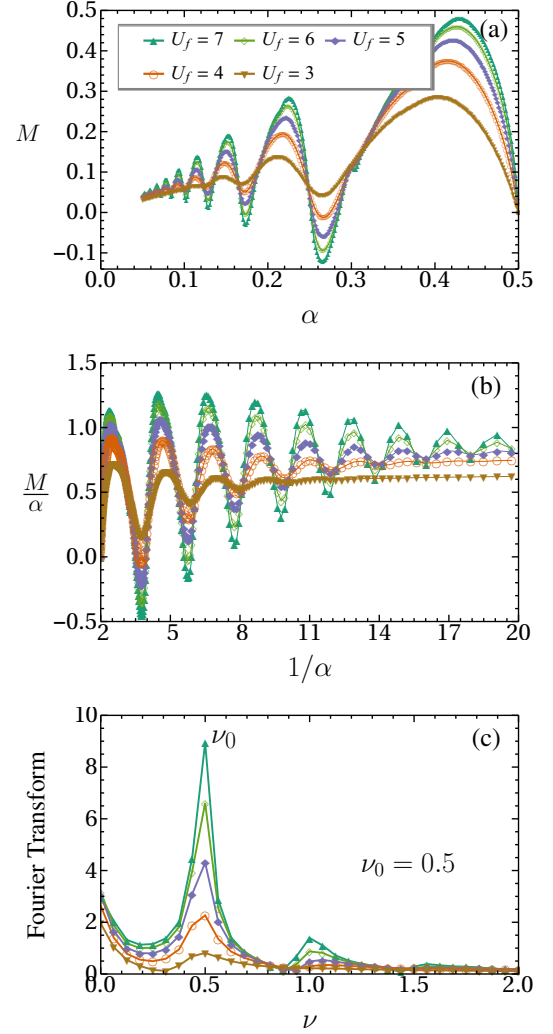
Figure 4.9: The dHvA oscillations in the insulating ground state of the symmetric periodic Anderson model on square lattice. On the left-hand side, we present the data for $V = 0.75, 0.72, 0.70$ (Kondo singlet) and $V = 0.65, 0.6, 0.5$ (Néel AFM) for a fixed $U_f = 4$. We see clear oscillations, both in the Kondo singlet and AFM phases, of frequency $\nu_0 = 0.5$ corresponding to the half-Brillouin zone (see Fig. 4.1). The data on the right side for different U_f's and $V = 0.6$, also shows the magnetic quantum oscillations with same features.

fixed V, it happens by increasing U_f. Remember that V^2/U_f is roughly speaking the measure of Kondo coupling in SPAM. Thus, we do get dHvA oscillations in the Kondo singlet phase close to critical point, but they are less prominent compared to the oscillations in the AFM phase for weaker couplings. However, for stronger

Kondo couplings ($V > V_{i3}$), we do not see any dHvA oscillations (hence, we don't show the data here), which affirms that the inversion of charge quasiparticles is very important for these oscillations to show-up. By doing the Fourier transformation of the M/α vs $1/\alpha$ data, we get the dominant frequency of dHvA oscillations, $\nu_0 = 0.5$, which corresponds to the half of the bulk Brillouin zone. Recall the relation, $A = (2\pi/a)^2\nu$, between the area A of an extremal orbit perpendicular to magnetic field on a constant energy surface in **k**-space and the frequency ν (in units of h/ea^2) of the dHvA oscillations. All these findings for SPAM are fully consistent with what we obtained for the KLM in the previous chapters.

4.5   Conclusion

In this chapter, we have investigated the symmetric periodic Anderson model using the theory of Kondo insulators that we developed for the half-filled Kondo lattice model. Our approach correctly produces the qualitative features of the Kondo insulating ground state of the SPAM. More importantly, it reveals the novel inversion phenomena also for the charge quasiparticles of SPAM, similar to what we got for the KLM. In fact, here, we get two inversion transitions, one each for a narrow (higher energy) and a board (lower energy) band of the charge quasiparticles. In the presence of uniform magnetic field coupled to the electronic motion, our theory also produces magnetic quantum oscillations of the frequency corresponding to the half-Brillouin zone (on bipartite lattice). The inversion has a direct bearing on these quantum oscillations which is clearly affirmed by the fact that the oscillations appear only after the quasiparticle bands have appropriately inverted. It is indeed very heartening and encouraging to see that our theory has produced a consistent physical understanding of all the three models of Kondo insulators, viz, the KLM, the H-KLM and the SPAM.

• • • • •

Chapter 5

Quantum Oscillations in Weakly Correlated Insulators

In the previous three chapters of this thesis, the theory that we developed to describe Kondo insulators was motivated to treat the interactions (Kondo exchange, Hubbard repulsion) respectfully. It basically approached the problem from the strong coupling side, and produced a consistent trend of physical behaviour in going towards weaker couplings in three different models of Kondo insulator. In particular, we found that the dHvA oscillations become more and more pronounced as the Kondo coupling gets weaker and weaker. Since the antiferromagnetically ordered insulating ground state in the weak coupling limit can be described very well by the spin density wave (SDW) mean-field theory (directly in terms of the electron operators) [91, 1], we are prompted to make an independent study of

magnetic quantum oscillations in the SDW insulators. This is what we do in the present chapter of this thesis.

A SDW state, caused by electron-electron interaction (howsoever small), is an instability of the metallic state. It involves the modulation of electronic spins with some characteristic periodicity (given by nesting wavevector, $\mathbf{Q}$), which is not necessarily commensurate with the underlying lattice. This spin density wave opens up a single-particle gap at the Fermi level, due to which, the system may either behave as an insulator if the gap opens on the entire Fermi surface (as in the quasi one dimensional Bechgaard salts $(TMTSF)_2PF_6$ [92]), or may continue to be a metal if the Fermi surface partially survives (say, as in Cr metal [93], or LaFePO [94, 95, 96]). On the half-filled hypercubic lattices, due to perfect nesting of the Fermi surface, [1] the spin density modulation leads to an insulating ground state with Néel AFM order commensurate with the lattice.

In this chapter, we calculate the orbital response to magnetic field in the weak-coupling Néel insulating ground states of the Hubbard and Kondo lattice models (on square and simple cubic lattices at half-filling) by doing a simple mean-field theory directly in terms of electron operators. As expected from our studies in Chapter 2, we do get clear dHvA oscillations in these weakly correlated insulating states. This study suggests that, apart from the Kondo insulators, the quantum oscillations of magnetization can also occur in other kinds of insulators (correlated or otherwise).

5.1 Small U Hubbard Model at Half-Filling

Motivated by the similarities between the effective charge dynamics of the KLM and Hubbard models in Kumar's representation, in Sec. 2.5 we had investigated and found the dHvA oscillations in the insulating ground state of the half-filled Hubbard model. The amplitude of these oscillations was found to grow with increase in t/U, suggesting that dHvA effect would occur also in the weakly correlated (small U) Hubbard model, a straightforward approach (directly in terms of the electron operators) that appropriately

---

[1]Say, with respect to $\mathbf{Q} = (\pi, \pi)$ on square lattice, or $\mathbf{Q} = (\pi, \pi, \pi)$ on simple cubic lattice.

describes the insulating AFM ground state is the SDW mean-field theory. In this section, we discuss the dHvA oscillations in the SDW insulating ground state of the half-filled Hubbard model on square and simple cubic lattices. In the next section, we will do the same for the half-filled KLM.

To study dHvA oscillations in an SDW insulator, we consider the following symmetric Hubbard model on bipartite lattice:

$$\hat{H} = -t \sum_{\mathbf{r},\boldsymbol{\delta}} \sum_{\sigma} e^{i\frac{e}{\hbar} \int_{\mathbf{r}}^{\mathbf{r}+\boldsymbol{\delta}} \mathbf{A}\cdot d\mathbf{r}} \hat{c}_{\mathbf{r},\sigma}^{\dagger} \hat{c}_{\mathbf{r}+\boldsymbol{\delta},\sigma} + U \sum_{\mathbf{r}} \left(\hat{n}_{\mathbf{r},\uparrow} - \frac{1}{2} \right) \left(\hat{n}_{\mathbf{r},\downarrow} - \frac{1}{2} \right) \qquad (5.1)$$

Here, $\mathbf{r}$ is sum over the lattice sites, $\boldsymbol{\delta}$ is summed over the nearest neighbours of $\mathbf{r}$, and $\sigma = \uparrow, \downarrow$ is spin label. The $\hat{c}_{\mathbf{r},\sigma}^{\dagger}(\hat{c}_{\mathbf{r},\sigma})$ are electron creation (annihilation) operators and $\hat{n}_{\mathbf{r},\sigma}$ is number operator. The first term in Eq. (5.1) of $\hat{H}$ is the kinetic energy with hopping, $t > 0$, between nearest neighbour sites, and magnetic field is coupled to the electron motion through Peierls phase factor in terms of vector potential, $\mathbf{A} = B(-y, 0, 0)$ for magnetic field B along $\hat{z}$ direction. The second term, with $U > 0$, is the onsite repulsion. If you expand this term, you get $U/2$ as the chemical potential, which guarantees half-filling on any bipartite lattice due to the particle-hole symmetry of this model. So, Eq. (5.1) is the Hamiltonian of the half-filled Hubbard model.

5.1.1 SDW mean-field theory on bipartite lattices

When U is not strong compared to the bandwidth, it has been found reasonable to treat the Hubbard interaction, $U \sum_{\mathbf{r}} \hat{n}_{\mathbf{r}\uparrow} \hat{n}_{\mathbf{r}\downarrow}$, in the Hartree-Fock approximation, which decouples the two-body interaction into self-consistently determined single particle terms. This simple mean-field decoupling is given as:

$$\hat{n}_{\mathbf{r},\uparrow} \hat{n}_{\mathbf{r},\downarrow} = \hat{n}_{\mathbf{r},\uparrow} \langle \hat{n}_{\mathbf{r},\downarrow} \rangle + \langle \hat{n}_{\mathbf{r},\uparrow} \rangle \hat{n}_{\mathbf{r},\downarrow} - \langle \hat{n}_{\mathbf{r},\uparrow} \rangle \langle \hat{n}_{\mathbf{r},\downarrow} \rangle .$$

The SDW, that is, the spin density wave approximation amounts to considering the following periodic spatial modulation for the mean fields [1].

$$
\begin{aligned}
\langle \hat{n}_{\mathbf{r},\sigma} \rangle &= \frac{n}{2} + \eta_{\sigma}\, m_s e^{i\boldsymbol{Q}\cdot\mathbf{r}} \\
&\text{with } \langle S_{\mathbf{r}}^{z} \rangle = \frac{1}{2} \langle \hat{n}_{\mathbf{r},\uparrow} - \hat{n}_{\mathbf{r},\downarrow} \rangle = m_s\, e^{i\boldsymbol{Q}\cdot\mathbf{r}}
\end{aligned}
\qquad (5.2)
$$

Here, n is the average number of electrons per site (which is 1 at half-filling), m_s is the magnitude of the staggered magnetic moment (which is to be determined self-consistently), and the wavevector $\boldsymbol{Q} = \boldsymbol{\pi}$ corresponds to the Néel SDW on hypercubic lattice. [2] This $\mathbf{Q}$ is so chosen, because $\boldsymbol{\pi}$ is the nesting wavevector for the Fermi surface of the half-filled tight binding model with nearest neighbour hoping on a hypercubic lattice. See Fig. 5.1
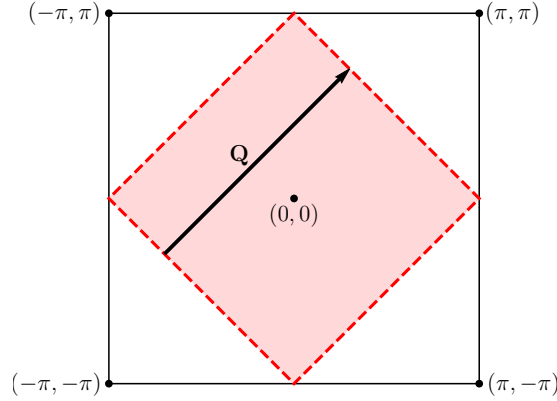

Figure 5.1: Nesting on square lattice. The large square enclosed by solid black lines is full-BZ however the faded light red region represents half-BZ. The edges of half-BZ describe the Fermi-surface at half-filling when $U = 0$. Here, $\mathbf{Q} = \boldsymbol{\pi}$ is the nesting vector which connects a large portion of Fermi surface to the other.

On a bipartite lattice, if the magnetic moment $\langle S_{\mathbf{r}}^z \rangle = m_s$ for $\mathbf{r} \in \mathcal{A}$ sublattice, then it is $-m_s$ on $\mathcal{B}$ sublattice, because $\mathbf{Q} = \boldsymbol{\pi}$. Moreover, $\eta_\uparrow = +1$ and $\eta_\downarrow = -1$. In this approximation, Eq. (5.1) takes the following form (written in the two sublattice notation):

$$\hat{H} = \sum_\sigma \left\{ -t \sum_{\mathbf{r} \in \mathcal{A}} \sum_{\boldsymbol{\delta}} \left[e^{i\frac{e}{\hbar} \int_{\mathbf{r}}^{\mathbf{r}+\boldsymbol{\delta}} \mathbf{A} \cdot d\mathbf{r}} \hat{a}_{\mathbf{r},\sigma}^\dagger \hat{b}_{\mathbf{r}+\boldsymbol{\delta},\sigma} + \text{h.c.} \right] + U \sum_{\mathbf{r} \in \mathcal{A}} \left[\frac{n-1}{2} - \eta_\sigma m_s \right] \hat{a}_{\mathbf{r},\sigma}^\dagger \hat{a}_{\mathbf{r},\sigma} \right.$$
$$\left. + U \sum_{\mathbf{r} \in \mathcal{B}} \left[\frac{n-1}{2} + \eta_\sigma m_s \right] \hat{b}_{\mathbf{r},\sigma}^\dagger \hat{b}_{\mathbf{r},\sigma} \right\} + e_0 L \tag{5.3}$$

Here, $e_0 = U(m_s^2 - \frac{n^2}{4} + \frac{1}{4})$ is a constant, L is total number of lattice sites, and $\hat{a}_{\mathbf{r},\sigma}^\dagger (\hat{a}_{\mathbf{r},\sigma})$ and $\hat{b}_{\mathbf{r},\sigma}^\dagger (\hat{b}_{\mathbf{r},\sigma})$ are electron creation (annihilation) operators at site $\mathbf{r}$ with spin σ on $\mathcal{A}$ and $\mathcal{B}$ sublattice, respectively. Since Eq. (5.3) is bilinear in the

---

[2]The wavevector $\boldsymbol{\pi}$ denotes $(\pi/a, \pi/a)$ for square lattice and $(\pi/a, \pi/a, \pi/a)$ for simple cubic lattice, with a as the lattice constant.

electronic creation and annihilation operators, therefore we can diagonalize it using Bogoliubov transformation. Before we compute the magnetic response in the ground state of Eq. (5.3), let us briefly describe the basic physics in the absence of magnetic field.

For $B = 0$, the SDW Hamiltonian of Eq. (5.3) is translationally invariant. To further simplify it, we use Fourier transformation as defined below

$$
\hat{a}_{\mathbf{r},\sigma} = \sqrt{\frac{2}{L}} \sum_{\mathbf{k}} e^{i\mathbf{k}\cdot\mathbf{r}} \, \hat{a}_{\mathbf{k},\sigma}
$$

$$
\hat{b}_{\mathbf{r},\sigma} = \sqrt{\frac{2}{L}} \sum_{\mathbf{k}} e^{i\mathbf{k}\cdot\mathbf{r}} \, \hat{b}_{\mathbf{k},\sigma} \tag{5.4}
$$

Here, $\mathbf{k} \in$ half Brillouin zone (BZ) or magnetic Brillouin zone (see in Fig. 5.1). The SDW Hamiltonian in the $\mathbf{k}$-space reads as:

$$
\hat{H} = \sum_{\mathbf{k},\sigma} \Bigg\{ -t \left(\gamma_{\mathbf{k}} \hat{a}^{\dagger}_{\mathbf{k},\sigma} \hat{b}_{\mathbf{k},\sigma} + \text{h.c.} \right) + U m_s \eta_{\sigma} \left(\hat{b}^{\dagger}_{\mathbf{k},\sigma} \hat{b}_{\mathbf{k},\sigma} - \hat{a}^{\dagger}_{\mathbf{k},\sigma} \hat{a}_{\mathbf{k},\sigma} \right)
$$

$$
+ \frac{U(n-1)}{2} \left(\hat{a}^{\dagger}_{\mathbf{k},\sigma} \hat{a}_{\mathbf{k},\sigma} + \hat{b}^{\dagger}_{\mathbf{k},\sigma} \hat{b}_{\mathbf{k},\sigma} \right) \Bigg\} + e_0 L \tag{5.5}
$$

with $\gamma_{\mathbf{k}} = \sum_{\boldsymbol{\delta}} e^{i\mathbf{k}\cdot\boldsymbol{\delta}}$. Now we use the Bogoliubov transformation,

$$
\hat{a}_{\mathbf{k},\sigma} = \cos\theta_{\mathbf{k}} \, \alpha_{\mathbf{k},\sigma} - e^{i\phi_{\mathbf{k}}} \sin\theta_{\mathbf{k}} \, \beta_{\mathbf{k},\sigma}
$$

$$
\hat{b}_{\mathbf{k},\sigma} = e^{-i\phi_{\mathbf{k}}} \sin\theta_{\mathbf{k}} \, \alpha_{\mathbf{k},\sigma} + \cos\theta_{\mathbf{k}} \, \beta_{\mathbf{k},\sigma}, \tag{5.6}
$$

with $\theta_{\mathbf{k}} = \frac{1}{2} \tan^{-1} \left[\frac{t|\gamma_{\mathbf{k}}|}{U m_s \eta_{\sigma}} \right]$, to diagonalize Eq. (5.5). The SDW Hamiltonian in the diagonalized form can be written as:

$$
\hat{H} = e_0 L + \sum_{\mathbf{k},\sigma} \left[E_{\mathbf{k},-} \, \alpha^{\dagger}_{\mathbf{k},\sigma} \alpha_{\mathbf{k},\sigma} + E_{\mathbf{k},+} \, \beta^{\dagger}_{\mathbf{k},\sigma} \beta_{\mathbf{k},\sigma} \right] \tag{5.7}
$$

where $E_{\mathbf{k},\pm} = \frac{U(n-1)}{2} \pm \sqrt{(U m_s)^2 + (t|\gamma_{\mathbf{k}}|)^2}$ are the electronic dispersions.

Since $n = 1$ at half-filling, the only mean-field parameter m_s is determined self-consistently by minimizing the ground state energy of Eq. (5.7). In the ground state of Eq. (5.7) at half-filling, the $E_{\mathbf{k},+}$ band is fully empty, while the $E_{\mathbf{k},-}$ band is fully filled. Therefore, the ground state energy per site (e_g) is given by

$$
e_g = e_0 + \frac{2}{L} \sum_{\mathbf{k}} E_{\mathbf{k},-} \tag{5.8}
$$

The energy minimization condition, $\frac{\partial e_g}{\partial m_s} = 0$, gives the following equation for m_s.

$$m_s = \frac{1}{L} \sum_{\mathbf{k}} \frac{m_s U}{\sqrt{(U m_s)^2 + (t|\gamma_{\mathbf{k}}|)^2}} \tag{5.9}$$

This equation obviously has a paramagnetic (PM) solution, $m_s = 0$, which is not the lowest energy solution. The non-zero m_s in the ground state is given by the solution of the equation, $1 = \frac{1}{L} \sum_{\mathbf{k}} \frac{U}{\sqrt{(U m_s)^2 + (t|\gamma_{\mathbf{k}}|)^2}}$.
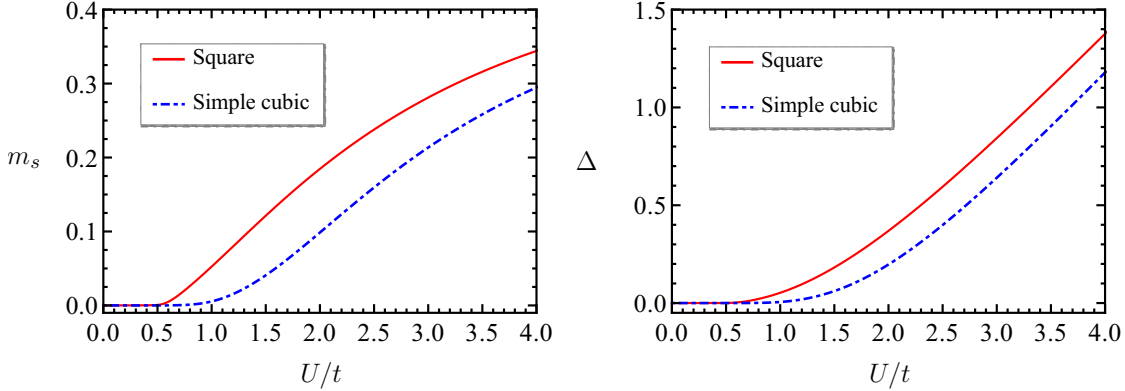
Figure 5.2: The staggered magnetization, m_s, and the band gap, Δ, vs. U/t of the SDW ground state of the half-filled Hubbard model. They are always non-zero, but for $U/t \ll 1$, they are expectedly exponentially small.
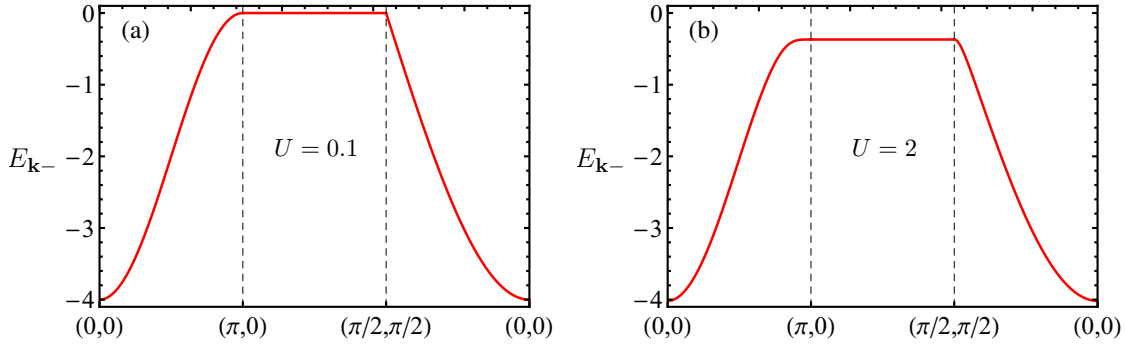
Figure 5.3: Square lattice: 2d plot of dispersion, $E_{\mathbf{k}-}$ along symmetric lines, for $U = 0.1$ and $U = 2.0$. The dispersion is always minimum (maximum) at $\mathbf{k} = 0$ ($|\gamma_{\mathbf{k}}| = 0$) point. As we see, there is no inversion or Lifshitz like phenomenon observed in the insulating ground state of SDW quasiparticles dispersion for any value of U, and this is also true for simple cubic.

The top (bottom) of the fully occupied (empty) band, $E_{\mathbf{k},-}$ ($E_{\mathbf{k}+}$), lies at the $|\gamma_{\mathbf{k}}| = 0$. This gives a band gap, $\Delta = 2U m_s$. The staggered magnetization, m_s,

and the gap, Δ, are plotted as a function of U/t for the square and simple cubic lattices in Fig. (5.2). We have taken $t = 1$ for all the calculation. The gap, Δ, is found to be non-zero for any U, howsoever small. Thus, the Néel SDW ground state of the half-filled Hubbard model is always gapped, and hence insulating. For U very small compared to t, the SDW state is known to behave as $m_s \sim \Delta \sim e^{-t/U}$, which is why get tiny gap and staggered moment for very mall U/t. Next we study dHvA oscillations in this SDW insulating ground state.

5.1.2 dHvA oscillations in the SDW insulating state

To investigate dHvA oscillations in the SDW insulator, we numerically compute M in the ground state of the following Hamiltonian, which is Eq. (5.3) for $n = 1$ (half-filling) in the magnetic field, B, given by $\mathbf{A} = -By\hat{x}$ and parameterized as, $\alpha = eBa^2/h$.

$$\hat{H} = \sum_\sigma \left\{ -t \sum_{\mathbf{r} \in \mathcal{A}} \sum_{\boldsymbol{\delta}} \left[e^{2\pi i \alpha \mathbf{r}_y \hat{x} \cdot \hat{\boldsymbol{\delta}}} \, \hat{a}^\dagger_{\mathbf{r},\sigma} \hat{b}_{\mathbf{r}+\boldsymbol{\delta},\sigma} + \text{h.c.} \right] \right.$$
$$\left. + U m_s \eta_\sigma \left(\sum_{\mathbf{r} \in \mathcal{B}} \hat{b}^\dagger_{\mathbf{r},\sigma} \hat{b}_{\mathbf{r},\sigma} - \sum_{\mathbf{r} \in \mathcal{A}} \hat{a}^\dagger_{\mathbf{r},\sigma} \hat{a}_{\mathbf{r},\sigma} \right) \right\} \tag{5.10}$$

Here, $\mathbf{r}_y$ is the y component of $\mathbf{r}$ in units of a, and $\hat{\boldsymbol{\delta}} = \boldsymbol{\delta}/|\boldsymbol{\delta}|$ for the nearest neighbour sites. We calculate the ground state energy, $e_g[B]$, of Eq. (5.10) as a function of $\alpha = p/q$ for integer $p = 1, 2, .., q$ with q upto 1021 for square lattice and 907 for simple cubic lattice. We do this by numerical Bogoliubov diagonalization of Eq. (5.10), and then summing over all the negative energy eigenvalues [see the Eq. (B.23) of Appendix B]. The ground state energy per site is given as follows:

$$e_g[\alpha] = -\frac{2}{L} \sum_{\mathbf{k}} \sum_{n_q=1}^{q} \epsilon_{\mathbf{k}}(n_q) \tag{5.11}$$

Here, $\mathbf{k} \equiv (k_1, k_2)$ where $-\pi < k_1 < \pi$ and $-\frac{\pi}{q} < k_2 < \frac{\pi}{q}$. From the ground state energy, we compute the magnetization, $M = -\frac{\partial e_g}{\partial \alpha}$, numerically.

It is important to note that in the presence of magnetic field, the order parameter, m_s, in Eq. (5.10) should in principle be calculated self-consistently as a function of the field. But this is a computationally demanding task, because to determine m_s self-consistently, we have to diagonalize $q \times q$ matrices very many

times for each value of magnetic field, α, which is not feasible for large q. Therefore, we simply use the zero field value of m_s to compute M vs. α, for $q = 1021$ and 907 respectively on square and simple cubic lattice. This calculation shows clear magnetic quantum oscillations, as anticipated. Then, for comparison, we also do an M vs. α calculation by using the field dependent m_s for a small $q = 307$ on square lattice. This second calculation also gives similar quantum oscillations with same dominant frequency.

Magnetization behaviour with zero-field m_s

The results of the magnetization calculation in the ground state of Eq. (5.10) with zero-field value of m_s are presented in Fig. 5.4 for square and simple cubic lattices. This magnetization data shows clear dHvA oscillations with respect to α (magnetic field), whose amplitude is found to gradually decrease with increasing U/t. This trend is consistent with what we obtained in Sec. 2.5 coming from the large U/t side.

The Fourier transform of M/α (with flat background subtracted) for $4 < 1/\alpha < 20$ on square lattice is presented in left panel of Fig. 5.4(c), where we see the dominant Fourier peak for different U's occurring at the same frequency, $f_0 = 0.5$. We also see its higher harmonics at $f = 1$ and 1.5. The semiclassical relation, $F = (2\pi/a)^2 f$, between the area F of an extremal orbit perpendicular to magnetic field on a constant energy surface in $\mathbf{k}$ space and the frequency f (in units of h/ea^2) of dHvA oscillations [5, 26, 28, 27] implies that the $f_0 = 0.5$ corresponds to the area of the half BZ, which points to the $|\gamma_{\mathbf{k}}| = 0$ as its origin. Note that the contour $|\gamma_{\mathbf{k}}| = 0$ is where the highest energy states of the fully occupied band, $E_{\mathbf{k},-}$, sit. Therefore, it suggests that for the dHvA oscillations the highest occupied levels in an insulator act as the Fermi surface, in spite of the fact that it is not a metal.

Likewise, on simple cubic lattice, as shown in right panel of Fig. 5.4(c), the Fourier transform of the M/α vs. $1/\alpha$ data gives the dominant frequency, $f_0 = 0.185$, independent of the value of U. This dominant frequency corresponds to the extremal area enclosed by the $|\gamma_{\mathbf{k}}| = 0$ contour on $k_z = 0$ plane [see Fig. 2.10-(c)]. The dominant frequencies, obtained on square and simple cubic lattices, show that the dHvA oscillations in the SDW insulator measure the surface of the highest
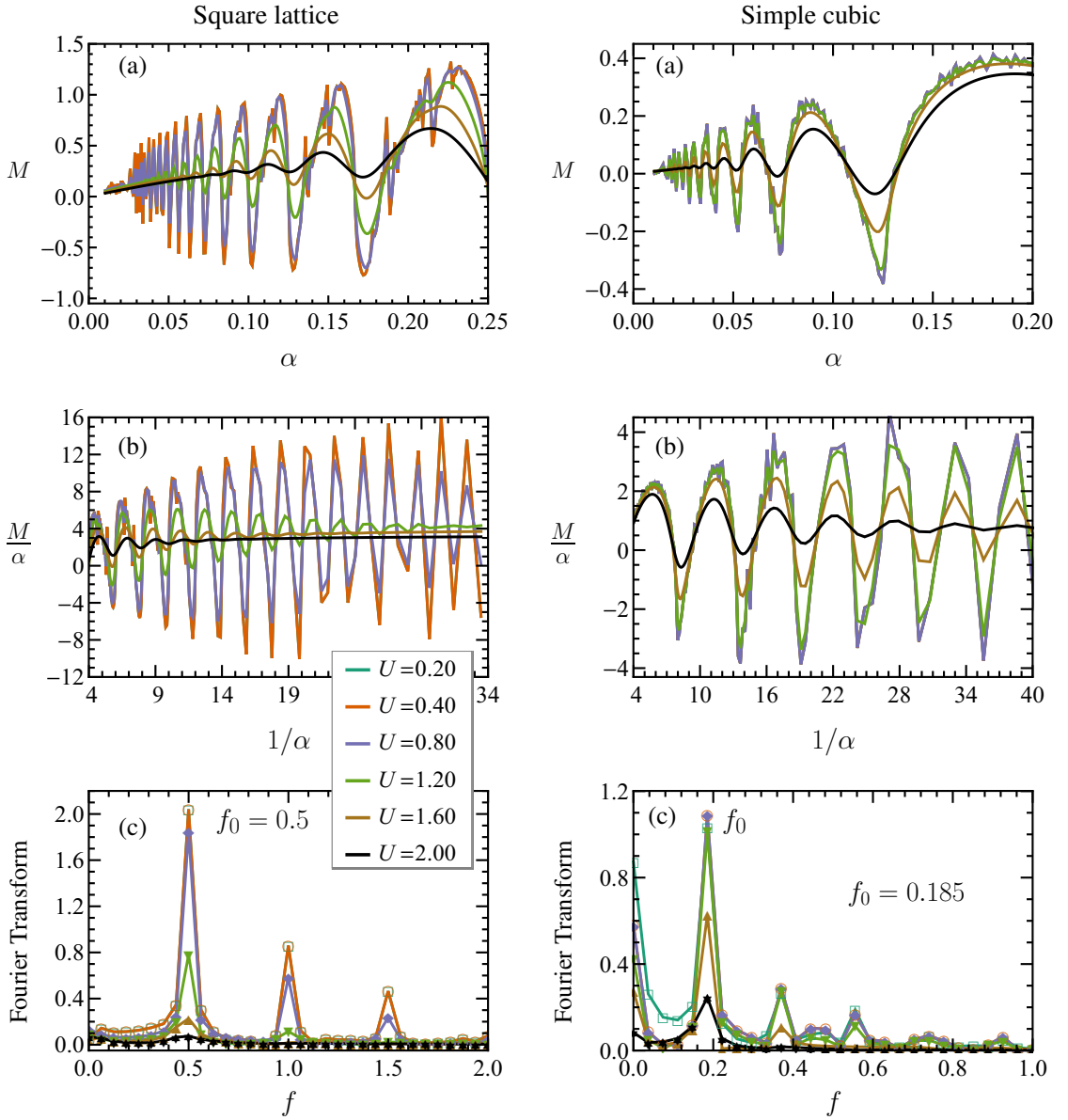
Figure 5.4: The dHvA oscillations in the SDW insulating state on square and simple cubic lattices. The magnetization data in the ground state of Eq. (5.10) for zero-field m_s is plotted variously as M vs. α and M/α vs. $1/\alpha$ for different U's. The Fourier transform (amplitude is divided by 100 for clear visibility) of M/α data gives $f_0 = 0.5$ (square) and $f_0 = 0.185$ (simple cubic) as the dominant frequency of oscillations.

energy levels of the fully-filled band.

Magnetization behaviour with field dependent m_s

Here, we study the dHvA oscillations by calculating the SDW mean-field parameter, m_s, self-consistently for different values of the magnetic field. Since the computation now becomes more demanding due to very many repeated numerical diagonalizations of the $q \times q$ matrices, we can not take large values for q. Recall that $\alpha = p/q$, where $p = 1, 2, \ldots, q$. Nevertheless, we do this exercise on square lattice for $q = 307$ to see if the dHvA oscillations obtained above (with zero-field value of m_s) is significantly modified, or if it remains qualitatively the same.
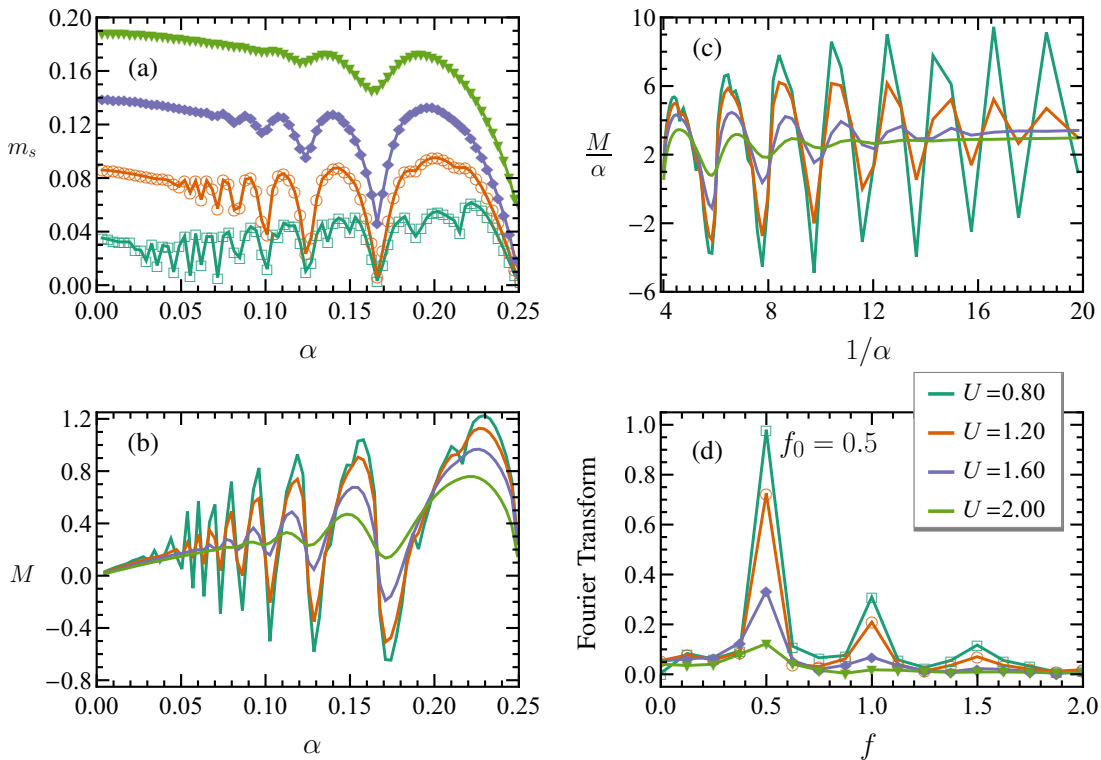
Figure 5.5: Square lattice: (a) The field dependent m_s for different U's. (b) Magnetization, M, with respect to magnetic field, α, for different U's calculated by using field dependent mean-field, m_s. M/α as a function of inverse magnetic field, $1/\alpha$ in (c). The Fourier transform of M/α is given in (d) with dominant frequency, $f_0 = 0.5$.

In Fig. 5.5(a), we plot m_s as calculated by varying α for different values of U. We observe that the m_s also shows oscillatory behaviour that changes from rapid to slow when U increases. We calculate the magnetization by using the formula $M = -\partial e_g/\partial \alpha$, where the ground state energy per site, e_g, is defined in

Eq. (5.11). Fig. 5.5, shows the magnetization data obtained in this case. It looks similar to what we found with zero-field m_s, as shown in Fig. 5.4. In fact, the Fourier transform of M/α shown in Fig. 5.5 gives the same dominant oscillations frequency, $f_0 = 0.5$, as obtained from the calculations with zero-field m_s. Hence, the dHvA oscillations in the two ways of treating m_s for magnetization calculation are found to be essentially same.

Remarks on the effect of Zeeman coupling

In this thesis, we have neglected the Zeeman coupling of magnetic field to the electron spin. This is because our primary motivation here has been to understand the response of the (Kondo) insulating state to magnetic field coupled via Peierls phase to electron motion. We now very briefly look at how it may affect the dHvA oscillations. Consider the Zeeman term, $-g\mu_B \sum_{\mathbf{r}}(\hat{n}_{\mathbf{r}\uparrow} - \hat{n}_{\mathbf{r}\downarrow})/2$, which can be recast as:

$$-4\pi t\, \alpha g_r m_r \sum_\sigma \eta_\sigma \left\{ \sum_{\mathbf{r}\in\mathcal{A}} \hat{a}^\dagger_{\mathbf{r},\sigma}\hat{a}_{\mathbf{r},\sigma} + \sum_{\mathbf{r}\in\mathcal{B}} \hat{b}^\dagger_{\mathbf{r},\sigma}\hat{b}_{\mathbf{r},\sigma} \right\}, \qquad (5.12)$$

where $\alpha = eBa^2/h$ is the reduced flux (that sits in the Peierls phase), $g_r = g/2$ is the Landé g factor relative to 2, and the relative effective mass, $m_r = m^*/m_e$, is the ratio of the effective mass from the tight-binding band-structure, $m^*(= \hbar^2/2ta^2)$, and the free electron mass, m_e. Ideally, both g_r and m_r would be 1, but in actual they would take different values for different materials.

According to Eq. (5.7), the single-particle gap is $\Delta = 2Um_s$, and $\uparrow$ and $\downarrow$ electron dispersions are degenerate. The Zeeman term would lift this degeneracy by $4\pi t\, \alpha g_r m_r$, but as long as $Um_s > 4\pi t\, \alpha g_r m_r$ is true, the ground state is gapped. Beyond it, the $\uparrow$ and $\downarrow$ electron bands will overlap, leading to a metallic ground state. Within this simple minded picture, a sufficiently strong magnetic field would destroy the SDW insulating state by overcoming the SDW gap. It can happen for small fields (of a few Tesla) if the SDW gap is tiny, and will require larger fields if the SDW gap is not so small. For a rough estimate, take $g_r m_r \sim 1$ and $t \sim 1$eV. Then, the condition for the survival of the SDW insulating phase reads as: $\Delta \gtrsim 10^{-4}B$. So, if $\Delta \sim 1$ meV, then $B \gtrsim 10$ T can overcome the SDW gap. This magnetic field is already quite large. But for slightly stronger Δ, one would require even larger

fields, beyond the typical laboratory fields, to make this happen. In either case, the quantum oscillations would survive. In the insulating case for smaller fields, they will be like what we have obtained above. But when the SDW gap is overcome by field, the resultant metallic state would show quantum oscillations with frequencies different from those in the insulating case. We leave the detailed investigation of dHvA oscillations for the case with both Peierls and Zeeman couplings, that is Eq. (5.10) + Eq. (5.12), for a future study.

5.2   Weak-Coupling KLM at Half-Filling

We know very well that for sufficiently small J/t, the half-filled KLM on any bipartite lattice realizes Néel insulating ground state. Hence, in the spirit of the previous section, we do a simple weak-coupling mean-field theory of the KLM, directly in terms of the electron operators. With Néel AFM order parameter, both for the localized moments and the conduction electrons, we study quantum oscillations of magnetization in this SDW like setting. We already know from Chapter 2 that the dHvA oscillations occur in the half-filled KLM for J/t ranging from intermediate to weak. This calculation, with the benefit of hindsight, is a vindication of that finding from a very simplistic approach motivated from the weak-coupling side.

5.2.1   Mean-field approximation with Néel order

The conduction electrons in KLM, Eq. (2.5), do not interact amongst themselves. But they interact with the localized spins via the Kondo interaction, $\frac{J}{2} \sum_{\mathbf{r}} \mathbf{S_r} \cdot \boldsymbol{\tau_r}$, between the electron spin, $\mathbf{S_r}$, and the localized spin-1/2 given by the Pauli operator, $\boldsymbol{\tau_r}$. At the simplest level, we can treat the Kondo interaction in the following mean-field approximation:

$$\mathbf{S_r} \cdot \boldsymbol{\tau_r} \approx \langle \mathbf{S_r} \rangle \cdot \boldsymbol{\tau_r} + \mathbf{S_r} \cdot \langle \boldsymbol{\tau_r} \rangle - \langle \mathbf{S_r} \rangle \cdot \langle \boldsymbol{\tau_r} \rangle$$
$$= \vec{M}_{\mathbf{r}} \cdot \boldsymbol{\tau_r} + \mathbf{S_r} \cdot \vec{m}_{\mathbf{r}} - \vec{M}_{\mathbf{r}} \cdot \vec{m}_{\mathbf{r}} \tag{5.13}$$

Here, $\langle \mathbf{S_r} \rangle = \vec{M}_{\mathbf{r}}$ and $\langle \boldsymbol{\tau_r} \rangle = \vec{m}_{\mathbf{r}}$, are the average magnetization vectors for the conduction electrons and localized spins, respectively. Since we know about the

Néel AFM ordering in the insulating ground state of the half-filled KLM, we choose,

$$\vec{M}_{\mathbf{r}} \text{ on } \mathcal{A} \text{ sublattice} = -\vec{M}_{\mathbf{r}} \text{ on } \mathcal{B} \text{ sublattice} = M\hat{\Omega}, \text{ and}$$

$$\vec{m}_{\mathbf{r}} \text{ on } \mathcal{A} \text{ sublattice} = -\vec{m}_{\mathbf{r}} \text{ on } \mathcal{B} \text{ sublattice} = -m\hat{\Omega}.$$

Here, the unit vector $\hat{\Omega}$ (which is arbitrary) specifies the direction of the vector order parameters, and M and m are their magnitudes. Under this approximation, the mean-field KLM reads as: $H_{\mathrm{MF}} \approx H_{\mathrm{electron}} + H_{\mathrm{moment}} + \frac{J}{2} M m L$.

$$H_{\mathrm{moment}} = \frac{JM}{2} \left[\sum_{\mathbf{r} \in \mathcal{A}} - \sum_{\mathbf{r} \in \mathcal{B}} \right] \hat{\Omega} \cdot \boldsymbol{\tau}_{\mathbf{r}} \tag{5.14}$$

$$H_{\mathrm{electron}} = -t \sum_{\mathbf{r} \in \mathcal{A}} \sum_{\boldsymbol{\delta}, s} \left(e^{i\frac{e}{\hbar} \int_{\mathbf{r}}^{\mathbf{r}+\boldsymbol{\delta}} \mathbf{A} \cdot \mathbf{dr}} f_{\mathbf{r},s}^{\dagger} f_{\mathbf{r}+\boldsymbol{\delta},s} + \mathrm{h.c.} \right) - \frac{Jm}{2} \left[\sum_{\mathbf{r} \in \mathcal{A}} - \sum_{\mathbf{r} \in \mathcal{B}} \right] \hat{\Omega} \cdot \mathbf{S}_{\mathbf{r}} \tag{5.15}$$

The H_{moment} is so very simple. For $\hat{\Omega} = (\sin\theta\cos\phi, \sin\theta\cos\phi\hat{y}, \cos\theta)$, it can be diagonalized by applying the following rotation on the localized spins operators on both the sublattices.

$$\hat{\mathcal{U}} = \begin{bmatrix} \cos\frac{\theta}{2} & -\sin\frac{\theta}{2} \, e^{-i\phi} \\ \sin\frac{\theta}{2} \, e^{i\phi} & \cos\frac{\theta}{2} \end{bmatrix} \tag{5.16}$$

The diagonalized form of H_{moment} is

$$\hat{\mathcal{U}}^{\dagger} H_{\mathrm{moment}} \hat{\mathcal{U}} = \tilde{H}_{\mathrm{moment}} = \frac{JM}{2} \left[\sum_{\mathbf{r} \in \mathcal{A}} - \sum_{\mathbf{r} \in \mathcal{B}} \right] \tau_{\mathbf{r}}^{z} \tag{5.17}$$

which immediately implies that the order parameter of the localized moments is trivially, $m = 1$, in the ground state. Given this, the electronic Hamiltonian in the basis rotated by the $\mathcal{U}$ defined above reads as:

$$H_{\mathrm{electron}} = \sum_{s=\uparrow,\downarrow} \left\{ -t \sum_{\mathbf{r} \in \mathcal{A}} \sum_{\boldsymbol{\delta}} \left(e^{i\frac{e}{\hbar} \int_{\mathbf{r}}^{\mathbf{r}+\boldsymbol{\delta}} \mathbf{A} \cdot \mathbf{dr}} \tilde{f}_{\mathbf{r},s}^{\dagger} \tilde{f}_{\mathbf{r}+\boldsymbol{\delta},s} + \mathrm{h.c.} \right) \right.$$

$$\left. - \frac{J}{4} \left[\sum_{\mathbf{r} \in \mathcal{A}} - \sum_{\mathbf{r} \in \mathcal{B}} \right] \eta_s \tilde{f}_{\mathbf{r},s}^{\dagger} \tilde{f}_{\mathbf{r},s} \right\} \tag{5.18}$$

where $\eta_{\uparrow(\downarrow)} = +(-)$, and the new electrons operators $\tilde{f}_{\mathbf{r},s}$ are related to the old $\hat{f}_{\mathbf{r},s}$ via the same unitary matrix as defined above in Eq. (5.16).

$$\begin{bmatrix} f_{\mathbf{r},\uparrow} \\ f_{\mathbf{r},\downarrow} \end{bmatrix} = \hat{\mathcal{U}} \begin{bmatrix} \tilde{f}_{\mathbf{r},\uparrow} \\ \tilde{f}_{\mathbf{r},\downarrow} \end{bmatrix} \tag{5.19}$$

Note the conspicuous absence of the electron's staggered magnetic order parameter, M, in Eq. (5.18). In this highly simple mean-field description of the Néel state of the half-filled KLM, it is so because m happens to be independent of M. Hence, once $m(= 1)$ is determined, we need not write any self-consistent equation for M.

In the absence of magnetic field, Eq. (5.18) can be diagonalized by successively applying the Fourier and Bogoliubov transformations. Since the Néel order distinguishes between the $\mathcal{A}$ and $\mathcal{B}$ sublattices, we incorporate this fact by explicitly including in the fermion creation and annihilation operators by using subscripts, a and b, for the two sublattices, respectively. With this slight change of notation, we define the Fourier transform of the fermion operators as: $\tilde{f}_{a,s}(\mathbf{r}) = \sqrt{\frac{2}{L}} \sum_{\mathbf{k}} e^{i\mathbf{k}\cdot\mathbf{r}} \tilde{f}_{a,s}(\mathbf{k})$ and $\tilde{f}_{b,s}(\mathbf{r}) = \sqrt{\frac{2}{L}} \sum_{\mathbf{k}} e^{i\mathbf{k}\cdot\mathbf{r}} \tilde{f}_{b,s}(\mathbf{k})$, where $\mathbf{k} \in$ the magnetic Brillouin zone. The diagonal form of H_{electron} is given as:

$$H_{\text{electron}}^{[B=0]} = \sum_{\mathbf{k}} \sum_{s} \omega_{\mathbf{k}} \left[\tilde{f}_{+,s}^{\dagger}(\mathbf{k}) \tilde{f}_{+,s}(\mathbf{k}) - \tilde{f}_{-,s}^{\dagger}(\mathbf{k}) \tilde{f}_{-,s}(\mathbf{k}) \right] \tag{5.20}$$

where $\omega_{\mathbf{k}} = \sqrt{(t\gamma_k)^2 + (\frac{J}{4})^2}$ is electron dispersion, and the new fermion operators, $\tilde{f}_{\pm,s}(\mathbf{k})$, are given by the following Bogoliubov transformation:

$$\tilde{f}_{a,s}(\mathbf{k}) = \cos\beta_{\mathbf{k}} \ \tilde{f}_{-,s}(\mathbf{k}) - \sin\beta_{\mathbf{k}} \ \tilde{f}_{+,s}(\mathbf{k})$$
$$\tilde{f}_{b,s}(\mathbf{k}) = \sin\beta_{\mathbf{k}} \ \tilde{f}_{-,s}(\mathbf{k}) + \cos\beta_{\mathbf{k}} \ \tilde{f}_{+,s}(\mathbf{k}) \tag{5.21}$$

with $\tan 2\beta_{\mathbf{k}} = \frac{t\gamma_k}{(J\eta_s/4)}$. In the ground state of $H_{\text{electron}}^{[B=0]}$, the positive energy bands corresponding to $\tilde{f}_{+,s}(\mathbf{k})$ are completely empty, while the negative energy bands corresponding to $\tilde{f}_{-,s}(\mathbf{k})$ are fully filled (satisfying half-filling). We see that $\omega_{\mathbf{k}}$ has minima at edge of half-BZ i.e. $|\gamma_{\mathbf{k}}| = 0$, so we find the single-particle gap to be, $\Delta_c = 2\,\omega_{\mathbf{k}=|\gamma_{\mathbf{k}}|=0} = J$. Hence, the Néel ordered ground state of KLM is an insulating state for any non zero J. Contrast this gap which decreases linearly with J, with the SDW gap of the Hubbard model which decreases exponentially at small U.
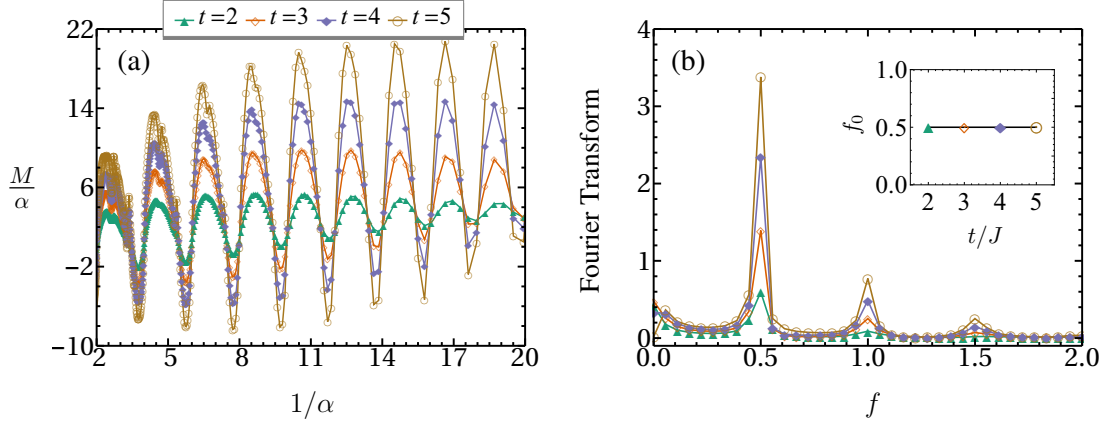
Figure 5.6: The dHvA oscillations in the mean-field Néel insulating ground state of the Kondo lattice model at half-filling [Eq. (5.18)] on square lattice. (a) M/α, versus inverse magnetic field, $1/\alpha$ for $t = 2, 3, 4, 5$ (with $J = 1$). (b) Its Fourier transform (amplitude is divided by 100), where the dominant fundamental frequency occurs at $f_0 = 0.5$. The inset shows that the f_0 remains constant on increasing t/J.
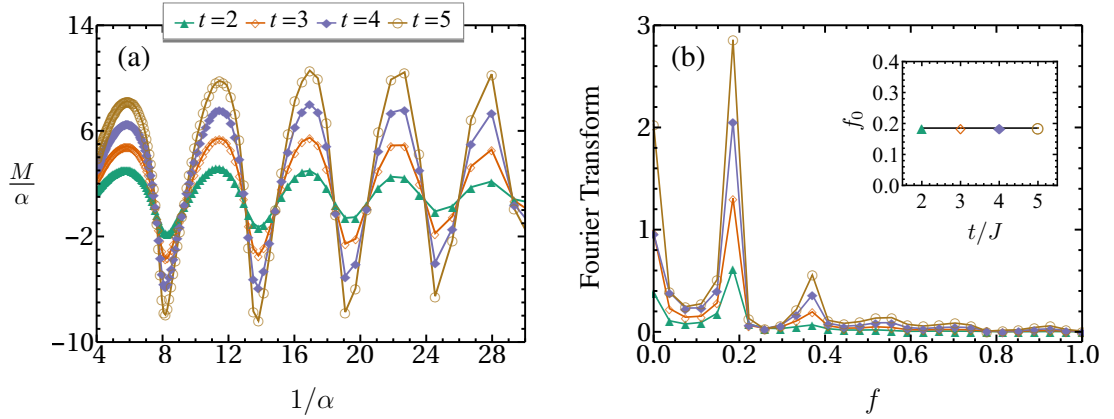

Figure 5.7: The dHvA oscillations in the mean-field Néel insulating ground state of the Kondo lattice model at half-filling [Eq. (5.18)] on simple cubic lattice. (a) M/α, versus inverse magnetic field, $1/\alpha$ for $t = 2, 3, 4, 5$ (with $J = 1$). (b) Its Fourier transform (amplitude is divided by 100), where the dominant fundamental frequency occurs at $f_0 = 0.185$. The inset shows that the f_0 remains constant on increasing t/J.

5.2.2 Magnetic quantum oscillations

To compute the magnetic response in this highly simplified description of the half-filled KLM, we put $\mathbf{A} = -yB\hat{x}$ in Eq. (5.18). The H_{electron} now reads as follows:

$$\hat{H} = \sum_{s=\uparrow,\downarrow} \left\{ -t \sum_{\mathbf{r} \in \mathcal{A}} \sum_{\boldsymbol{\delta}} \left[e^{2\pi i \alpha \mathbf{r}_y \hat{x} \cdot \boldsymbol{\delta}} \, \tilde{f}_{a,s}^{\dagger}(\mathbf{r}) \tilde{f}_{b,s}(\mathbf{r} + \boldsymbol{\delta}) + \text{h.c.} \right] \right.$$

$$-\frac{J}{4}\eta_s\left[\sum_{\mathbf{r}\in\mathcal{A}}\tilde{f}^\dagger_{a,s}(\mathbf{r})\tilde{f}_{a,s}(\mathbf{r}) - \sum_{\mathbf{r}\in\mathcal{B}}\tilde{f}^\dagger_{b,s}(\mathbf{r})\tilde{f}_{b,s}(\mathbf{r})\right]\Bigg\} \tag{5.22}$$

This is a standard Hofstadter problem, but with a staggered potential term. For each value of the spin quantum number s, we have an independent problem to solve. We calculate the ground state energy per site, $e_g[B]$, as a function of magnetic field, B, in the standard way by writing Eq. (5.22) in the Nambu notation, and then doing a Bogoliubov diagonalization numerically [for instance, see Eq. (B.24) of Appendix B]. Here, $\alpha = p/q$, where $p = 1, 2, \ldots, q$ and $q = 907$ (601) for square (simple cubic) lattice. From this, using $M = -\frac{\partial e_g}{\partial \alpha}$, we calculate magnetization. In Fig. 5.6(a), the behaviour of M/α with respect to $1/\alpha$ is shown for different values of t (for $J = 1$) on square lattice, where the oscillations are prominently visible. Expectedly, their amplitude decreases as we decrease t/J. The Fourier transform in Fig. 5.6(b) gives the dominant frequency $f_0 = 0.5$. We also calculate M on simple cubic lattice (data presented in Fig. 5.7), where too, we get clear magnetic quantum oscillations with a dominant frequency at $f_0 = 0.185$.

The quantum oscillation results obtained from this overly simplified calculation on KLM are, as anticipated, in line with what we found through the systematic theory in Chapter 2 and Ref. [42]. Notably, here too, as in the other calculations presented in this thesis, the dominant frequencies correspond to the contours, $\gamma_{\mathbf{k}} = 0$, which is where the maxima of the fully-filled bands of Eq. (5.20) lie. This clearly implies that the magnetic quantum oscillations in an insulator measure the surface of the highest occupied energy levels of electrons (effective chemical potential), analogous to the Fermi surface in metals.

5.3   Conclusion

In summary, we have investigated magnetic quantum oscillations in the insulating SDW ground state of the half-filled Hubbard model, and done similar mean-field calculations for the weak-coupling KLM at half-filling, on square and simple cubic lattices. The occurrence of these oscillations was clearly anticipated by us in Ref. [42]. This chapter is a simple byproduct of the main body of calculations presented in the previous chapters based on our original theory of Kondo insula-

tors. In our studies here, we have again found the fundamental frequency of dHvA oscillations in the insulating states to correspond to the chemical potential surface (highest energy levels of the fully-occupied band). Since it is relatively straightforward to formulate an SDW theory on non-bipartite lattices, and include Zeeman coupling, it is our future goal to carry forward these studies to different physical settings.

● ● ● ● ●

AppendixA

Diagonalization of the Charge Dynamics, $H_c^{[B]}$

In this appendix, we show a detailed calculation of the ground state energy per site (e_g) of the charge dynamics Hamiltonian, $\hat{H}_c^{[B]}$ given in Eq. (2.30a) to find the magnetization, M, as a function of magnetic field, B. Here, we only describe the calculation steps for the bipartite square lattice in detail. However, the calculation for the simple cubic lattice case is similar to the square lattice, and it is straightforward. To diagonalize the charge dynamics Hamiltonian, we recall the $\hat{H}_c^{[B]}$ which is given as:

$$\hat{H}_c^{[B]} = -\frac{it}{2} \sum_{\mathbf{r} \in \mathcal{A}} \sum_{\boldsymbol{\delta}} \cos\left(2\pi\alpha\, \mathbf{r}_y\, \hat{x} \cdot \hat{\boldsymbol{\delta}}\right) \left[\hat{\psi}_{a,\mathbf{r}} \hat{\phi}_{b,\mathbf{r}+\boldsymbol{\delta}} + \rho_1 \hat{\psi}_{b,\mathbf{r}+\boldsymbol{\delta}} \hat{\phi}_{a,\mathbf{r}}\right]$$

$$+ \frac{J\rho_0}{4}\left[\sum_{\mathbf{r} \in \mathcal{A}} \hat{n}_{a,\mathbf{r}} + \sum_{\mathbf{r} \in \mathcal{B}} \hat{n}_{b,\mathbf{r}}\right] \tag{A.1}$$

The bipartite square lattice is given in Fig. A.1 with primitive vectors, $\boldsymbol{a_1} = 2a\hat{x}$ and $\boldsymbol{a_2} = a(-\hat{x} + \hat{y})$. We can find the corresponding reciprocal vectors, $\boldsymbol{b_1} = \frac{\pi}{a}(\hat{x} + \hat{y})$ and $\boldsymbol{b_2} = \frac{2\pi}{a}\hat{y}$. The Bravais lattice vector is taken to be $\boldsymbol{R} = m\boldsymbol{a_1} + n\boldsymbol{a_2}$ with integers $m = \frac{x+y}{2a}$ and $n = \frac{y}{a}$, where a is lattice constant, and x and y denote the actual position of lattice sites.

Here, the nearest-neighbour unit vectors are $\hat{\boldsymbol{\delta}} = \{\hat{x}, -\hat{x}, \hat{y}, -\hat{y}\}$ and the position of site $\mathbf{r}$ is given as $\mathbf{r}_x = m$ and $\mathbf{r}_y = n$. Using these informations we rewrite the Hamiltonian given in Eq. (A.1) in $\mathbf{r} \equiv (m, n)$ coordinate notation as:

$$\hat{H}_c^{[B]} = -\frac{it}{2} \sum_{m=1}^{L_1} \sum_{n=1}^{L_2} \left(\cos(2\pi\alpha n) \left[\hat{\psi}_a(m, n)\hat{\phi}_b(m, n) + \rho_1 \hat{\psi}_b(m, n)\hat{\phi}_a(m, n)\right]\right.$$
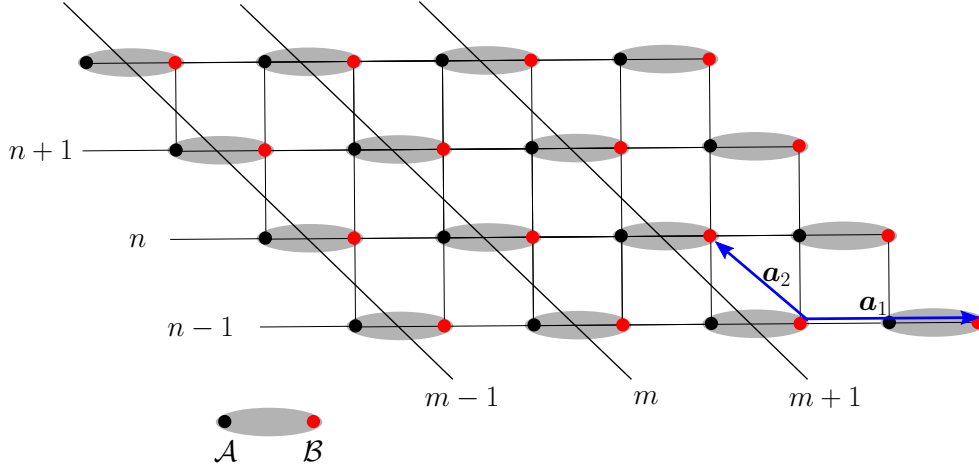
Figure A.1: Bipartite square lattice: The filled black and red circles are taken as $\mathcal{A}$-sublattice and $\mathcal{B}$-sublattice, respectively.

$$
\begin{aligned}
&+ \cos(2\pi\alpha n)\left[\hat{\psi}_a(m,n)\hat{\phi}_b(m-1,n) + \rho_1\hat{\psi}_b(m-1,n)\hat{\phi}_a(m,n)\right] \\
&+ \left[\hat{\psi}_a(m,n)\hat{\phi}_b(m,n+1) + \rho_1\hat{\psi}_b(m,n+1)\hat{\phi}_a(m,n)\right] \\
&+ \left[\hat{\psi}_a(m,n)\hat{\phi}_b(m-1,n-1) + \rho_1\hat{\psi}_b(m-1,n-1)\hat{\phi}_a(m,n)\right]\Bigg) \\
&+ \frac{J\rho_0}{4}\sum_{m=1}^{L_1}\sum_{n=1}^{L_2}\left(\hat{a}_{m,n}^{\dagger}\hat{a}_{m,n} + \hat{b}_{m,n}^{\dagger}\hat{b}_{m,n}\right)
\end{aligned}
\tag{A.2}
$$

with, $L_1 = 2L_x$ and $L_2 = L_y$ where L_x and L_y are total length along $\hat{x}$ and $\hat{y}$. By using the definition of Majorana fermions in terms of spinless fermions i.e. $i\hat{\psi}_a = \hat{a}^{\dagger} - \hat{a}$, $\hat{\phi} = \hat{a}^{\dagger} + \hat{a}$ and $i\hat{\psi}_b = \hat{b}^{\dagger} - \hat{b}$, $\hat{\phi}_b = \hat{b}^{\dagger} + \hat{b}$, we derive the following expression for $\hat{H}_c^{[B]}$ as:

$$
\begin{aligned}
\hat{H}_c^{[B]} = -\frac{t}{2}\sum_{m=1}^{L_1}\sum_{n=1}^{L_2}\Bigg(&(1+\rho_1)\cos(2\pi\alpha n)\left[(\hat{a}_{m,n}^{\dagger}\hat{b}_{m,n} + h.c.) + (\hat{a}_{m,n}^{\dagger}\hat{b}_{m-1,n} + h.c.)\right] \\
&+ (1+\rho_1)\left[(\hat{a}_{m,n}^{\dagger}\hat{b}_{m,n+1} + h.c.) + (\hat{a}_{m,n}^{\dagger}\hat{b}_{m-1,n-1} + h.c.)\right] \\
&+ (1-\rho_1)\cos(2\pi\alpha n)\left[(\hat{a}_{m,n}^{\dagger}\hat{b}_{m,n}^{\dagger} + h.c.) + (\hat{a}_{m,n}^{\dagger}\hat{b}_{m-1,n}^{\dagger} + h.c.)\right] \\
&+ (1-\rho_1)\left[(\hat{a}_{m,n}^{\dagger}\hat{b}_{m,n+1}^{\dagger} + h.c.) + (\hat{a}_{m,n}^{\dagger}\hat{b}_{m-1,n-1}^{\dagger} + h.c.)\right]\Bigg) \\
&+ \frac{J\rho_0}{4}\sum_{m=1}^{L_1}\sum_{n=1}^{L_2}\left(\hat{a}_{m,n}^{\dagger}\hat{a}_{m,n} + \hat{b}_{m,n}^{\dagger}\hat{b}_{m,n}\right)
\end{aligned}
\tag{A.3}
$$

We define a Fourier transform along m direction as:

$$\hat{a}_{m,n} = \frac{1}{\sqrt{L_1}} \sum_{k_1} e^{ik_1 m} \, \hat{a}_{k_1,n}$$

$$\hat{b}_{m,n} = \frac{1}{\sqrt{L_1}} \sum_{k_1} e^{ik_1(m+\frac{1}{2})} \, \hat{b}_{k_1,n} \tag{A.4}$$

where, we take the actual position of $\hat{a}_{m,n}$ and $\hat{b}_{m,n}$. Using the Fourier transformation given in Eq. (A.4), Eq. (A.3) becomes,

$$\begin{aligned}
\hat{H}_c^{[B]} = -\frac{t}{2} \sum_{k_1} \sum_{n=1}^{L_2} \bigg(& 2(1+\rho_1)\cos(k_1/2)\cos(2\pi\alpha n)\Big[\hat{a}_{k_1,n}^\dagger \hat{b}_{k_1,n} + h.c.\Big] \\
& + 2(1-\rho_1)\cos(k_1/2)\cos(2\pi\alpha n)\Big[\hat{a}_{k_1,n}^\dagger \hat{b}_{-k_1,n}^\dagger + h.c.\Big] \\
& + (1+\rho_1)\Big[(e^{ik_1/2}\hat{a}_{k_1,n}^\dagger \hat{b}_{k_1,n+1} + h.c.) + (e^{-ik_1/2}\hat{a}_{k_1,n}^\dagger \hat{b}_{k_1,n-1} + h.c.)\Big] \\
& + (1-\rho_1)\Big[(e^{ik_1/2}\hat{a}_{k_1,n}^\dagger \hat{b}_{-k_1,n+1}^\dagger + h.c.) + (e^{-ik_1/2}\hat{a}_{k_1,n}^\dagger \hat{b}_{-k_1,n-1}^\dagger + h.c.)\Big] \\
& + \frac{J\rho_0}{4} \sum_{k_1} \sum_{n=1}^{L_2} \Big[\hat{a}_{k_1,n}^\dagger \hat{a}_{k_1,n} + \hat{b}_{k_1,n}^\dagger \hat{b}_{k_1,n}\Big] \tag{A.5}
\end{aligned}$$

The above equation is like Harper's equation [97, 67]. We can see that $\hat{H}_c^{[B]}$ in Eq. (A.5) does not incorporate the periodicity along n, but by choosing the magnetic field α as a rational number i.e. $\alpha = p/q$ where p and q are integers, we retain the periodicity along n with q sites in a unit cell. Hence, we take a super-unit-cell of q sites and define $n = q(n'-1) + n_q$, where $n_q = 1, 2, ..., q$ and $n' = 1, 2, ..., L_2'$. Then the total no. of sites, L_2, along n is decomposed as q times L_2' i.e. $L_2 = qL_2'$. This is shown below,

$$\overbrace{1\ 2\ 3\ \cdots\ q}^{n'=1}\quad \overbrace{1\ 2\ 3\ \cdots\ q}^{n'=2}\quad \cdots\quad \overbrace{1\ 2\ 3\ \cdots\ q}^{n'=L_2'}$$

and sum over n becomes:

$$\sum_{n=1}^{L_2} \Rightarrow \sum_{n_q=1}^{q} \sum_{n'=1}^{L_2'}$$

. Therefore, We define a Fourier transform along n as:

$$\hat{a}_{k_1,n} \equiv \hat{a}_{k_1,n'}(n_q) = \frac{1}{\sqrt{L_2'}} \sum_{k_2} e^{ik_2[q(n'-1)+n_q]} \, \hat{a}_{k_1,k_2}(n_q)$$

$$\hat{b}_{k_1,n} \equiv \hat{b}_{k_1,n'}(n_q) = \frac{1}{\sqrt{L_2'}} \sum_{k_2} e^{ik_2[q(n'-1)+n_q]} \, \hat{b}_{k_1,k_2}(n_q) \tag{A.6}$$

Using the above Fourier transformation to Eq. (A.5), we get the following form of the Hamiltonian,

$$
\begin{aligned}
\hat{H}_c^{[B]} = -\frac{t}{2} \sum_{k_1} \sum_{k_2} \sum_{n_q=1}^{q} &\bigg(2(1+\rho_1)\cos(k_1/2)\cos(2\pi\alpha n_q)\Big[\hat{a}_{k_1,k_2}^\dagger(n_q)\hat{b}_{k_1,k_2}(n_q) + h.c.\Big] \\
&+ 2(1-\rho_1)\cos(k_1/2)\cos(2\pi\alpha n_q)\Big[\hat{a}_{k_1,k_2}^\dagger(n_q)\hat{b}_{-k_1,-k_2}^\dagger(n_q) + h.c.\Big] \\
&+ (1+\rho_1)\Big[(e^{i(\frac{k_1}{2}+k_2)}\hat{a}_{k_1,k_2}^\dagger(n_q)\hat{b}_{k_1,k_2}(n_q+1) + h.c.) \\
&+ (e^{-i(\frac{k_1}{2}+k_2)}\hat{a}_{k_1,k_2}^\dagger(n_q)\hat{b}_{k_1,k_2}(n_q-1) + h.c.)\Big] \\
&+ (1-\rho_1)\Big[(e^{i(\frac{k_1}{2}+k_2)}\hat{a}_{k_1,k_2}^\dagger(n_q)\hat{b}_{-k_1,-k_2}^\dagger(n_q+1) + h.c.) \\
&+ (e^{-i(\frac{k_1}{2}+k_2)}\hat{a}_{k_1,k_2}^\dagger(n_q)\hat{b}_{-k_1,-k_2}^\dagger(n_q-1) + h.c.)\Big]\bigg) \\
&+ \frac{J\rho_0}{4} \sum_{k_1} \sum_{n=1}^{L_2} \Big[\hat{a}_{k_1,k_2}^\dagger(n_q)\hat{a}_{k_1,k_2}(n_q) + \hat{b}_{k_1,k_2}^\dagger(n_q)\hat{b}_{k_1,k_2}(n_q)\Big] \tag{A.7}
\end{aligned}
$$

with the conditions, $\hat{a}_{k_1,k_2}(n_q+q) = \hat{a}_{k_1,k_2}(n_q)$ and $\hat{b}_{k_1,k_2}(n_q+q) = \hat{b}_{k_1,k_2}(n_q)$. From Eq. (A.4) and (A.6), we can derive that $-\pi < k_1 < \pi$ and $-\frac{\pi}{q} < k_2 < \frac{\pi}{q}$. Hence, Brillouin zone along k_2 is reduced by a factor of q.

We can also rewrite the above Eq. (A.7) by defining, $\mathbf{k} \equiv (k_1, k_2)$, $\Lambda_{\mathbf{k}}(n_q) = -t\cos(\frac{k_1}{2})\cos(2\pi\alpha n_q)$ and $\lambda_{\mathbf{k}} = -\frac{t}{2}e^{ik_1/2}e^{ik_2}$.

$$
\begin{aligned}
\hat{H}_c^{[B]} = \sum_{k_1} \sum_{k_2} \sum_{n_q=1}^{q} &\bigg((1+\rho_1)\Lambda_{\mathbf{k}}(n_q)\Big[(\hat{a}_{\mathbf{k}}^\dagger(n_q)\hat{b}_{\mathbf{k}}(n_q) + h.c.)\Big] \\
&+ (1+\rho_1)\Big[(\lambda_{\mathbf{k}}\hat{a}_{\mathbf{k}}^\dagger(n_q)\hat{b}_{\mathbf{k}}(n_q+1) + h.c.) + (\lambda_{\mathbf{k}}^*\hat{a}_{\mathbf{k}}^\dagger(n_q)\hat{b}_{\mathbf{k}}(n_q+1) + h.c.)\Big] \\
&+ (1-\rho_1)\Lambda_{\mathbf{k}}(n_q)\Big[(\hat{a}_{\mathbf{k}}^\dagger(n_q)\hat{b}_{-\mathbf{k}}^\dagger(n_q) + h.c.)\Big] \\
&+ (1-\rho_1)\Big[(\lambda_{\mathbf{k}}\hat{a}_{\mathbf{k}}^\dagger(n_q)\hat{b}_{-\mathbf{k}}^\dagger(n_q+1) + h.c.) + (\lambda_{\mathbf{k}}^*\hat{a}_{\mathbf{k}}^\dagger(n_q)\hat{b}_{-\mathbf{k}}^\dagger(n_q+1) + h.c.)\Big]\bigg) \\
&+ \frac{J\rho_0}{4} \sum_{k_1} \sum_{k_2} \sum_{n_q=1}^{q} \Big[\hat{a}_{\mathbf{k}}^\dagger(n_q)\hat{a}_{\mathbf{k}}(n_q) + \hat{b}_{\mathbf{k}}^\dagger(n_q)\hat{b}_{\mathbf{k}}(n_q)\Big] \tag{A.8}
\end{aligned}
$$

To diagonalize Eq. (A.8), we write it in the Nambu basis notation as:

$$\hat{H}_c^{[B]} = \left(\frac{J\rho_0}{8}\right)L + \frac{1}{2}\sum_{k_1}\sum_{k_2} \Psi_{\mathbf{k}}^\dagger \mathcal{H}_{\mathbf{k}} \Psi_{\mathbf{k}} \tag{A.9}$$

Here, $\mathcal{H}_{\mathbf{k}}$ is a $4q \times 4q$ hermitian matrix for a given value of $\mathbf{k}$ is

$$\mathcal{H}_{\mathbf{k}} = \begin{bmatrix} A & B & 0 & B \\ B & A & -B & 0 \\ 0 & -B & -A & -B \\ B & 0 & -B & -A \end{bmatrix} \tag{A.10}$$

with $A = \left(\frac{J\rho_0}{4}\right)\mathbb{I}_{q\times q}$ where $\mathbb{I}_{q\times q}$ is $q \times q$ identity matrix, and

$$B = \begin{bmatrix} \Lambda_{\mathbf{k}}(1) & \lambda_{\mathbf{k}} & 0 & 0 & \ldots & \lambda_{\mathbf{k}}^* \\ \lambda_{\mathbf{k}}^* & \Lambda_{\mathbf{k}}(2) & \lambda_{\mathbf{k}} & 0 & \ldots & 0 \\ 0 & \lambda_{\mathbf{k}}^* & \Lambda_{\mathbf{k}}(3) & \lambda_{\mathbf{k}} & \ldots & 0 \\ \vdots & \vdots & \ddots & \ddots & \ddots & \vdots \\ 0 & 0 & \ldots & \lambda_{\mathbf{k}}^* & \Lambda_{\mathbf{k}}(q-1) & \lambda_{\mathbf{k}} \\ \lambda_{\mathbf{k}} & 0 & \ldots & 0 & \lambda_{\mathbf{k}}^* & \Lambda_{\mathbf{k}}(q) \end{bmatrix}. \tag{A.11}$$

The Nambu basis operator $\Psi_{\mathbf{k}}^\dagger$ with row vector is defined as:

$$\Psi_{\mathbf{k}}^\dagger = [\hat{a}_{\mathbf{k}}^\dagger(1), \hat{a}_{\mathbf{k}}^\dagger(2), ..., \hat{a}_{\mathbf{k}}^\dagger(q), \hat{b}_{\mathbf{k}}^\dagger(1), \hat{b}_{\mathbf{k}}^\dagger(2), ..., \hat{b}_{\mathbf{k}}^\dagger(q), \hat{a}_{-\mathbf{k}}(1), \hat{a}_{-\mathbf{k}}(2), ..., \hat{a}_{-\mathbf{k}}(q),$$
$$\hat{b}_{-\mathbf{k}}(1), \hat{b}_{-\mathbf{k}}(2), ..., \hat{b}_{-\mathbf{k}}(q)]. \tag{A.12}$$

We numerically diagonalize the $\mathcal{H}_{\mathbf{k}}$ by using a Bogoliubov transformation [described in below Sec. A.1] and calculate the ground state energy using Eq. (A.25). Hence, the final form of the ground state energy per site (e_g) is given as:

$$e_g = \left(\frac{J\rho_0}{8}\right) - \frac{1}{2L}\sum_{k_1}\sum_{k_2}\sum_{n_q=1}^{2q} \epsilon_{\mathbf{k},n_q} \tag{A.13}$$

Using Eq. (A.13), we find the magnetization (M) as a function of α using the formula, $M = -\frac{\partial e_g}{\partial \alpha}$.

Further, for the simple cubic lattice, the calculation procedure is similar to square lattice except there will be another sum over a wave vector k_3 and the form of $\lambda_{\mathbf{k}}$ and $\Lambda_{\mathbf{k}}(n_q)$ is modified. We find the following form of e_g for simple cubic as,

$$e_g = \left(\frac{J\rho_0}{8}\right) - \frac{1}{2L}\sum_{k_1}\sum_{k_2}\sum_{k_3}\sum_{n_q=1}^{2q} \epsilon_{\mathbf{k},n_q} \tag{A.14}$$

with $\mathbf{k} \equiv (k_1, k_2, k_3)$, $\Lambda_{\mathbf{k}}(n_q) = -t[\cos(\frac{k_1}{2})\cos(2\pi\alpha n_q) + \cos(\frac{k_1}{2} + k_2)]$ and $\lambda_{\mathbf{k}} = -\frac{t}{2}e^{ik_1/2}e^{ik_3}$. However, the range of wave-vectors are $-\pi < k_1 < \pi$, $-\pi < k_2 < \pi$ and $-\frac{\pi}{q} < k_3 < \frac{\pi}{q}$.

A.1 Bogoliubov Transformation

Here, we describe the Bogoliubov transformation to diagonalize the fermionic Hamiltonian, $\mathcal{H}_{\mathbf{k}}$, by redefining the Eq. (A.12) of $\Psi_{\mathbf{k}}^{\dagger}$ label index as follows,

$$\Psi_{\mathbf{k}}^{\dagger} = [\mu_{\mathbf{k},1}^{\dagger}, \mu_{\mathbf{k},2}^{\dagger}, ..., \mu_{\mathbf{k},q}^{\dagger}, \mu_{\mathbf{k},q+1}^{\dagger}, \mu_{\mathbf{k},q+2}^{\dagger}, ..., \mu_{\mathbf{k},2q}^{\dagger}, \mu_{-\mathbf{k},1}, \mu_{-\mathbf{k},2}, ..., \mu_{-\mathbf{k},q},$$

$$\mu_{-\mathbf{k},q+1}, \mu_{-\mathbf{k},q+2}, ..., \mu_{-\mathbf{k},2q}] \tag{A.15}$$

where,

$$\begin{bmatrix} \mu_{\mathbf{k},1}^{\dagger} \\ \mu_{\mathbf{k},2}^{\dagger} \\ \vdots \\ \mu_{\mathbf{k},q}^{\dagger} \\ \mu_{\mathbf{k},q+1}^{\dagger} \\ \mu_{\mathbf{k},q+2}^{\dagger} \\ \vdots \\ \mu_{\mathbf{k},2q}^{\dagger} \end{bmatrix} = \begin{bmatrix} \hat{a}_{\mathbf{k}}^{\dagger}(1) \\ \hat{a}_{\mathbf{k}}^{\dagger}(2) \\ \vdots \\ \hat{a}_{\mathbf{k}}^{\dagger}(q) \\ \hat{b}_{\mathbf{k}}^{\dagger}(1) \\ \hat{b}_{\mathbf{k}}^{\dagger}(2) \\ \vdots \\ \hat{b}_{\mathbf{k}}^{\dagger}(q) \end{bmatrix} \quad \text{and} \quad \begin{bmatrix} \mu_{-\mathbf{k},1} \\ \mu_{-\mathbf{k},2} \\ \vdots \\ \mu_{-\mathbf{k},q} \\ \mu_{-\mathbf{k},q+1} \\ \mu_{-\mathbf{k},q+2} \\ \vdots \\ \mu_{-\mathbf{k},2q} \end{bmatrix} = \begin{bmatrix} \hat{a}_{-\mathbf{k}}(1) \\ \hat{a}_{-\mathbf{k}}(2) \\ \vdots \\ \hat{a}_{-\mathbf{k}}(q) \\ \hat{b}_{-\mathbf{k}}(1) \\ \hat{b}_{-\mathbf{k}}(2) \\ \vdots \\ \hat{b}_{-\mathbf{k}}(q) \end{bmatrix} \tag{A.16}$$

The anticommutation relations of the spinless fermions, $\hat{a}$'s and $\hat{b}$'s, in new operators μ's become

$$\{\mu_{\mathbf{k},i} \ , \ \mu_{\mathbf{k}',j}^{\dagger}\} = \delta_{i,j}\delta_{\mathbf{k},\mathbf{k}'} \tag{A.17a}$$

$$\{\mu_{\mathbf{k},i} \ , \ \mu_{\mathbf{k}',j}\} = 0 \tag{A.17b}$$

$$\{\mu_{\mathbf{k},i}^{\dagger} \ , \ \mu_{\mathbf{k}',j}^{\dagger}\} = 0 \tag{A.17c}$$

We also rewrite, $\mathcal{H}_{\mathbf{k}}$, given in Eq. (A.10) as following

$$\mathcal{H}_{\mathbf{k}} = \begin{bmatrix} \mathcal{D} & \mathcal{F} \\ -\mathcal{F} & -\mathcal{D} \end{bmatrix} \quad \text{with} \quad \mathcal{D} = \begin{bmatrix} A & B \\ B & A \end{bmatrix}_{2q \times 2q}, \ \mathcal{F} = \begin{bmatrix} 0 & B \\ -B & 0 \end{bmatrix}_{2q \times 2q} \tag{A.18}$$

Now, we define a new transformation for a given $\mathbf{k}$ and label index i

$$\mu_{\mathbf{k},i} = \sum_{j=1}^{2q} \left(U_{i,j}\tilde{\mu}_{\mathbf{k},j} + V_{i,j}\tilde{\mu}_{-\mathbf{k},j}^{\dagger} \right) \tag{A.19}$$

such that the new operators $\tilde{\mu}_j$'s also follow the fermionic (anticommutation) algebra. Therefore, using this transformation the Hamiltonian, $\hat{H}_c^{[B]}$, of Eq. (A.9) becomes:

$$\hat{H}_c^{[B]} = \left(\frac{J\rho_0}{8}\right)L + \frac{1}{2}\sum_{k_1}\sum_{k_2} \underbrace{\Psi_{\mathbf{k}}^\dagger \mathcal{U}_{\mathbf{k}}}_{\tilde{\Psi}_{\mathbf{k}}^\dagger} \underbrace{\mathcal{U}_{\mathbf{k}}^\dagger \mathcal{H}_{\mathbf{k}} \mathcal{U}_{\mathbf{k}}}_{\mathcal{E}_{\mathbf{k}}} \underbrace{\mathcal{U}_{\mathbf{k}}^\dagger \Psi_{\mathbf{k}}}_{\tilde{\Psi}_{\mathbf{k}}} \tag{A.20}$$

where,

$$\Psi_{\mathbf{k}}^\dagger \mathcal{U}_{\mathbf{k}} = \tilde{\Psi}_{\mathbf{k}}^\dagger \quad, \text{and} \quad \mathcal{U}_{\mathbf{k}} = \begin{bmatrix} U & V \\ V^* & U^* \end{bmatrix} \tag{A.21}$$

with U and V are $2q \times 2q$ matrices and $U_{i,j}$ and $V_{i,j}$ are their elements. We can find relation (in matrix form) between U and V by using the anticommutation relations given in Eqs. (A.17) as:

$$\begin{bmatrix} U & V \\ V^* & U^* \end{bmatrix} \begin{bmatrix} U^\dagger & V^T \\ V^\dagger & U^T \end{bmatrix} = \begin{bmatrix} \boldsymbol{I}_{2q\times 2q} & 0 \\ 0 & \boldsymbol{I}_{2q\times 2q} \end{bmatrix} \tag{A.22}$$

where, $\boldsymbol{I}_{2q\times 2q}$ is identity matrix in $2q$-dimension. Hence, $\mathcal{U}_{\mathbf{k}}$ is a unitary matrix of order $4q$. Finally, the demand of $\hat{H}_c^{[B]}$ is diagonalized in terms of new operators, $\tilde{\mu}_{\mathbf{k},i}$'s, provides the following condition on

$$\mathcal{U}_{\mathbf{k}}^\dagger \mathcal{H}_{\mathbf{k}} \mathcal{U}_{\mathbf{k}} = \mathcal{E}_{\mathbf{k}} \tag{A.23}$$

with

$$\mathcal{E}_{\mathbf{k}} = \begin{bmatrix} \Sigma_{\mathbf{k}} & 0 \\ 0 & -\Sigma_{\mathbf{k}} \end{bmatrix} \tag{A.24}$$

where, $\Sigma_{\mathbf{k}} = \text{Diag}[\epsilon_{\mathbf{k},1}, \epsilon_{\mathbf{k},2}, \epsilon_{\mathbf{k},3}, \cdots, \epsilon_{\mathbf{k},2q}]$. Hence, the diagonalized form of $\hat{H}_c^{[B]}$ is given as:

$$\hat{H}_c^{[B]} = \left(\frac{J\rho_0}{8}\right)L + \sum_{k_1}\sum_{k_2}\sum_{n_q=1}^{2q} \epsilon_{\mathbf{k},n_q}\left[\tilde{\mu}_{\mathbf{k},n_q}^\dagger \tilde{\mu}_{\mathbf{k},n_q} - \frac{1}{2}\right] \tag{A.25}$$

AppendixB

Diagonalization of the SDW Hofstadter Hamiltonian

In this appendix, we calculate the field dependent ground state energy per site, $e_g[\alpha]$, of the SDW Hamiltonian given in Eq. (5.10) using a Bogoliubov transformation to find magnetization, M, as a function of magnetic field, α. We recall the Hamiltonian $\hat{H}$ as follows:

$$
\hat{H} = \sum_\sigma \left\{ -t \sum_{\mathbf{r} \in \mathcal{A}} \sum_{\boldsymbol{\delta}} \left[e^{2\pi i \alpha \mathbf{r}_y \hat{x} \cdot \boldsymbol{\delta}} \, \hat{a}_{\mathbf{r},\sigma}^\dagger \hat{b}_{\mathbf{r}+\boldsymbol{\delta},\sigma} + \text{h.c.} \right] \right.
$$
$$
\left. + U m_s \eta_\sigma \left(\sum_{\mathbf{r} \in \mathcal{B}} \hat{b}_{\mathbf{r},\sigma}^\dagger \hat{b}_{\mathbf{r},\sigma} - \sum_{\mathbf{r} \in \mathcal{A}} \hat{a}_{\mathbf{r},\sigma}^\dagger \hat{a}_{\mathbf{r},\sigma} \right) \right\} \tag{B.1}
$$

Here, $\hat{a}_{\mathbf{r},\sigma}^\dagger (\hat{a}_{\mathbf{r},\sigma})$ and $\hat{b}_{\mathbf{r},\sigma}^\dagger (\hat{b}_{\mathbf{r},\sigma})$ are actual electron creation (annihilation) operators at site $\mathbf{r}$ with spin $\sigma (\equiv \uparrow, \downarrow)$ on $\mathcal{A}$ and $\mathcal{B}$ sublattice, respectively. Using the convention developed in Appendix A for square lattice [see Fig. A.1], the Hamiltonian $\hat{H}$ in Eq. (B.1) becomes,

$$
\hat{H} = -t \sum_{m=1}^{L_1} \sum_{n=1}^{L_2} \sum_\sigma \left[\left\{ e^{2\pi i \alpha n} \, \hat{a}_\sigma^\dagger(m,n) \hat{b}_\sigma(m,n) + h.c. \right\} \right.
$$
$$
+ \left\{ e^{-2\pi i \alpha n} \, \hat{a}_\sigma^\dagger(m,n) \hat{b}_\sigma(m-1,n) + h.c. \right\}
$$
$$
\left. + \left\{ \hat{a}_\sigma^\dagger(m,n) \left(\hat{b}_\sigma(m-1,n-1) + \hat{b}_\sigma(m,n+1) \right) + h.c. \right\} \right]
$$
$$
+ U m_s \eta_\sigma \sum_{m=1}^{L_1} \sum_{n=1}^{L_2} \sum_\sigma \left[\hat{a}_\sigma^\dagger(m,n) \hat{a}_\sigma(m,n) - \hat{b}_\sigma^\dagger(m,n) \hat{b}_\sigma(m,n) \right] \tag{B.2}
$$

Since, Eq. (B.2) is translationally invariant along m, so we define a Fourier transform as:

$$\hat{a}_\sigma(m,n) = \frac{1}{\sqrt{L_1}} \sum_{k_1} e^{ik_1 m} \, \hat{a}_\sigma(k_1,n) \tag{B.3a}$$

$$\hat{b}_\sigma(m,n) = \frac{1}{\sqrt{L_1}} \sum_{k_1} e^{ik_1(m+\frac{1}{2})} \, \hat{b}_\sigma(k_1,n) \tag{B.3b}$$

Using Eqs. (B.3) in Eq. (B.2) we get the following form of H,

$$
\begin{aligned}
\hat{H} = -t \sum_{k_1} \sum_{n=1}^{L_2} \sum_{\sigma} & \Bigg[\Big\{ 2\cos(2\pi i\alpha n + k_1/2)\, \hat{a}_\sigma^\dagger(k_1,n)\hat{b}_\sigma(k_1,n) + h.c.\Big\} \\
& + \Big\{ \Big(e^{ik_1/2}\hat{a}_\sigma^\dagger(k_1,n)\hat{b}_\sigma(k_1,n+1) + e^{-ik_1/2}\hat{a}_\sigma^\dagger(k_1,n)\hat{b}_\sigma(k_1,n-1)\Big) + h.c.\Big\} \Bigg] \\
& + Um_s\eta_\sigma \sum_{k_1}\sum_{n=1}^{L_2}\sum_{\sigma} \Big[\hat{a}_\sigma^\dagger(k_1,n)\hat{a}_\sigma(k_1,n) - \hat{b}_\sigma^\dagger(k_1,n)\hat{b}_\sigma(k_1,n) \Big]
\end{aligned} \tag{B.4}
$$

As described in Appendix A, we choose the magnetic field $\alpha = p/q$ where p and q are integers, which retain the periodicity along n with q sites in a unit cell. Hence, by defining $n = q(n'-1) + n_q$, where $n_q = 1, 2, ..., q$ and $n' = 1, 2, ..., L_2'$ with $L_2 = qL_2'$ we can also apply the following Fourier transform

$$\hat{a}_\sigma(k_1,n) \equiv \hat{a}_\sigma(k_1,n';n_q) = \frac{1}{\sqrt{L_2'}} \sum_{k_2} e^{ik_2[q(n'-1)+n_q]} \, \hat{a}_\sigma(k_1,k_2;n_q) \tag{B.5a}$$

$$\hat{b}_\sigma(k_1,n) \equiv \hat{b}_\sigma(k_1,n';n_q) = \frac{1}{\sqrt{L_2'}} \sum_{k_2} e^{ik_2[q(n'-1)+n_q]} \, \hat{b}_\sigma(k_1,k_2;n_q) \tag{B.5b}$$

to Eq. (B.4) and obtain,

$$
\begin{aligned}
\hat{H} = -t \sum_{k_1,k_2} \sum_{n_q=1}^{q} \sum_{\sigma} & \Bigg[\Big\{ 2\cos(2\pi i\alpha n_q + k_1/2)\, \hat{a}_\sigma^\dagger(k_1,k_2;n_q)\hat{b}_\sigma(k_1,k_2;n_q) + h.c.\Big\} \\
& + \Big\{ \Big(e^{i(\frac{k_1}{2}+k_2)}\hat{a}_\sigma^\dagger(k_1,k_2;n_q)\hat{b}_\sigma(k_1,k_2;n_q+1) + h.c.\Big) \\
& + \Big(e^{-i(\frac{k_1}{2}+k_2)}\hat{a}_\sigma^\dagger(k_1,k_2;n_q)\hat{b}_\sigma(k_1,k_2;n_q-1) + h.c.\Big)\Big\} \Bigg] \\
& + Um_s\eta_\sigma \sum_{k_1,k_2}\sum_{n_q=1}^{q}\sum_{\sigma} \Big[\hat{a}_\sigma^\dagger(k_1,k_2;n_q)\hat{a}_\sigma(k_1,k_2;n_q) - \hat{b}_\sigma^\dagger(k_1,k_2;n_q)\hat{b}_\sigma(k_1,k_2;n_q) \Big]
\end{aligned} \tag{B.6}
$$

We rewrite Eq. (B.6) in compact form as:

$$\hat{H} = -t \sum_{\mathbf{k}} \sum_{n_q=1}^{q} \sum_{\sigma} \Bigg[\Big\{ \Lambda_{\mathbf{k}}(n_q)\, \hat{a}_{\mathbf{k}\sigma}^\dagger(n_q)\hat{b}_{\mathbf{k}\sigma}(n_q) + h.c.\Big\}$$

$$+ \left\{ \left(\lambda_{\mathbf{k}} \hat{a}_{\mathbf{k}\sigma}^\dagger(n_q) \hat{b}_{\mathbf{k}\sigma}(n_q + 1) + h.c. \right) + \left(\lambda_{\mathbf{k}}^* \hat{a}_{\mathbf{k}\sigma}^\dagger(n_q) \hat{b}_{\mathbf{k}\sigma}(n_q - 1) + h.c. \right) \right\} \right]$$

$$+ U m_s \eta_\sigma \sum_{\mathbf{k}} \sum_{n_q=1}^{q} \sum_\sigma \left[\hat{a}_{\mathbf{k}\sigma}^\dagger(n_q) \hat{a}_{\mathbf{k}\sigma}(n_q) - \hat{b}_{\mathbf{k}\sigma}^\dagger(n_q) \hat{b}_{\mathbf{k}\sigma}(n_q) \right] \tag{B.7}$$

where, $\mathbf{k} \equiv (k_1, k_2)$, $\lambda_{\mathbf{k}} = -t e^{i(\frac{k_1}{2} + k_2)}$ and $\Lambda_{\mathbf{k}}(n_q) = -2t \cos(2\pi i \alpha n_q + k_1/2)$. To diagonalize the above Eq. (B.7), we write in the Nambu basis notation as:

$$\hat{H} = \sum_\sigma \sum_{\mathbf{k}} \Psi_{\mathbf{k}\sigma}^\dagger \mathcal{H}_{\mathbf{k}\sigma} \Psi_{\mathbf{k}\sigma} \tag{B.8}$$

Here, $\mathcal{H}_{\mathbf{k}\sigma}$ is a matrix of order $2q$ which is given below for a value of $\mathbf{k}$ and σ as:

$$\mathcal{H}_{\mathbf{k}\sigma} = \begin{bmatrix} A & B \\ B & -A \end{bmatrix} \tag{B.9}$$

with $A = (U m_s \eta_\sigma) \mathbb{I}_{q \times q}$ where $\mathbb{I}_{q \times q}$ is $q \times q$ identity matrix, and

$$B = \begin{bmatrix} \Lambda_{\mathbf{k}}(1) & \lambda_{\mathbf{k}} & 0 & 0 & \ldots & \lambda_{\mathbf{k}}^* \\ \lambda_{\mathbf{k}}^* & \Lambda_{\mathbf{k}}(2) & \lambda_{\mathbf{k}} & 0 & \ldots & 0 \\ 0 & \lambda_{\mathbf{k}}^* & \Lambda_{\mathbf{k}}(3) & \lambda_{\mathbf{k}} & \ldots & 0 \\ \vdots & \vdots & \ddots & \ddots & \ddots & \vdots \\ 0 & 0 & \ldots & \lambda_{\mathbf{k}}^* & \Lambda_{\mathbf{k}}(q-1) & \lambda_{\mathbf{k}} \\ \lambda_{\mathbf{k}} & 0 & \ldots & 0 & \lambda_{\mathbf{k}}^* & \Lambda_{\mathbf{k}}(q) \end{bmatrix}. \tag{B.10}$$

However, the Nambu basis is chosen as:

$$\Psi_{\mathbf{k}\sigma}^\dagger = [\hat{a}_{\mathbf{k}\sigma}^\dagger(1), \hat{a}_{\mathbf{k}\sigma}^\dagger(2), \cdots, \hat{a}_{\mathbf{k}\sigma}^\dagger(q), \hat{b}_{\mathbf{k}\sigma}^\dagger(1), \hat{b}_{\mathbf{k}\sigma}^\dagger(2), \cdots, \hat{b}_{\mathbf{k}\sigma}^\dagger(q)]. \tag{B.11}$$

Bogoliubov transformation

Here, we describe a Bogoliubov transformation to diagonalize, $\mathcal{H}_{\mathbf{k}\sigma}$. To do so, we define old operators in terms of new operators via a transformation (for a given $\mathbf{k}$ and σ) given below:

$$\hat{a}_i = \sum_{j=1}^{q} \left[U_{i,j} \tilde{a}_j + V_{i,j} \tilde{b}_j \right] \tag{B.12a}$$

$$\hat{b}_i = \sum_{j=1}^{q} \left[V_{i,j}^* \tilde{a}_j + U_{i,j}^* \tilde{b}_j \right] \tag{B.12b}$$

such that the new operators $\tilde{a}_j$'s and $\tilde{b}_j$'s also follow the fermionic algebra. Therefore, using the above transformation in Eq. (B.7), we get

$$\hat{H} = \sum_\sigma \sum_{\mathbf{k}} \underbrace{\Psi^\dagger_{\mathbf{k}\sigma} \mathcal{U}_{\mathbf{k}\sigma}}_{\tilde{\Psi}^\dagger_{\mathbf{k}\sigma}} \underbrace{\mathcal{U}^\dagger_{\mathbf{k}\sigma} \mathcal{H}_{\mathbf{k}\sigma} \mathcal{U}_{\mathbf{k}\sigma}}_{\mathcal{E}_{\mathbf{k}}} \underbrace{\mathcal{U}^\dagger_{\mathbf{k}\sigma} \Psi_{\mathbf{k}\sigma}}_{\tilde{\Psi}_{\mathbf{k}\sigma}} \tag{B.13}$$

where,

$$\Psi^\dagger_{\mathbf{k}\sigma} \mathcal{U}_{\mathbf{k}\sigma} = \tilde{\Psi}^\dagger_{\mathbf{k}\sigma} \quad , \text{and} \quad \mathcal{U}_{\mathbf{k}\sigma} = \begin{bmatrix} U & V \\ V^* & U^* \end{bmatrix} \tag{B.14}$$

with U and V are $q \times q$ matrices and $U_{i,j}$ and $V_{i,j}$ are their elements. We can find relation between U and V by using the anticommutation relations of $\hat{a}_i$'s and $\hat{b}_i$'s as:

$$\{\hat{a}_i, \hat{a}^\dagger_j\} = \delta_{i,j} \Rightarrow UU^\dagger + VV^\dagger = \mathbb{I} \tag{B.15}$$

$$\{\hat{b}_i, \hat{b}^\dagger_j\} = \delta_{i,j} \Rightarrow V^*V^T + U^*U^T = \mathbb{I} \tag{B.16}$$

$$\{\hat{a}_i, \hat{b}^\dagger_j\} = 0 \Rightarrow UV^T + VU^T = 0 \tag{B.17}$$

$$\{\hat{b}_i, \hat{a}^\dagger_j\} = 0 \Rightarrow V^*U^\dagger + U^*V^\dagger = 0 \tag{B.18}$$

We can also write these relations in compact form:

$$\begin{bmatrix} U & V \\ V^* & U^* \end{bmatrix} \begin{bmatrix} U^\dagger & V^T \\ V^\dagger & U^T \end{bmatrix} = \begin{bmatrix} \mathbb{I} & 0 \\ 0 & \mathbb{I} \end{bmatrix} \tag{B.19}$$

Hence, it turns out that $\mathcal{U}_{\mathbf{k}\sigma}$ is a unitary matrix of order $2q$ i.e. $\mathcal{U}_{\mathbf{k}\sigma}\mathcal{U}^\dagger_{\mathbf{k}\sigma} = \mathcal{U}^\dagger_{\mathbf{k}\sigma}\mathcal{U}_{\mathbf{k}\sigma} = \boldsymbol{I}$, where $\boldsymbol{I}$ is $2q$-dimensional identity matrix. Finally, the demand of $\hat{H}$ is diagonalized in terms of the new operators, $\tilde{a}_{\mathbf{k},\sigma}(i)$'s and $\tilde{b}_{\mathbf{k},\sigma}(i)$'s, provides the following condition on

$$\mathcal{U}^\dagger_{\mathbf{k}\sigma} \mathcal{H}_{\mathbf{k}\sigma} \mathcal{U}_{\mathbf{k}\sigma} = \mathcal{E}_{\mathbf{k}} \tag{B.20}$$

with

$$\mathcal{E}_{\mathbf{k}} = \begin{bmatrix} \Sigma_{\mathbf{k}} & 0 \\ 0 & -\Sigma_{\mathbf{k}} \end{bmatrix} \tag{B.21}$$

where, $\Sigma_{\mathbf{k}} = \text{Diag}[\epsilon_{\mathbf{k}}(1), \epsilon_{\mathbf{k}}(2), \epsilon_{\mathbf{k}}(3), \cdots, \epsilon_{\mathbf{k}}(q)]$. Hence, the diagonalized form of $\hat{H}$ is,

$$\hat{H} = \sum_\sigma \sum_{\mathbf{k}} \sum_{n_q=1}^{q} \epsilon_{\mathbf{k}}(n_q) \left[\tilde{a}^\dagger_{\mathbf{k}\sigma}(n_q) \tilde{a}_{\mathbf{k}\sigma}(n_q) - \tilde{b}^\dagger_{\mathbf{k}\sigma}(n_q) \tilde{b}_{\mathbf{k}\sigma}(n_q) \right] \tag{B.22}$$

We note that $\epsilon_{\mathbf{k}}(n_q)$ is independent of σ. Since, at half-filling in ground state of Eq. (B.22) we have $\langle \tilde{a}^{\dagger}_{\mathbf{k}\sigma}(n_q)\tilde{a}_{\mathbf{k}\sigma}(n_q)\rangle = 0$ and $\langle \tilde{b}^{\dagger}_{\mathbf{k}\sigma}(n_q)\tilde{b}_{\mathbf{k}\sigma}(n_q)\rangle = 1$. Therefore, we calculate the ground state energy per site, $e_g[\alpha]$, using Eq. (B.22) as:

$$e_g[\alpha] = -\frac{2}{L}\sum_{\mathbf{k}}\sum_{n_q=1}^{q}\epsilon_{\mathbf{k}}(n_q) \tag{B.23}$$

However, we can diagonalize the weak-coupling KLM field dependent Hamiltonian, $\hat{H}$, given in Eq. (5.22) by replacing $Um_s \to (-J/4)$ in Eq. (B.1). Therefore, the ground state energy per site, $e_g[B]$, is also given by

$$e_g[B] = -\frac{2}{L}\sum_{\mathbf{k}}\sum_{n_q=1}^{q}\epsilon_{\mathbf{k}}(n_q) \tag{B.24}$$

AppendixC

Fourier Analysis

Fourier transform (FT) is a strong mathematical tool that converts a signal from *time domain* to its *frequency domain.* In other words it a powerful method which decomposes a function into the frequencies that constitute it. Since, it is always possible that we can describe virtually most of the natural phenomenon through a waveform, for example, sound waves, electromagnetic waves, and etc. Therefore, studying FT becomes essential to describe many physical properties. Our immediate goal is to obtain the magnetic quantum oscillations frequency by using the Fourier transform.

Mathematically, the Fourier transform of a function $f(t)$ from time to frequency domain is defined as:

$$f(\nu) = \int_{-\infty}^{\infty} f(t) \ e^{2\pi i \nu t} \ dt \tag{C.1}$$

where $f(\nu)$ is the Fourier transform of $f(t)$, and the inverse Fourier transform is defined in following way,

$$f(t) = \int_{-\infty}^{\infty} f(\nu) \ e^{-2\pi i \nu t} \ d\nu \tag{C.2}$$

Since, the Fourier transform is a generalization of complex Fourier series, therefore, we first discuss the Fourier series and then derive Eq. (C.1) and (C.2) in the next section.

C.1 Fourier Series

The Fourier series of a real function $f(x)$ is defined as:

$$f(x) = \frac{a_0}{2} + \sum_{n=1}^{\infty} a_n \cos(nx) + \sum_{n=1}^{\infty} b_n \sin(nx) \tag{C.3}$$

along with the integral identities (or orthogonality conditions) as:

$$\int_{-\pi}^{\pi} \sin(mx) \sin(nx) dx = \pi \delta_{mn} \tag{C.4a}$$

$$\int_{-\pi}^{\pi} \cos(mx) \cos(nx) dx = \pi \delta_{mn} \tag{C.4b}$$

$$\int_{-\pi}^{\pi} \sin(mx) \cos(nx) dx = 0 \tag{C.4c}$$

$$\int_{-\pi}^{\pi} \sin(nx) dx = 0 \tag{C.4d}$$

$$\int_{-\pi}^{\pi} \cos(nx) dx = 0 \tag{C.4e}$$

where m, n are nonzero integer and δ_{mn} is the Kronecker delta function defined below as:

$$\delta_{mn} = \begin{cases} 1 & \text{if } m = n \\ 0 & \text{otherwise} \end{cases} \tag{C.5}$$

It turns out that we can define the Fourier coefficient a_0, a_n and b_n by using the Eqs. C.4 as:

$$a_0 = \frac{1}{\pi} \int_{-\pi}^{\pi} f(x) dx \tag{C.6a}$$

$$a_n = \frac{1}{\pi} \int_{-\pi}^{\pi} f(x) \cos(nx) dx \tag{C.6b}$$

$$b_n = \frac{1}{\pi} \int_{-\pi}^{\pi} f(x) \sin(nx) dx \tag{C.6c}$$

We can use Euler's equation, $e^{i\theta} = \cos\theta + i\sin\theta$, to extend the Fourier series Eq. (C.3) in complex coefficient domain,

$$f(x) = \sum_{n=-\infty}^{\infty} c_n e^{-inx} \tag{C.7}$$

where c_n is a complex number and is defined as,

$$c_n = \frac{1}{2\pi} \int_{-\pi}^{\pi} f(x) e^{inx} \, dx \tag{C.8}$$

$$
= \begin{cases} \frac{1}{2}(a_n + ib_n) & \text{for } n < 0 \\ \frac{1}{2}(a_n - ib_n) & \text{for } n > 0 \\ \frac{1}{2}a_0 & \text{for } n = 0 \end{cases} \tag{C.9}
$$

However, the orthogonality relation becomes,

$$
\int_{-\pi}^{\pi} (e^{imx})^* e^{inx} \, dx = 2\pi \; \delta_{mn} \tag{C.10}
$$

Proof

To prove the Fourier transform relation, we consider a function $f(t)$ which is periodic in the interval $[-T/2, T/2]$, then the Fourier series can be defined as:

$$
f(t) = \sum_{n=-\infty}^{\infty} c_n \, e^{-2\pi i (\frac{n}{T})t} \tag{C.11}
$$

and its coefficient is,

$$
c_n = \frac{1}{T} \int_{-T/2}^{T/2} f(t) \, e^{2\pi i (\frac{n}{T})t} \, dt \tag{C.12}
$$

Let us define n^{th} frequency as

$$
\nu_n = n/T \Rightarrow \Delta\nu = \nu_{n+1} - \nu_n = \frac{n+1}{T} - \frac{n}{T} = \frac{1}{T}
$$

. Therefore,

$$
f(t) = \sum_{n=-\infty}^{\infty} c_n \, e^{-2\pi i (n\Delta\nu)t} \tag{C.13}
$$

whereas

$$
c_n = \Delta\nu \int_{-T/2}^{T/2} f(t) \, e^{2\pi i (n\Delta\nu)t} \, dt \tag{C.14}
$$

By putting c_n in $f(t)$ equation and then taking limit $T \to \infty$ the discrete sum becomes integral and with $\Delta\nu \to d\nu$, $n\Delta\nu \to \nu$ we arrive at the final form of Fourier transform,

$$
f(\nu) = \int_{-\infty}^{\infty} f(t) \, e^{2\pi i \nu t} \, dt \tag{C.15}
$$

and its inverse transform is

$$
f(t) = \int_{-\infty}^{\infty} f(\nu) \, e^{-2\pi i \nu t} \, d\nu \tag{C.16}
$$

C.2   Discrete Fourier Transform

The continuous Fourier transform is relevant for well defined analytical functions that are doable by hand. However, to analyze the simulation or experimental data on digital computers, it is necessary to replace the continuum values to a set of discrete values. In order to do that, the integration is replaced by summation and the continuous Fourier transform becomes the discrete Fourier transform. Below we follow the steps of Arfken and Weber given in Ref. [98].

For the time interval $(0, T)$, we consider N discrete values of t_k as,

$$t_k = \frac{kT}{N}, \qquad k = 0, 1, 2, ..., N - 1 \tag{C.17}$$

and the corresponding functions are $f(t_0), \ f(t_1), \ f(t_2), ..., f(t_{N-1})$. Then, from Eq. (C.15), we get

$$f(\nu) = \frac{1}{\sqrt{N}} \sum_{k=0}^{N-1} f(t_k) \ e^{2\pi i \nu t_k} \tag{C.18}$$

In principle, we can calculate the above Fourier transform for any value of ν. Since, we are providing N data points as a input therefore only the final N output data points will be physically relevant. So, we define N values in ν-space as:

$$\nu_p = \frac{p}{T}, \qquad p = 0, 1, 2, ..., N - 1. \tag{C.19}$$

Hence, the discrete Fourier transform is given as:

$$f(\nu_p) = \frac{1}{\sqrt{N}} \sum_{k=0}^{N-1} f(t_k) \ e^{2\pi i \nu_p t_k} \tag{C.20}$$

and its inverse Fourier transform is defined as:

$$f(t_k) = \frac{1}{\sqrt{N}} \sum_{p=0}^{N-1} f(\nu_p) \ e^{-2\pi i \nu_p t_k} \tag{C.21}$$

We can also write Eq. (C.20) in matrix form given below

$$
\begin{bmatrix}
f(\nu_0) \\
f(\nu_1) \\
f(\nu_2) \\
f(\nu_3) \\
... \\
f(\nu_{N-1})
\end{bmatrix}
=
\begin{bmatrix}
1 & 1 & 1 & 1 & ... & 1 \\
1 & W & W^2 & W^3 & ... & W^{N-1} \\
1 & W^2 & W^4 & W^6 & ... & W^{N-2} \\
1 & W^3 & W^6 & W^9 & ... & W^{N-3} \\
... & & & & & \\
1 & W^{N-1} & W^{N-2} & W^{N-3} & ... & W
\end{bmatrix}
\begin{bmatrix}
f(t_0) \\
f(t_1) \\
f(t_2) \\
f(t_3) \\
... \\
f(t_{N-1})
\end{bmatrix}
\tag{C.22}
$$

with, $W = e^{i2\pi/N}$.

C.2.1   Limitations

The discrete Fourier transformation is a standard method to analyze any waveform, but it also has limitations when we apply Eqs. (C.20) and (C.21) to physical systems. For example, when N is small the physical interpretation of the Fourier transformed data and the limit $f(\nu_p) \to f(\nu)$ becomes quite difficult to explain. Therefore, to avoid the trouble we can take the most essential precaution by choosing N sufficiently large. We illustrate this point by choosing an appropriate example given below.

Example(1):

We consider a simple function $f(t) = \cos(2\pi t)$ of length, $T = 1$ and $N = 4$ particular points as:

$$t_k = \frac{kT}{N} = \frac{k}{4}, \quad k = 0, 1, 2, 3 \tag{C.23}$$

then the $f(t_k)$ can be represented by a four-component vector

$$f(t_k) = (1, 0, -1, 0) \tag{C.24}$$

and the corresponding frequencies are given by equation

$$\nu_p = \frac{p}{T} = p \quad p = 0, 1, 2, 3. \tag{C.25}$$

Clearly the function, $\cos(2\pi t)$, only corresponds to the frequency component $p = 1$. By solving

$$\begin{bmatrix} f(\nu_0) \\ f(\nu_1) \\ f(\nu_2) \\ f(\nu_3) \end{bmatrix} = \frac{1}{2} \begin{bmatrix} 1 & 1 & 1 & 1 \\ 1 & i & -1 & -i \\ 1 & -1 & 1 & -1 \\ 1 & -i & -1 & i \end{bmatrix} \begin{bmatrix} 1 \\ 0 \\ -1 \\ 0 \end{bmatrix} \tag{C.26}$$

we get

$$f(\nu_p) = (0, 1, 0, 1) \tag{C.27}$$

We can use the inverse Fourier transform of Eq. (C.21) to obtain our original function

$$
\begin{aligned}
f(t_k) &= e^{-i2\pi t_k} + e^{-i2\pi 3t_k} & \text{(C.28)} \\
\Re f(t_k) &= \cos(2\pi t_k) + \cos(2\pi 3t_k) & \text{(C.29)}
\end{aligned}
$$

But, we get one extra wave-function of frequency, $\nu = 3$, other than actual $\nu = 1$. Hence, $\cos(2\pi t_k)$ and $\cos(2\pi 3t_k)$ mimic each other because of limited number of data points or a particular choice to data points. In literature, it is known as *aliasing*. The results are plotted in Fig. C.1.
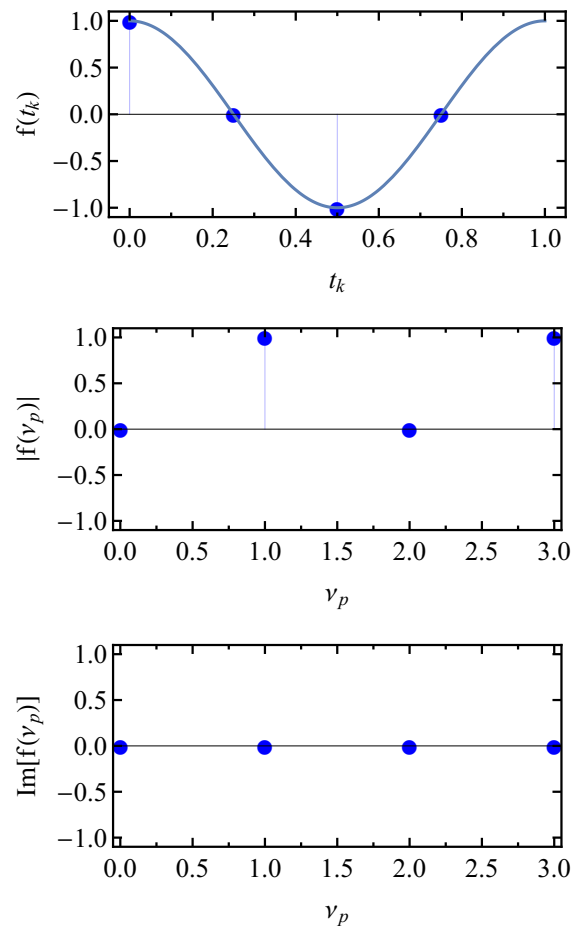

Figure C.1: The function, $f(t) = \cos(2\pi t)$ and its Fourier transform, $f(\nu_p)$. We can see the error frequency $\nu = 3$ in the middle plot which have non-zero amplitude.

C.3 Fourier Transform Using Mathematica

In this section we describe here how to perform Fourier analysis in *Mathematica*. We can find the Mathematica expression of the discrete Fourier transform (or inverse) by performing a minor change in Eq. (C.20) and (C.21) as:

$$t_k = \frac{kT}{N} = \frac{(k-1)T}{N} \quad \text{and} \quad \nu_p = \frac{p}{T} = \frac{p-1}{T} \tag{C.30}$$

where $p, k = 1, 2, ..., N$. We can see that in Mathematica the zero frequency correspond to $p = 1$. Then

$$f(\nu_p) = \frac{1}{\sqrt{N}} \sum_{k=1}^{N} f(t_k) \ e^{2\pi i(p-1)(k-1)/N} \tag{C.31}$$

The above expression is used to calculate the discrete Fourier transform. Its inverse Fourier transform is given by

$$f(t_k) = \frac{1}{\sqrt{N}} \sum_{p=1}^{N} f(\nu_p) \ e^{-2\pi i(p-1)(k-1)/N} \tag{C.32}$$

Below we describe how to perform Fourier analysis in Mathematica. The Mathematica uses `Fourier` function to find the discrete Fourier transform of any equally spaced data.

Example(2):

In this example we consider a simple function $f(t) = \cos(2\pi t)$ of Length, $T = 4$ and $N = 100$ equally spaced data points.

Some Important Steps:

- Make a data file (say, *source*) and save the function value $f(t_k) = \cos(2\pi t_k)$ in it for the discrete value $t_k = \frac{kT}{N}$, $k = 1, 2, ..., N$ using `Table` command as:
  $source = $ `Table`$[f(t_k), \{k, 1, N\}]$

- Apply `Fourier` command on *source* to calculate Fourier transform (named as *FTvalues*). Since, $f(\nu_p)$ is complex valued function therefore after applying `Fourier` we get a set of complex numbers. We find Fourier amplitude (or intensity) by also applying absolute command `Abs`.
  $FTvalues = $ `Abs`$[$`Fourier`$[source]]$

- The corresponding frequencies are calculated using the formula:

$$\nu_p = \frac{p-1}{T} = \frac{p-1}{N \times \Delta t}, \quad p = 1, 2, .., N$$

since, $\Delta t = t_{k+1} - t_k = T/N$. We call this data file '*freq*' which is given as:

freq=`Table`[ν_p, $\{p, 1, N\}$]

- At last we combine frequency data ('*freq*') to Fourier transform data ('*FT-values*') as:

FTvalues=`Table`[$\{freq[[i]], FTvalues[[i]]\}$, $\{i, 1, $`Length`$[FTvalues]\}$]

Through this procedures we find the Fourier transform of the function $f(t)$ taken in example(2) [See Fig. C.2].
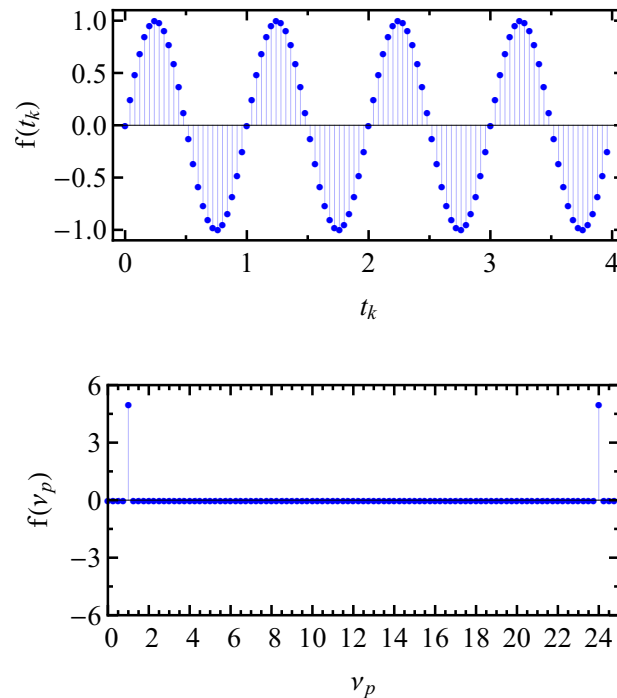

Figure C.2: The function, $f(t) = \cos(2\pi t)$ of the example and its Fourier transform. We can see the Fourier transform correctly determines the function frequency, $\nu = 1$. The other frequency around $\nu = 24$ is a mimic of $\nu = 1$ because the Fourier transform also calculates for negative frequency [see Eq. (C.31)].

Bibliography

[1] P. Fazekas, *Lecture Notes on Electron Correlation and Magnetism* (World Scientific).

[2] P. Misra, *Heavy-Fermion Systems* (Elsevier, Amsterdam, 2008).

[3] P. Coleman, *Introduction to Many-Body Physics* (Cambridge University Press, UK, 2015).

[4] K. Andres, J. E. Graebner, and H. R. Ott, Phys. Rev. Lett. **35**, 1779 (1975).

[5] N. W. Ashcroft and N. D. Mermin, *Solid State Physics* (Saunders College Publishing, USA, 1976).

[6] C. Kittel, *Introduction to Solid State Physics*, 6th ed. (John Wiley & Sons, Inc., New York, 1986).

[7] F. Steglich, J. Aarts, C. D. Bredl, W. Lieke, D. Meschede, W. Franz, and H. Schäfer, Phys. Rev. Lett. **43**, 1892 (1979).

[8] H. R. Ott, H. Rudigier, Z. Fisk, and J. L. Smith, Phys. Rev. Lett. **50**, 1595 (1983).

[9] G. R. Stewart, Z. Fisk, J. O. Willis, and J. L. Smith, Phys. Rev. Lett. **52**, 679 (1984).

[10] A. Menth, E. Buehler, and T. H. Geballe, Phys. Rev. Lett. **22**, 295 (1969).

[11] G. Li, Z. Xiang, F. Yu, T. Asaba, B. Lawson, P. Cai, C. Tinsman, A. Berkley, S. Wolgast, Y. S. Eo, D.-J. Kim, C. Kurdak, J. W. Allen, K. Sun, X. H. Chen, Y. Y. Wang, Z. Fisk, and L. Li, Science **346**, 1208 (2014).

[12] B. S. Tan, Y.-T. Hsu, B. Zeng, M. C. Hatnean, N. Harrison, Z. Zhu, M. Hart-
     stein, M. Kiourlappou, A. Srivastava, M. D. Johannes, T. P. Murphy, J.-H.
     Park, L. Balicas, G. G. Lonzarich, G. Balakrishnan, and S. E. Sebastian,
     Science **349**, 287 (2015).

[13] P. Nyhus, S. L. Cooper, Z. Fisk, and J. Sarrao, Phys. Rev. B **52**, R14308
     (1995).

[14] B. Gorshunov, N. Sluchanko, A. Volkov, M. Dressel, G. Knebel, A. Loidl, and
     S. Kunii, Phys. Rev. B **59**, 1808 (1999).

[15] X. N., B. P. K., D. J. H., D. R. S., L. G., M. S., M. C. E., S. X., P. N. C.,
     R. M., P. E., C. K., A. A., B. S. V., Y. R., W. H.-M., F. Z., D. X., M. J.,
     D. H., and S. M., Nature Communications **5**, 4566 (2014).

[16] F. Lu, J. Zhao, H. Weng, Z. Fang, and X. Dai, Phys. Rev. Lett. **110**, 096401
     (2013).

[17] W. de Haas, J. de Boer, and G. van dën Berg, Physica **1**, 1115 (1934).

[18] Proceedings of the Royal Society of London A: Mathematical, Physical and
     Engineering Sciences **263**, 494 (1961).

[19] A. C. Hewson, *The Kondo Problem to Heavy Fermions*, Cambridge Studies in
     Magnetism (Cambridge University Press, 1993).

[20] J. Kondo, Progress of Theoretical Physics **32**, 37 (1964).

[21] S. Doniach, Physica B **91**, 231 (1977).

[22] M. A. Ruderman and C. Kittel, Phys. Rev. **96**, 99 (1954).

[23] K. Yosida, Phys. Rev. **106**, 893 (1957).

[24] P. W. Anderson, Phys. Rev. **124**, 41 (1961).

[25] M. Jarrell, Phys. Rev. B **51**, 7429 (1995).

[26] D. Shoenberg, *Magnetic Oscillations in Metals*, Cambridge Monographs on
     Physics (Cambridge University Press, 1984).

[27] L. Onsager, Phil. Mag. **43**, 1006 (1952).

[28] A. A. Abrikosov, *Fundamentals of the Theory of Metals* (North-Holland, Amsterdam, 1988).

[29] M. Dzero, K. Sun, V. Galitski, and P. Coleman, Phys. Rev. Lett. **104**, 106408 (2010).

[30] T. Takimoto, Journal of the Physical Society of Japan **80**, 123710 (2011).

[31] S. Wolgast, Y. S. Eo, T. Öztürk, G. Li, Z. Xiang, C. Tinsman, T. Asaba, B. Lawson, F. Yu, J. W. Allen, K. Sun, L. Li, i. m. c. Kurdak, D.-J. Kim, and Z. Fisk, Phys. Rev. B **92**, 115110 (2015).

[32] G. Baskaran, arXiv:1507.03477 (2015).

[33] M. Hartstein, W. H. Toews, Y. T. Hsu, B. Zeng, X. Chen, M. C. Hatnean, Q. R. Zhang, S. Nakamura, A. S. Padgett, G. Rodway-Gant, J. Berk, M. K. Kingston, G. H. Zhang, M. K. Chan, S. Yamashita, T. Sakakibara, Y. Takano, J. H. Park, L. Balicas, N. Harrison, N. Shitsevalova, G. Balakrishnan, G. G. Lonzarich, R. W. Hill, M. Sutherland, and S. E. Sebastian, Nature Physics **14**, 166 EP (2017).

[34] I. Sodemann, D. Chowdhury, and T. Senthil, Phys. Rev. B **97**, 045152 (2018).

[35] K. Kishigi and Y. Hasegawa, Phys. Rev. B **90**, 085427 (2014).

[36] J. Knolle and N. R. Cooper, Phys. Rev. Lett. **115**, 146401 (2015).

[37] L. Zhang, X.-Y. Song, and F. Wang, Phys. Rev. Lett. **116**, 046404 (2016).

[38] H. K. Pal, F. Piéchon, J.-N. Fuchs, M. Goerbig, and G. Montambaux, Phys. Rev. B **94**, 125140 (2016).

[39] H. Shen and L. Fu, Phys. Rev. Lett. **121**, 026403 (2018).

[40] N. Harrison, Phys. Rev. Lett. **121**, 026602 (2018).

[41] H. Liu, M. Hartstein, G. J. Wallace, A. J. Davies, M. C. Hatnean, M. D. Johannes, N. Shitsevalova, G. Balakrishnan, and S. E. Sebastian, Journal of Physics: Condensed Matter **30**, 16LT01 (2018).

[42] P. Ram and B. Kumar, Phys. Rev. B **96**, 075115 (2017).

[43] B. Kumar, Phys. Rev. B **77**, 205115 (2008).

[44] P. Fulde, V. Zevin, and G. Zwicknagl, Zeitschrift für Physik B Condensed Matter **92**, 133 (1993).

[45] Q. Si and F. Steglich, Science **329**, 1161 ((2010)).

[46] J. P. L. Faye, M. N. Kiselev, P. Ram, B. Kumar, and D. Sénéchal, Phys. Rev. B **97**, 235151 (2018).

[47] M. Feldbacher, C. Jurecka, F. F. Assaad, and W. Brenig, Phys. Rev. B **66**, 045103 (2002).

[48] G. Aeppli and Z. Fisk, Comments Cond. Mat. Phys. **16**, 155 (1992).

[49] O. Erten, P. Ghaemi, and P. Coleman, Phys. Rev. Lett. **116**, 046403 (2016).

[50] M. Dzero, J. Xia, V. Galitski, and P. Coleman, Annu. Rev. Condens. Matter Phys. **7**, 249 (2016).

[51] Y. Xu, S. Cui, J. K. Dong, D. Zhao, T. Wu, X. H. Chen, K. Sun, H. Yao, and S. Y. Li, Phys. Rev. Lett. **116**, 246403 (2016).

[52] B. Kumar, Phys. Rev. B **79**, 155121 (2009).

[53] B. Kumar, Phys. Rev. B **87**, 195105 (2013).

[54] B. Bertini, E. Tartaglia, and P. Calabrese, Journal of Statistical Mechanics: Theory and Experiment **2017**, 103107 (2017).

[55] A. Nocera, F. H. L. Essler, and A. E. Feiguin, Phys. Rev. B **97**, 045146 (2018).

[56] S. Östlund and M. Granath, Phys. Rev. Lett. **96**, 066404 (2006).

[57] A. Angelucci, Phys. Rev. B **51**, 11580 (1995).

[58] S. Doniach, Physica B **91**, 231 (1977).

[59] S. Sachdev and R. N. Bhatt, Phys. Rev. B **41**, 9323 (1990).

[60] B. Kumar, Phys. Rev. B **82**, 054404 (2010).

[61] F. F. Assaad, Phys. Rev. Lett. **83**, 796 (1999).

[62] Z.-P. Shi, R. R. P. Singh, M. P. Gelfand, and Z. Wang, Phys. Rev. B **51**, 15630 (1995).

[63] Z. Wang, X.-P. Li, and D.-H. Lee, Physica B **199 & 200**, 463 (1994).

[64] R. Kumar and B. Kumar, Phys. Rev. B **77**, 144413 (2008).

[65] S. Trebst, H. Monien, A. Grzesik, and M. Sigrist, Phys. Rev. B **73**, 165101 (2006).

[66] I. M. Lifshitz, Sov. Phys. JETP **11**, 1130 (1960).

[67] D. R. Hofstadter, Phys. Rev. B **14**, 2239 (1976).

[68] E. Manousakis, Rev. Mod. Phys. **63**, 1 (1991).

[69] P. W. Anderson, Phys. Rev. **86**, 694 (1952).

[70] N. Shibata, T. Nishino, K. Ueda, and C. Ishii, Phys. Rev. B **53**, R8828 (1996).

[71] T. Schork, S. Blawid, and J.-i. Igarashi, Phys. Rev. B **59**, 9888 (1999).

[72] Z. Wang, X.-P. Li, and D.-H. Lee, Phys. Rev. B **47**, 11935 (1993).

[73] J. R. Iglesias, C. Lacroix, and B. Coqblin, Phys. Rev. B **56**, 11820 (1997).

[74] H. Tsunetsugu, M. Sigrist, and K. Ueda, Rev. Mod. Phys. **69**, 809 (1997).

[75] G.-M. Zhang, Q. Gu, and L. Yu, Phys. Rev. B **62**, 69 (2000).

[76] J. R. Schrieffer and P. A. Wolff, Phys. Rev. **149**, 491 (1966).

[77] Proceedings of the Royal Society of London A: Mathematical, Physical and Engineering Sciences **276**, 238 (1963).

[78] R. Shinzaki, J. Nasu, and A. Koga, Journal of Physics: Conference Series **683**, 012041 (2016).

[79] A. Georges, G. Kotliar, W. Krauth, and M. J. Rozenberg, Rev. Mod. Phys. **68**, 13 (1996).

[80] N. S. Vidhyadhiraja and D. E. Logan, The European Physical Journal B - Condensed Matter and Complex Systems **39**, 313 (2004).

[81] J. W. Allen and R. M. Martin, Phys. Rev. Lett. **49**, 1106 (1982).

[82] A. McMahan, C. Huscroft, R. Scalettar, and E. Pollock, Journal of Computer-Aided Materials Design **5**, 131 (1998).

[83] J. H. Pixley, L. Deng, K. Ingersent, and Q. Si, Phys. Rev. B **91**, 201109 (2015).

[84] K. Ueda, H. Tsunetsugu, and M. Sigrist, Phys. Rev. Lett. **68**, 1030 (1992).

[85] V. E. Smith, D. E. Logan, and H. Krishnamurthy, Eur. Phys. J. B **32**, 49 (2003).

[86] S. Sachdev and R. N. Bhatt, Phys. Rev. B **41**, 9323 (1990).

[87] S.-J. Sun, T.-M. Hong, and M. F. Yang, Physica B: Condensed Matter **216**, 111 (1995).

[88] M. Vekić, J. W. Cannon, D. J. Scalapino, R. T. Scalettar, and R. L. Sugar, Phys. Rev. Lett. **74**, 2367 (1995).

[89] W. Hu, R. T. Scalettar, E. W. Huang, and B. Moritz, Phys. Rev. B **95**, 235122 (2017).

[90] B. Möller and P. Wölfle, Phys. Rev. B **48**, 10320 (1993).

[91] A. W. Overhauser, Journal of Applied Physics **34**, 1019 (1963).

[92] G. Grüner, Rev. Mod. Phys. **66**, 1 (1994).

[93] E. Fawcett, Rev. Mod. Phys. **60**, 209 (1988).

[94] D. J. Campbell, C. Eckberg, K. Wang, L. Wang, H. Hodovanets, D. Graf, D. Parker, and J. Paglione, Phys. Rev. B **96**, 075120 (2017).

[95] A. Carrington, A. Coldea, J. Fletcher, N. Hussey, C. Andrew, A. Bangura, J. Analytis, J.-H. Chu, A. Erickson, I. Fisher, and R. McDonald, Physica C: Superconductivity **469**, 459 (2009).

[96] B. Vignolle, D. Vignolles, D. LeBoeuf, S. Lepault, B. Ramshaw, R. Liang, D. Bonn, W. Hardy, N. Doiron-Leyraud, A. Carrington, N. Hussey, L. Taillefer, and C. Proust, Comptes Rendus Physique **12**, 446 (2011).

[97] P. G. Harper, Proceedings of the Physical Society. Section A **68**, 874 (1955).

[98] G. B. Arfken, H. J. Weber, and F. E. Harris, *Mathematical Methods for Physicists (Seventh Edition)*, seventh edition ed., edited by G. B. Arfken, H. J. Weber, and F. E. Harris (Academic Press, Boston, 2013) pp. 935–962.